

Preferential Synaptic Type of GABA-A Receptor Ligands Enhancing Neuronal Survival and Facilitating Functional Recovery After Ischemic Stroke

Barbara Mordyl,[¶] Nikola Fajkis-Zajczkowska,[¶] Katarzyna Szafrńska, Agata Siwek, Monika Głuch-Lutwin, Paweł Żmudzki, Jakub Jończyk, Tadeusz Karcz, Karolina Słoczyńska, Elżbieta Pękala, Bartosz Pomierny, Weronika Krzyżanowska, Jakub Jurczyk, Alicja Skórkowska, Aleksandra Sałach, Magdalena Jastrzębska-Więsek, Maria Walczak, Maciej Tadeusz Gawlik, Magdalena Smolik, Marcin Kolaczowski, and Monika Marcinkowska*



Cite This: <https://doi.org/10.1021/acs.jmedchem.4c01578>



Read Online

ACCESS |



Metrics & More

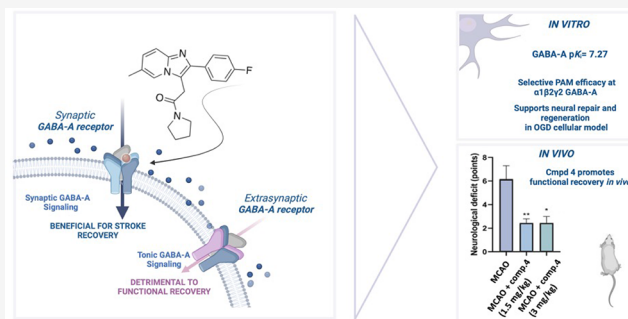


Article Recommendations



Supporting Information

ABSTRACT: Selective enhancement of synaptic GABA signaling mediated by GABA-A receptors has been previously reported to promote functional recovery after ischemic stroke, while tonic GABA signaling has been detrimental. To identify agents that enhance synaptic signaling, we synthesized GABA-A ligands based on three chemotypes with affinity values $pK_i = 6.44$ – 8.32 . Representative compounds showed a preference in functional responses toward synaptic type of GABA-A receptors, compared to the extrasynaptic ones. In a cellular ischemia model (OGD), selected compounds showed the potential to improve neuronal recovery. The selected lead, compound 4, demonstrated the ability to reduce mitochondrial dysfunction, regulate intracellular calcium levels, decrease caspase 3 levels, and promote neurite outgrowth in *in vitro* assays. In an animal model, compound 4 enhanced motor recovery and showed neuroprotective activity by reducing infarct volume and decreasing poststroke acidosis. These findings underscore the value of selective ligands modulating synaptic GABA-A receptors in promoting recovery from ischemic stroke.



INTRODUCTION

Ischemic stroke causes a significant burden on society due to almost 5.9 million deaths each year and approximately 102 million long-term disabilities among stroke survivors.^{1,2} Stroke typically disrupts motor systems, rendering half of stroke survivors permanently disabled, with a third dependent on others for everyday activities.³ To date, physical rehabilitation remains the gold standard intervention for stroke survivors to reduce functional disability,⁴ as there are no effective pharmacological treatments available to promote recovery after stroke.⁵ This highlights the need to develop effective pharmacological strategies promoting recovery from stroke and stroke related dysfunctions.

One of the characteristic hallmarks of postischemic injury is a pathological increase in tonic GABAergic currents, a form of GABAergic neurotransmission mediated by extrasynaptic GABA-A receptors (GABA-AR).⁶ It has been demonstrated that tonic GABA signaling, by changing neuronal excitability and plasticity, delays functional recovery from stroke.^{6,7} However, GABA signaling may also play a beneficial role in recovery. Synaptic-type of GABA-A receptors that modulate cortical map boundaries in the normal brain,⁸ also facilitates poststroke

recovery.⁹ Experimental studies revealed that selective, acute potentiation of synaptic GABA transmission, has been found to promote stroke-induced cortical remapping and neuronal healing, a process vital for brain repair and functional recovery.^{9,10} In addition, GABA-A receptor-mediated synaptic signaling promotes neuronal healing by facilitating neurite growth and adult neurogenesis,^{10–14} adding another layer of contribution to poststroke brain repair.^{9,15,16}

It is essential to note that the pentameric ion channels that build the GABA-A receptors differ in their subunit architecture. The subpopulation of receptors involved in restorative synaptic currents is localized within the synaptic cleft and predominantly consists of $\alpha 1$ – 3 subunits,^{17,18} The GABA-A receptors situated extrasynaptically, that mediate tonic GABA currents largely

Received: July 10, 2024

Revised: November 25, 2024

Accepted: December 6, 2024

consist of $\alpha 5$ subunit-containing receptors.^{19–21} These tonically active extrasynaptic $\alpha 5$ -GABA-A receptors have been shown to be deleterious to stroke recovery (Figure 1).^{6,22} Studies in

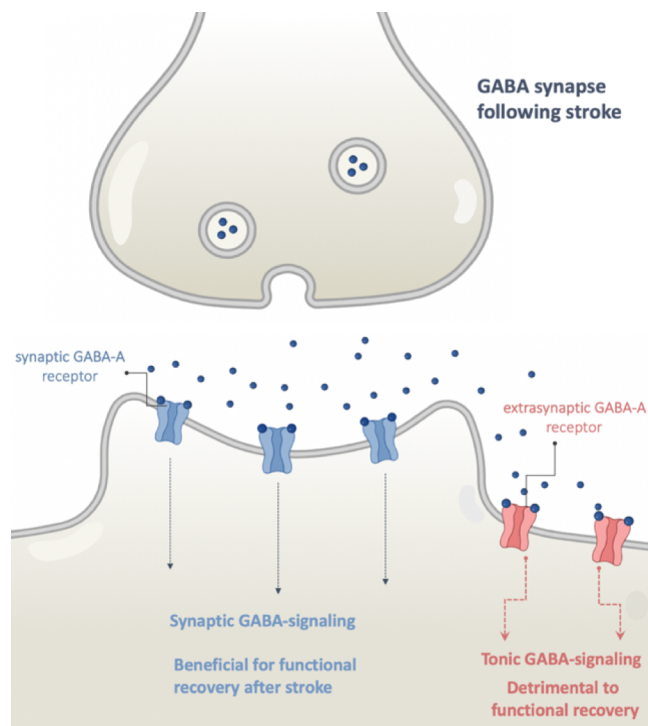


Figure 1. Simplified illustration of poststroke pathology. Stroke leads to pathologically raised tonic GABA signaling in the peri-infarct zone. Raised tonic GABA signaling, mediated mainly by $\alpha 5$ GABA-AR was found to suppress brain repair after stroke.⁶ In contrast, selective, acute enhancement of synaptic (phasic) GABA signaling was found to be beneficial for functional recovery after ischemic stroke.⁹

animal models have shown that genetic or pharmacological blockade of $\alpha 5$ -GABA-A receptors improves recovery, indicating that tonic GABAergic signaling is detrimental to functional recovery from stroke.^{6,22} These findings also suggest a potential pharmacological intervention to reduce altered tonic signaling and improve poststroke recovery using $\alpha 5$ GABA-A antagonists or negative allosteric modulators (NAMs).^{9,23,24} While this concept showed promising results in animal experiments, it failed to yield clinical benefit and did not translate successfully into clinical application.²⁵ Moreover, blockade of $\alpha 5$ GABA-A receptors proved challenging due to the limited therapeutic time window, as blocking these receptors too early after stroke may exacerbate excitotoxicity, leading to increased neuronal damage rather than aiding recovery.⁶ These features make $\alpha 5$ GABA-A receptors a less favorable target for stroke recovery.²⁵

Alternative strategy to promote GABA-mediated stroke recovery is through the selective potentiation of synaptic GABA-A currents which in animal models has been shown to promote poststroke plasticity-related recovery and improve overall functional outcomes.⁹ Notably, numerous case reports have demonstrated that treatment with low, sub-sedative doses of the FDA-approved drug zolpidem, which exhibits preferential positive allosteric modulatory properties at synaptic $\alpha 1$ -GABA-A receptors, improves brain function in stroke patients and reverses stroke-related symptoms.^{26–28} Moreover, in contrast to the $\alpha 5$ GABA-A receptor NAMs strategy, modulation of $\alpha 1$ -GABA-A mediated transmission offers a broader therapeutic

window for intervention, ranging from 1-h postreperfusion to several days after stroke.⁹ However, currently there are few compounds selective for synaptic-type GABA-A receptors with high affinity for $\alpha 1$ subtypes that do not interact with $\alpha 5$ GABA-A,^{29,30} as previous research in the field has mainly focused on the development of $\alpha 1$ -sparing, $\alpha 2/3$ PAMs for the treatment of anxiety and other disorders,³¹ or selective $\alpha 5$ NAMs for cognitive dysfunctions.^{32,33}

Herein we describe our efforts toward identifying GABA-AR ligands selective for synaptic GABA-A receptors, with a preference for the $\alpha 1$ synaptic subpopulation while sparing extrasynaptic $\alpha 5$ -GABA-AR. From the library of two distinct chemotypes, we selected the most promising compound 4, which exhibited pronounced functional efficacy at $\alpha 1$ GABA-A receptors, a favorable ADMET profile, and the ability to enhance neuronal regeneration in *in vitro* studies, as well as promote functional recovery in an animal model of stroke.

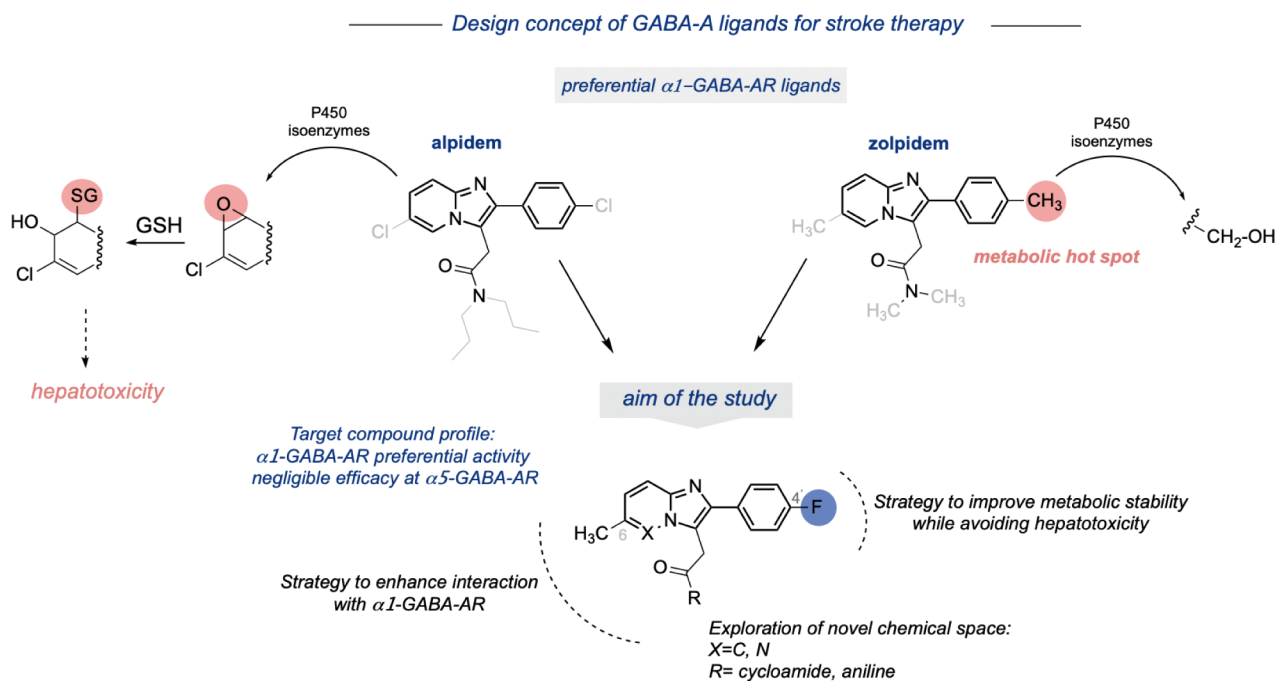
RESULTS AND DISCUSSION

Design of GABA-A Ligands for Poststroke Recovery.

There is a large body of historical literature focused on identifying various GABA-A ligands with diverse functional profiles.³³ Most studies have concentrated on developing $\alpha 2/3$ functionally selective ligands that spare the $\alpha 1$ subunit, as $\alpha 1$ activity has been associated with unwanted sedation in clinical settings.³⁴ This has led to the identification of only a few compounds with high preferential activity for $\alpha 1$, such as zolpidem, alpidem, and CL 218,872.^{29,30} However, zolpidem was found to be rapidly metabolized, resulting in a poor pharmacokinetic profile, with a half-life of 30 min in rats^{35,36} and 2–3 h in humans.³⁷ In fact, the stroke recovery-promoting effects of zolpidem in patients were transient, lasting only 2–3 h, which can be attributed to its short pharmacokinetic profile.^{26,38} Alpidem, an anxiolytic drug, had to be withdrawn from the market due to severe hepatotoxicity,³⁹ while the research compound CL 218,872 does not display an ideal functional selectivity profile.⁴⁰ Although it shows high affinity for $\alpha 1$ receptors, it also interacts with $\alpha 5$ GABA-A receptors at higher concentrations, which may pose a risk to stroke patients. Additionally, alternative studies in the field have identified selective antagonists or NAMs for the $\alpha 5$ GABA-A receptor.²⁵ However, this functional activity ultimately failed to yield the desired clinical efficacy, as mentioned earlier.

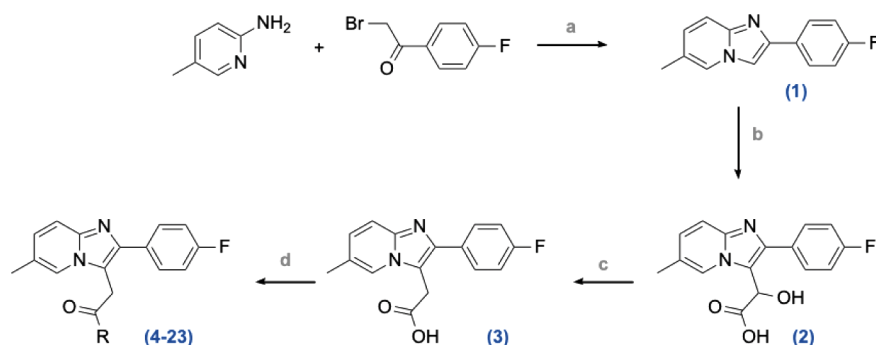
These considerations guided our decision to focus on $\alpha 1$ -preferring GABA-AR PAMs that possess negligible activity at $\alpha 5$ -GABA-A receptors and alongside an appropriate pharmacokinetic profile and no hepatotoxicity. We reasoned that this subunit functional profile would be well-suited for stroke patients, based on evidence from preclinical studies and clinical case reports. Although $\alpha 1$ -preferring GABA-A receptor compounds typically induce sedation in the noninjured brain in clinical settings, their response in stroke patients^{41,42} and animal models of experimental stroke predominantly results in enhanced motor function at low doses.^{9,43} This feature has been attributed to a widespread reorganization of neuronal circuits related to stroke and compensatory increased numbers of $\alpha 1$ receptor subunit-containing GABAergic synapses in the specific cortical areas.⁹ Moreover, typical side effects associated with the chronic use of drugs acting on $\alpha 1$ GABA-AR were not reported in various case studies of patients with brain injuries and associated motor dysfunction who were treated with long-term zolpidem.^{26,41}

Scheme 1. Design Concept of GABA-A Ligands for Stroke Therapy, Incorporating Previous Literature Data

Table 1. Binding Affinities of Series I Compounds for GABA-A Receptors^a and hERG Channel^b

Compd	R	GABA-A pK_i	hERG pIC_{50}	Compd	R	GABA-A pK_i	hERG pIC_{50}
4		7.27 ± 0.21	4.52 ± 0.08	14		7.08 ± 0.13	5.32 ± 0.08
5		6.70 ± 0.11	4.56 ± 0.08	15		6.66 ± 0.09	4.55 ± 0.07
6		6.75 ± 0.10	4.72 ± 0.09	16		7.02 ± 0.12	4.96 ± 0.08
7		7.37 ± 0.17	4.58 ± 0.07	17		7.31 ± 0.15	5.30 ± 0.10
8		7.79 ± 0.12	4.22 ± 0.08	18		6.44 ± 0.13	4.87 ± 0.10
9		7.37 ± 0.25	4.70 ± 0.07	19		7.36 ± 0.13	4.86 ± 0.10
10		7.66 ± 0.21	4.94 ± 0.06	20		7.99 ± 0.14	5.61 ± 0.11
11		7.93 ± 0.16	5.24 ± 0.10	21		7.19 ± 0.12	4.76 ± 0.09
12		6.95 ± 0.17	4.70 ± 0.06	22		6.50 ± 0.10	7.66 ± 0.10
13		6.80 ± 0.11	5.06 ± 0.07	23		6.70 ± 0.10	4.69 ± 0.09
Verapamil			6.28 ± 0.10	Zolpidem		7.18 ± 0.09	4.43 ± 0.09
				Diazepam		8.25 ± 0.11	4.45 ± 0.07

^aBinding affinity values are presented as pK_i (i.e., $-\log K_i$) and are reported as mean \pm SEM, derived from a minimum of three independent experiments achieved in duplicate. ^bhERG inhibition was determined in CHO cells stably expressing the human hERG potassium channel (Kv11.1) with the use of an automated patch clamp platform.

Scheme 2. Synthesis of Series I Compounds^a

^a(a) NaHCO₃, toluene, 100 °C, microwave, 1 h (91%), (b) glyoxylic acid, DCM, 45 °C, 16 h (quantitative yield), (c) Pd/C, HCOOH, 100 °C, 16 h (93%), (d) amine, CDI, THF, 40 °C, 12 h (19–82%).

In the design of GABA-A ligands, we employed a knowledge-based strategy to guide the selection of key structural elements, ensuring optimal interaction with the α/γ binding site of the receptor. The majority of ligands exhibiting high efficacy at $\alpha 1$ GABA-A receptors reported to date typically bind to the allosteric site of GABA-A receptors, defined between the α and γ subunits.^{44,45} These positive allosteric modulators (PAMs) share a 2-phenylimidazo[1,2-*a*]pyridine core as a privileged scaffold; therefore, we adopted this as our initial template.^{46,47} To confer the necessary interaction with the $\alpha 1$ and $\gamma 1-3$ subunits of the GABA-A receptor, highly active ligands contain methyl or chlorine substituents located at the 4' and 6 positions of the 2-phenylimidazo[1,2-*a*]pyridine core. However, the pendant methyl groups as found in zolpidem, have been identified as metabolic hotspots, making them vulnerable to CYP-mediated oxidation,³⁶ resulting in a poor half-life of approximately 30 min in rats and 2–3 h in humans (Scheme 1). On the other hand, placing a chlorine atom, as in alpidem, reduces metabolic clearance but simultaneously directs metabolism toward the formation of a reactive epoxide intermediate in the chloroimidazopyridine ring, leading to glutathione depletion and leads to acute liver toxicity in patients.^{39,48}

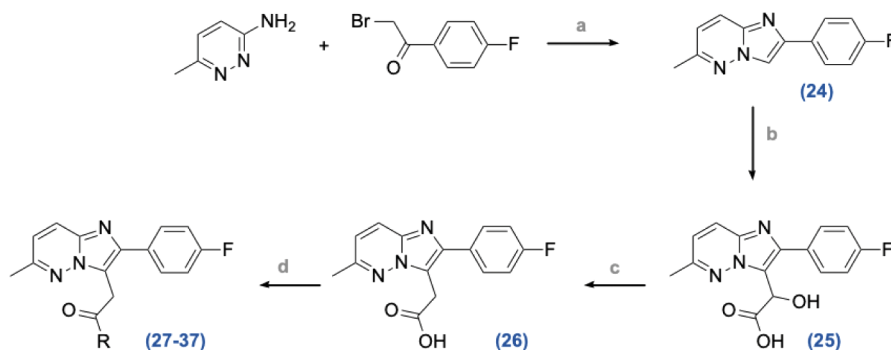
Therefore, to prevent the formation of reactive arene oxide on the imidazopyridine ring while maintaining a scaffold with optimal metabolic stability, we applied single-site fluorination at the most sensitive position—specifically the 4' position of the phenyl ring.^{49,50} Unlike alpidem, the 2-(4-fluorophenyl)-6-methylimidazo[1,2-*a*]pyridine ring is not subjected to oxidation on the imidazopyridine ring, preventing the formation of an arene oxide, as the most sensitive 4' position is blocked by a fluorine atom.⁴⁹

The second site of modifications were centered on introducing various cyclic amine and aniline-based moieties within the amide tail (Scheme 1 and Table 1). This strategy was guided by prior studies showing that large amine-containing groups at the amide moiety interact favorably with the binding pocket at the $\alpha 1/\gamma 2$ interface, enhancing receptor interaction and potentially leading to greater positive allosteric modulation (PAM) activity.⁴⁹ Moreover, in contrast to alkyl amide substituents, which tend to undergo rapid hydroxylation during hepatic metabolism, cyclic amide moieties have demonstrated greater stability.^{36,49} To conduct extensive structure–activity relationship studies around the amide terminal, we selected various substituents, with the selection based on synthetic feasibility, as well as compliance with Lipinski's Rule of 5 and

CNS MPO scores⁵¹ (refer to Table S1). An initial set of 20 designed molecules (Series I) was subsequently subjected to chemical synthesis and radioligand binding studies (Scheme 1 and Table 1).

Synthesis and Structure–Activity Relationships of Series I. The imidazo[1,2-*a*]pyridine series I library was synthesized utilizing a four-step protocol, starting with the condensation of commercially available 5-methylpyridin-2-amine with 2-bromo-1-(4-fluorophenyl)ethan-1-one, to yield the core structure 1 (Scheme 2). Subsequent functionalization of 2-(4-fluorophenyl)-6-methylimidazo[1,2-*a*]pyridine (1) with glyoxylic acid at the 3 position gave α -hydroxyacetamide precursor (2), which was then dehydroxylated in the presence of Pd/C and HCOOH to give intermediate acid (3). The final compounds (4–23) were synthesized by reacting the acid (3) with the corresponding amines in the presence of 1,1'-carbonyldiimidazole (CDI) in THF. In the first-line experiments, we screened all the synthesized compounds for their affinity for GABA-A receptors through a competitive radioligand binding study using [³H]flunitrazepam (Table 1).

The obtained p*K*_i values were ranging from 6.44 to 7.99. Among the aliphatic amides in series I, the highest p*K*_i values were observed for compounds bearing a piperazine ring (7, p*K*_i = 7.37) and a pyrrolidine ring (4, p*K*_i = 7.27) both being at a similar level to the reference drug zolpidem (p*K*_i = 7.18). Introduction of a morpholine (5, p*K*_i = 6.70) or a thiomorpholine (6, p*K*_i = 6.75) ring impaired the affinity, relative to the pyrrolidine analogue (4). Placing a phenyl ring in the amide side chain yielded compound 8, which demonstrated enhanced affinity for GABA-A receptor (p*K*_i = 7.79) in comparison to compound 4. Next, we evaluated how the introduction of substituents within the phenyl ring impacts affinity, using commonly employed substituents such as F, Cl, Me, OCH₃, and CF₃. In general, introduction of a substituent in the *para* position was well tolerated, with compounds bearing *para*-methoxy (20, p*K*_i = 7.99) and *para*-fluoro (11, p*K*_i = 7.93) moieties, displaying the highest p*K*_i values within series 1. On the other hand, introduction of a substituent at the *ortho* position of the phenyl ring decreased the affinity for GABA-A receptor, relative to the aniline analogue (8). This effect was particularly pronounced with the *ortho*-methoxy derivative (18, p*K*_i = 6.44) and the *ortho*-methyl analogue (15, p*K*_i = 6.66). Among compounds with substituents at the *meta* position, a modest decrease in affinity in comparison to 8, was observed for the *meta*-fluoro derivative (10, p*K*_i = 7.66) and the *meta*-methoxy analogue (19, p*K*_i = 7.36). Introduction of a trifluoromethyl group at the *meta*

Scheme 3. Synthesis of Series II Compounds^a

^a(a) NaHCO₃, toluene, 110 °C, 12 h (67%), (b) glyoxylic acid, DCM, 60 °C, 12 h (43%), (c) PPh₃, I₂, toluene, 100 °C, 12 h (52%), (d) TBTU, DIPEA, DCM, 30 °C, 5 min microwave (23–71%) (Method B).

position of the phenyl ring led to a significant decrease in affinity (22, p*K*_i = 6.50) comparing to 8.

Given that stroke survivors represent a specific group of patients who often suffer from various cardiovascular diseases,^{52,53} we reasoned that derisking the new potential pharmacological agents in terms of potential pro-arrhythmia properties should be of high priority. Inhibition of hERG channels may result in the prolongation of the QT interval, thereby increasing the risk of arrhythmias and sudden cardiac death, a particularly dangerous outcome for stroke survivors.⁵⁴ That being said, the novel compounds should be devoid of significant interaction with the hERG channel. The entire set of compounds was evaluated for hERG interaction to select those with the lowest potential risk of cardiotoxicity (Table 1). The majority of compounds exhibited low hERG pIC₅₀ values (pIC₅₀ < 5, IC₅₀ > 10 μM), similarly to the zolpidem (pIC₅₀ = 4.43). The only exception was compound 22, with a pIC₅₀ of 7.66, falling below the 10 μM cutoff value.^{55,56} Therefore, compound 22 was excluded from further investigation. For the remaining set of compounds, we calculated the difference in affinity between the GABA-A receptor and hERG. This value exceeded 2 (*K*_i difference >100-fold) for the majority of ligands, suggesting that the difference between the affinity for the GABA-A receptor and the hERG channel is sufficiently high⁵⁵ to advance these molecules for further evaluation. Compounds which did not meet these criteria included derivatives with *meta*- and *para*-chlorophenyl moieties (13, 14), *para*-methyl (17), and *ortho*-methoxy substituents (18), where the difference fell below 2. Hence, these derivatives, along with compound 22, were omitted from further investigations.

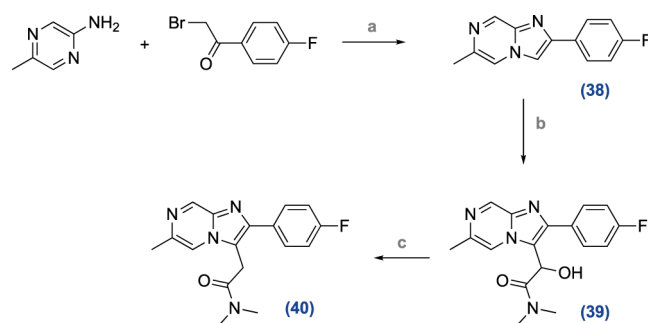
Structure–Activity Relationships. Series II and III.

Having established the SAR around the 2-(4-fluorophenyl)-6-methylimidazo[1,2-*a*]pyridine scaffold in series I, follow-up studies involved exchanging the imidazo[1,2-*a*]pyridine core with various aza bioisosteres, as altering the nitrogen placement within the heterocyclic core or adding an extra nitrogen to the core has previously been shown to influence the subtype selectivity of GABA-A receptor ligands.^{57,58} Based on these considerations, we chose to explore the 2-(4-fluorophenyl)-6-methylimidazo[1,2-*b*]pyridazine (series II) and 2-(4-fluorophenyl)-6-methylimidazo[1,2-*a*]pyrazine (series III) scaffolds, replacing the prototype imidazo[1,2-*a*]pyridine core while retaining selected cycloamide and aromatic amide moieties that contributed to the high affinity observed in series I.

Using a method analogous to that employed for series I, the core structure of series II: 2-(4-fluorophenyl)-6-methylimidazo-

[1,2-*b*]pyridazine (24), was obtained through the condensation of 3-amino-6-methylpyridazine with 2-bromo-4'-fluoroacetophenone (Scheme 3). Subsequently, the intermediate (24) was reacted with glyoxylic acid in dichloromethane to incorporate an aliphatic chain at the 3-position, yielding 2-[2-(4-fluorophenyl)-6-methylimidazo[1,2-*b*]pyridazin-3-yl]-2-hydroxyoctanoic acid (25). Dehydroxylation of intermediate (25) in the presence of PPh₃ and I₂, delivered the acid (26), which was further converted to the final amines (27–37) using TBTU, DIPEA in DCM. A representative compound from series III, compound 40 was prepared in a three-step synthesis (Scheme 4).

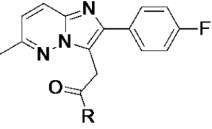
Scheme 4. Synthesis of a Representative Compound^a



^a(a) NaHCO₃, acetonitrile, reflux, 12 h (56%), (b) *N,N*-dimethyl-2-oxoacetamide, CH₃COOH, 65 °C, MW, 1 h, (39%), (c) PBr₃, THF, 45 °C, MW, Na₂CO_{3(aq)}.

Condensation between 5-methylpyrazin-2-amine and 2-bromo-1-(4-fluorophenyl)ethan-1-one gave core structure (38), which was next reacted with *N,N*-dimethyl-2-oxoacetamide to afford key intermediate (39). The final compound (40) was obtained by dehydroxylation in the presence of phosphorus tribromide as previously reported.⁵⁹

Within series II, we observed that compounds bearing cycloamide substituents at the amide site (27, 28, 29, 30) exhibited higher activity, with p*K*_i values ranging from 7.21 to 8.22 (Table 2), in comparison to the aromatic derivatives (31–37, p*K*_i = 6.36–6.98). The most active analogue in this series was compound 30, bearing a thiomorpholine ring (p*K*_i = 8.43) and a pyrrolidine ring (p*K*_i = 8.32), surpassing the reference drug zolpidem (p*K*_i = 7.18) and approaching the affinity of diazepam (p*K*_i = 8.25), a high-affinity but nonselective GABA-A binder. Introduction of an aniline ring resulted in reduced affinity for GABA-A receptor (31, p*K*_i = 6.85), as compared to the

Table 2. Binding Affinities of Series II Compounds for GABA-A Receptors^a and hERG Channel^{b,c}


Compd	R	GABA-A pK _i	hERG pIC ₅₀	Compd	R	GABA-A pK _i	hERG pIC ₅₀
27		7.21 ± 0.20	4.46 ± 0.09	33		6.70 ± 0.14	4.69 ± 0.09
28		8.32 ± 0.20	4.44 ± 0.08	34		6.70 ± 0.14	4.54 ± 0.08
29 ^c		7.44 ± 0.16	4.79 ± 0.09	35		6.36 ± 0.12	4.37 ± 0.08
30		8.43 ± 0.20	4.37 ± 0.07	36		6.76 ± 0.11	4.56 ± 0.09
31		6.85 ± 0.14	4.60 ± 0.08	37		6.98 ± 0.13	4.81 ± 0.10
32		6.55 ± 0.16	4.57 ± 0.08	Zolpidem		7.18 ± 0.09	4.43 ± 0.09
Verapamil			6.28 ± 0.10	Diazepam		8.25 ± 0.11	4.45 ± 0.07

^aBinding affinity values are presented as pK_i (i.e., $-\log K_i$) and are reported as mean ± SEM, derived from a minimum of three independent experiments achieved in duplicate. ^bhERG inhibition was determined in CHO cells stably expressing the human hERG potassium channel (Kv11.1) with the use of an automated patch clamp platform. ND—not active. Blank spaces—not tested. ^cCompound 29 has been reported previously, however, no K_i data regarding its affinity toward GABA-A or its ADMET profile are available. Therefore, it was resynthesized in our study and investigated in terms of *in vitro* pharmacology and SAR studies.⁵⁸

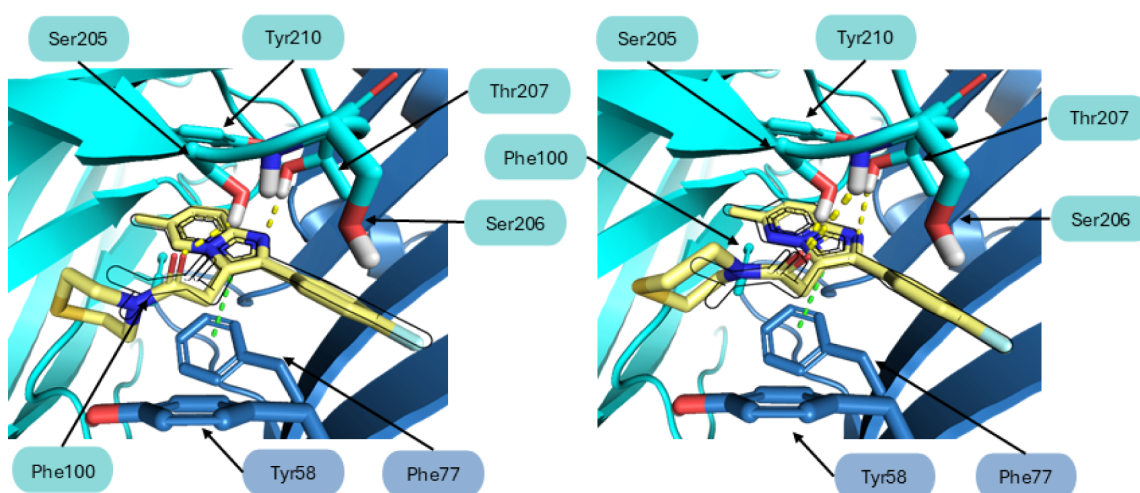


Figure 2. Predicted interaction modes of compounds 6 and 30 with the $\alpha 1\beta 2\gamma 2$ GABA-A receptor (PDB: 8DD2) at the benzodiazepine binding site. The $\alpha 1$ -subunit is marked in cyan and the $\gamma 2$ in dark blue, with interacting amino acids represented by sticks. Yellow dots indicate hydrogen bonds and green represents aromatic interactions, including both CH- π and π - π . The black outline shows the arrangement of the reference molecule—Zolpidem.

thiomorpholine analogue (30, pK_i = 8.43). The introduction of substituents around the phenyl ring did not improve affinities, as pK_i values ranged from 6.80 to 6.20. Replacement of the 2-(4-fluorophenyl)-6-methylimidazo[1,2-*b*]pyridazine template with the 2-(4-fluorophenyl)-6-methylimidazo[1,2-*a*]pyridazine core in series III proved detrimental to GABA-A receptor affinity, as representative compound 40 exhibited no affinity (GABA-A pK_i = N.D.).

In line with our investigations on compounds within series I, we also assessed the pIC₅₀ values for hERG in Series II. The inhibitory potency of the series II compounds remained below

the 10 μ M (pK_i < 5) cutoff. The calculated differences in affinity between the GABA-A receptor and hERG, for the majority of molecules, surpassed 2 orders of magnitude, indicating a substantial separation in affinity of the tested compounds for GABA-A receptor and the hERG channel. However, three compounds (32, 33 and 35) failed to meet these criteria and were consequently excluded from any further investigations.

The Molecular Modeling Investigation. According to the structure–activity relationships (SAR), the 2-phenylimidazo[1,2-*b*]pyridazine derivatives bearing cycloamine at the amide backbone exerted higher binding affinities compared to their

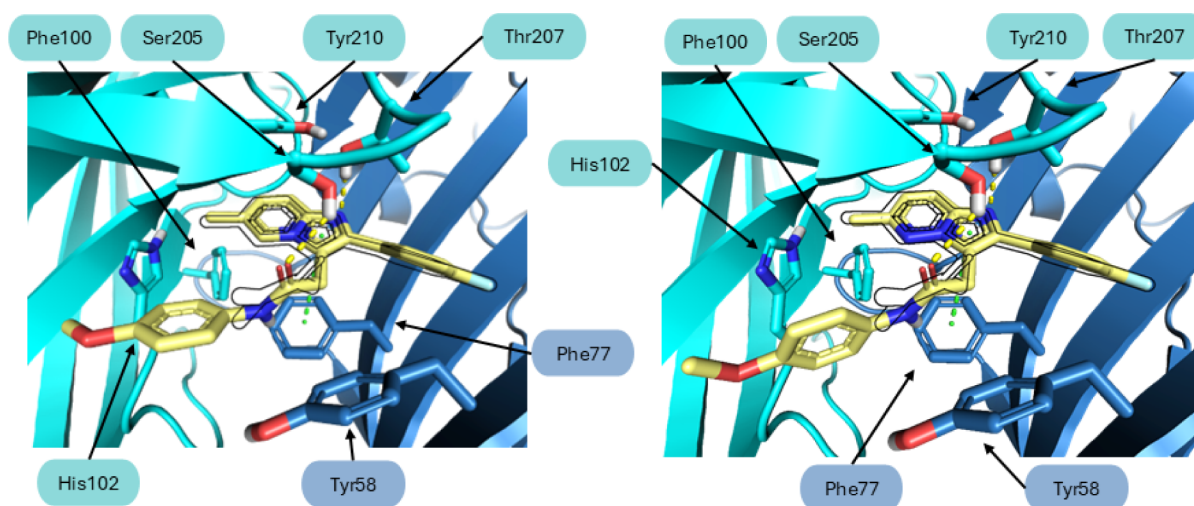


Figure 3. Predicted interaction modes of compounds **20** and **37** with the GABA-A receptor (PDB: 8DD2) at the benzodiazepine binding site. The $\alpha 1$ -subunit is marked in cyan and the $\gamma 2$ in dark blue, with interacting amino acids represented by sticks. Yellow dots indicate hydrogen bonds and green represents aromatic interactions, including both CH- π and π - π . The black outline shows the arrangement of the reference molecule—Zolpidem.

imidazo[1,2-*a*]pyridine counterparts. For example compound **30**, a thiomorpholine derivative from series II—imidazo[1,2-*b*]pyridazine, exhibited an approximately 10-fold change in potency ($pK_i = 8.43 \pm 0.20$ for **30**) compared to its imidazo[1,2-*a*]pyridine counterpart, compound **6** ($pK_i = 6.75 \pm 0.10$). The observed differences in the potency of series I and series II ligands prompted us to elucidate the underlying factors influencing their activity of compounds in these series through computational studies. As a reference point, we used cryo-EM structure of a human $\alpha 1/\beta 2/\gamma 2$ GABA-A receptor subtype complex bound with GABA and Zolpidem (PDB: 8DD2).⁶⁰ The results indicate that zolpidem has the potential to bind to both the traditional binding pocket at $\alpha 1/\gamma 2$ extracellular domain (ECD) and two general anesthetic-binding pockets found between the $\beta 2/\alpha 1$ transmembrane domain (TMD) interfaces. While the role of the $\alpha 1/\gamma 2$ ECD site in GABA-A modulation has been well described, the functional role of $\beta 2/\alpha 1$ TMD sites in the case of zolpidem are not yet fully understood. Moreover, the conservation of the amino acids involved in zolpidem interactions at the TMD $\beta 2/\alpha 1$ interfaces among α subunits suggests that they do not play a significant role in subtype selectivity. Consequently, our research efforts were concentrated on analyzing the disparities in binding modes exhibited by the investigated ligands within the $\alpha 1/\gamma 2$ ECD site. The docking poses of selected ligands at the TMD $\beta 2/\alpha 1$ site were also documented and can be found in Figure S12. The predicted binding mode of compounds **6** and **30** in with the $\alpha 1/\gamma 2$ ECD site of GABA-A receptor revealed that their binding poses resembled those of the confirmed position of zolpidem in the analyzed cryo-EM structure of the $\alpha 1/\beta 2/\gamma 2$ GABA-A receptor, particularly in terms of the arrangement of the heterocyclic systems. Both compounds **6** and **30** demonstrated a strong preference for aligning the amide fragment parallel to the aromatic ring of Tyr58. This preferred orientation of the aromatic system of Tyr58 and the carbonyl group might indicate the occurrence of lp- π type interactions.^{61,62} The key difference in binding modes that possibly explains the differences in pK_i activities between compounds **6** and **30** is that the presence of nitrogen atom in the 2-phenylimidazo[1,2-*b*]pyridazine derivatives allows for the alignment of the carbonyl group with polar amino acids (Ser205 and Ser206) in loop C. The pose acquired

for imidazo[1,2-*a*]pyridine derivative (**6**), shown in Figure 2, suggests potential difficulties in achieving an ideal fit due to the very close proximity of protons between the aromatic system and the heterocyclic substituent (ranging from 2.23 to 2.97 Å). Overall, these differences in binding modes may explain the variations in experimental pK_i values.

For molecules bearing aromatic rings at the amide moiety, radioligand binding studies indicated a contrary trend. Compounds within series I, featuring imidazo[1,2-*a*]pyridine scaffold, tended to show greater potency compared to their 2-phenylimidazo[1,2-*b*]pyridazine analogues. Specifically, a 4-methoxyaniline derivative from series I (compound **20**) demonstrated 10-fold higher potency compared to its 2-phenylimidazo[1,2-*b*]pyridazine counterpart, compound **37**. Yet, the docking studies revealed no significant differences in the binding modes of these two molecules, as both compounds exhibited similar arrangements with only minor variations (Figure 3). The arrangement of the bicyclic systems of **20** and **37** were similar to cycloamide derivatives (**6** and **30**) and the reference drug zolpidem in the cryo-EM complex. We observed analogous preference for aligning the amide fragment parallel to the aromatic ring of Tyr58, which can be explained by lp- π interactions. Both compounds formed aromatic interactions with Phe77 and hydrophobic interactions with Phe100 and Tyr210 and hydrogen bonds formed between the compounds and Ser205 and Thr207 of the $\alpha 1$ -subunit of the GABA-A receptor. The sole difference was observed in the binding mode of compound **20**, where the aromatic part of *N*-phenylacetamide engaged in aromatic CH- π interactions with His102 (Figure 3). However, these minor variations in binding modes between compounds **20** and **37** may not substantially influence the differences in compound potencies.

We suspected that there might be a difference in the energetically favorable conformation of the ligands in their unbound state that may account for the overall differences in their affinity, prior to interacting with the $\alpha 1/\beta 2/\gamma 2$ GABA-A receptor. Therefore, we used a quantum-mechanical (QM) approach known as GFN2-xTB and ULYSSES tool:⁶³ to calculate the favorable conformation in the unbound state of compounds **20** and **37**. The analysis revealed that in the unbound state, there are key differences between the two

molecules. The 2-phenylimidazo[1,2-*b*]pyridazine analogue, compound **37**, forms an intramolecular hydrogen bond between the nitrogen atom of the pyrimidine ring and the amide group (Figure 4) that is not observed in the imidazo[1,2-*a*]pyridine

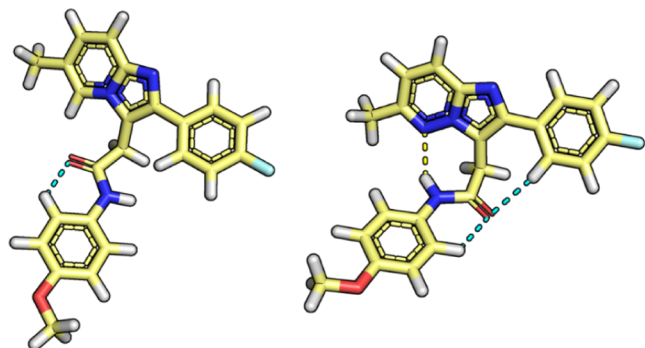


Figure 4. Comparison of QM-optimized analogs **20** and **37**. Yellow dashed lines represent hydrogen bonds, while aromatic hydrogen bonds are marked in cyan.

series (**20**). The stability of this molecular arrangement in which the molecule forms intramolecular hydrogen bond is enhanced by the presence of aromatic hydrogen bonds formed by the *N*-(3-methoxyphenyl)acetamide fragment. The analysis shows that aromatic amides are particularly prone to the formation of intramolecular hydrogen bonds because the conformation is stabilized by the additional aromatic interactions.

In this scenario, we can assume that the disruption of intramolecular hydrogen bonds upon ligand binding to a protein may incur significant energetic costs. The energy required to break these bonds necessitates compensation through interactions formed at the receptor binding site. If the energy gained from forming new interactions with the protein does not sufficiently offset the energy required to break the intramolecular bonds, the overall binding affinity might be lower.

In order to estimate the deformation energy, further computational experiments were carried out. This energy is defined as the difference in energy between the protein–ligand complex pose and the energetically optimal conformation of the

free ligand with the observed hydrogen bond. Compound **37** exhibited a deformation energy of 17.92 kcal/mol, indicating high energetic penalty resulting from the breaking of the internal hydrogen bond during binding. The ΔE_{def} between ligands **20** and **37** is 1.56 kcal/mol, favoring compound **20**, which indicates its higher shape complementarity with the GABA-A binding site. This phenomenon could explain the differences in binding affinities observed in experimental pK_i values of **20** and **37** despite similar binding modes at the $\alpha 1\beta 2\gamma 2$ GABA-A receptor.

GABA-A Functional Studies. Numerous literature reports have demonstrated that selecting compounds based solely on binding affinity is challenging and often does not translate into pharmacological efficacy in *in vivo* models.^{64,65}

Efforts to optimize functional selectivity rather than binding affinity have ultimately proved successful, leading to the identification of a broad range of both clinical and preclinical compounds.³³ Therefore, we focused on functionally selective PAMs rather than binding-selective ligands. Our goal was to select a compound with preferential PAM activity at $\alpha 1$ GABA-A receptors, while ensuring negligible activity at $\alpha 5$ GABA-A receptors to achieve the desired pharmacological profile for stroke treatment.^{6,9} The 10 most active compounds from series I and II, with K_i values in the range of 10^{-7} M to 10^{-8} M ($pK_i = 7-8$) were tested in the functional selectivity assay measuring PAM efficacy at synaptic ($\alpha 1\beta 2\gamma 2$, $\alpha 2\beta 3\gamma 2$, and $\alpha 3\beta 3\gamma 2$) and extrasynaptic ($\alpha 5\beta 3\gamma 2$) GABA-A receptors (Table 3). The compounds were tested at a single concentration of 10 μM , as many research groups have observed significant functional differences between GABA-A α subunits at this concentration.^{11,60,66,67} Given our particular interest in minimizing activity at $\alpha 5$ GABA-A receptors, we reasoned that selecting the 10 μM concentration would help us better distinguish even subtle differences between GABA-A subunits, especially ensuring negligible activity at $\alpha 5$ GABA-A receptors.

We observed that all the compounds exhibited a preference in functional activities toward synaptic type of ($\alpha 1-3$ containing) GABA-A receptors compared to extrasynaptic, $\alpha 5$ -GABA-A receptors. Among the tested compounds, several (**4**, **20**, **27**) exhibited negligible functional activity at $\alpha 5$ GABA-A receptors, with values ranging from 102.63% to 115.32%, closely approaching the baseline GABA response. In terms of functional

Table 3. Evaluation of Positive Allosteric Modulation (PAM) Properties for Selected Compounds at Synaptic ($\alpha 1\beta 2\gamma 2$, $\alpha 2\beta 3\gamma 2$, and $\alpha 3\beta 3\gamma 2$) and Extrasynaptic ($\alpha 5\beta 3\gamma 2$) GABA-A Receptors ($n = 2-3$)^a

Compound	% of control GABA response at $\alpha 1$ GABA-A mean \pm SEM	% of control GABA response at $\alpha 2$ GABA-A mean \pm SEM	% of control GABA response at $\alpha 3$ GABA-A mean \pm SEM	% of control GABA response at $\alpha 5$ GABA-A mean \pm SEM
4	201.4 \pm 4.41	139.80 \pm 5.97	139.10 \pm 7.07	102.63 \pm 1.80
8	163.67 \pm 6.17	166.64 \pm 3.25	218.25 \pm 7.22	163.62 \pm 1.90
9	151.4 \pm 11.85	154.52 \pm 1.59	226.53 \pm 6.93	166.39 \pm 13.97
11	204.33 \pm 12.45	155.12 \pm 15.37	178.50 \pm 12.78	133.92 \pm 0.575
20	198.33 \pm 2.33	184.20 \pm 4.96	203.44 \pm 4.40	108.17 \pm 3.37
27	145.75 \pm 9.37	153.79 \pm 6.78	203.71 \pm 15.38	115.32 \pm 1.38
28	216.33 \pm 2.33	158.04 \pm 3.42	211.40 \pm 15.86	127.38 \pm 1.65
29	175.33 \pm 15.86	200.68 \pm 17.64	200.46 \pm 11.00	130.19 \pm 0.135
30	206.67 \pm 25.33	187.43 \pm 3.97	229.60 \pm 14.02	169.88 \pm 2.11
37	143.67 \pm 3.18	150.90 \pm 3.92	232.32 \pm 5.37	148.35 \pm 2.26
Diazepam	230.0 \pm 1.1	212.67 \pm 23.00	287.57 \pm 3.47	226.56 \pm 4.61
Zolpidem ^b	180.0 \pm 14.0	132.0 \pm 4.0	121.0 \pm 3.0	102.0 \pm 2.0

^aData represent a mean \pm SEM of at least two independent measurements. The results show a fold increase in GABA-gated current amplitude after administration of the tested compounds at 10 μM , compared to the efficacy of GABA alone. Diazepam tested at 1 μM . All compounds' presented data have been normalized to the baseline peak current induced by the addition of EC₂₀ GABA. ^bEnhancement in % of control in GABA response provided according to Ramerstorfer et al.⁴⁰

activity these values can be regarded as negligible as previously stated. The observed activities were comparable to those of the reference drug zolpidem, a well-known compound recognized for its sparing activity at the $\alpha 5$ GABA-A receptor.^{40,68} The remaining compounds, such as **11**, **28**, and **29**, showed weak PAM efficacy ranging from 127.38% to 133.92%. These values were still lower than those observed for diazepam, a nonselective GABA-AR PAM, whose activity at the $\alpha 5$ -GABA-A subtype exceeds 200%.

Regarding the dominant functional responses within the synaptic subtype of GABA-A receptors, certain compounds showed a preference for $\alpha 3$ -containing GABA-A receptors, including **8** and **9** from series I and **27** and **37** from series II. The latter one also showed the highest modulatory efficacy toward $\alpha 3$, with 232.32% of the ion current. This result is somewhat surprising, as previous studies have shown that the presence of an additional nitrogen atom in the heterocyclic core shifts selectivity toward the $\alpha 1$ GABA-A subunit. However, it is important to note that this trend was observed in binding selectivity assays rather than functional assays, which may explain the differences observed in our study.

Several compounds exhibited high functional responses at $\alpha 1$ -containing GABA-A receptors, the most important subunit for stroke treatment, with PAM efficacy >198%, showing values similar to those of zolpidem. This includes a pyrrolidine (**4**) and a *para*-fluoroaniline derivative (**11**) and *para*-methoxyaniline (**20**) from series I and a pyrrolidine derivative (**28**) and thiophene (**30**) from series II. In terms of the desired functional profile—preferential activity at $\alpha 1$ with minimal activity at $\alpha 5$ GABA-AR, several compounds are particularly appealing, including compounds **4**, **11**, and **20**. Among them the most interesting functional profile was exhibited by compound **4**, showing a strong preference for $\alpha 1$ -containing receptors ($\alpha 1$ PAM = $201.4 \pm 4.41\%$) over the remaining subtypes ($\alpha 2$ PAM = 139%, $\alpha 3$ PAM = 139%, and $\alpha 5$ PAM = 102%), rendering it an $\alpha 1$ dominant GABA-AR ligand.

Preliminary Physicochemical Profiling. Alongside, the selected set of compounds was evaluated for thermodynamic solubility in PBS at pH 7.4⁶⁹ and for artificial permeability using the parallel artificial membrane permeability (PAMPA) assay,⁷⁰ both of which are critical parameters that influence permeation through biological membranes. The thermodynamic solubility of the tested compounds ranged from 0.13 ± 0.02 to >2.00 mg/mL (Table 4). According to early stage drug discovery criteria, where the goal for solubility is greater than 0.06 mg/mL, these compounds can be classified as sufficiently soluble.⁷¹ In the PAMPA assay, the permeability of tested compounds was ranging from $P_e = 1.03 \pm 0.10 \times 10^{-6}$ cm/s up to $P_e = 29.7 \pm 0.86 \times 10^{-6}$ cm/s. The highest P_e value was observed for compound **4** ($P_e = 29.7 \pm 0.86$) being close to the reference zolpidem ($P_e = 21.6 \pm 1.26$). Analyses of FDA-approved central nervous system (CNS) therapeutics have revealed a correlation where compounds with P_e values in PAMPA assay greater than 4.0×10^{-6} cm/s typically exhibit high blood-brain barrier (BBB) penetration, whereas those with P_e values less than 2.0×10^{-6} cm/s are generally indicative of poor BBB permeability.⁷⁰ The majority of tested compounds demonstrated P_e values exceeding 4.0×10^{-6} cm/s, indicating suitability for CNS-acting molecules. Solely compound **20**, with a P_e of $1.03 \pm 0.10, \times 10^{-6}$ cm/s fell below this threshold and was excluded from further investigation.

In Vitro Studies. Neuroprotection Assessment Against Experimental Ischemia. Evidence shows that, apart from

Table 4. Thermodynamic Solubility and Artificial Permeability PAMPA Assay for Selected Compounds

Compound	Permeability $P_e \pm SD$ [$\cdot 10^{-6}$ cm/s] ^a	Solubility [mg/mL] ^b
4	29.7 ± 0.86	1.87 ± 0.740
8	5.29 ± 0.07	1.61 ± 0.13
9	6.25 ± 0.28	>2.00
11	6.06 ± 0.32	0.98 ± 0.07
20	1.03 ± 0.10	0.52 ± 0.06
27	9.79 ± 2.41	>2.00
28	22.9 ± 0.2	1.21 ± 0.22
29	9.99 ± 0.78	1.59 ± 0.61
30	11.7 ± 1.3	0.32 ± 0.06
37	4.53 ± 0.43	0.13 ± 0.02
zolpidem ^c	21.6 ± 1.26	>2.00
perfenazine		0.031 ± 0.032
sulpiride	0.016 ± 0.003	
caffeine	15.2 ± 3.0	

^aDetermined using precoated PAMPA Plate System Gentest (Corning, Tewksbury, MA, USA). ^bThermodynamic solubility of tested compounds in PBS (pH = 7.4). Compounds were prepared as tartaric acid salts 1:1. Black spaces—not tested. ^cPAMPA assay performed on zolpidem tartrate.⁷²

promoting synaptic GABA neurotransmission which contributes to neuroplasticity and functional recovery,⁹ GABA-A ligands exert neuroprotective ability and support neural repair and regeneration, thereby further supporting the recovery process from stroke.⁷³ Experimental ischemia was induced by subjecting neuronal cultures (N2A cells) to the oxygen-glucose deprivation model (OGD) lasting for 4 h. Following this, the neuronal cells were restored to normoglycemic and normoxic conditions, treated with the selected compounds, and allowed for a recovery period of 24 h. Zolpidem, which has demonstrated neuroprotective efficacy in multiple assays,^{74,75} was used as the positive control and reference drug. The OGD conditions resulted in significant cell death comparing to control (Figure 5). Post ischemia treatment with tested compounds reduced cell damage, as evidenced by higher cell viability. Significant neuroprotective activity was observed for series I compounds bearing imidazo[1,2-*a*]pyridine ring, particularly the pyrrolidine (**4**), aniline (**8**) and *para*-methoxyaniline (**20**) derivatives, when administered post treatment at 10 μ M concentration (Figure 5). Among 2-(4-fluorophenyl)-6-methylimidazo[1,2-*b*]pyridazine derivatives (series II), compounds bearing dimethylamide (**27**) and tiomorpholine substituents (**30**) elicited significant neuroprotective activity at 10 μ M concentration. These neuroprotective effects were comparable to those of the reference compound zolpidem, which was active at 10 μ M. Among the active compounds, compounds **4**, **20**, and **30** are characterized by high efficacy at the $\alpha 1$ GABA-A receptor, while compounds **8** and **27** are preferential PAMs at the $\alpha 3$ GABA-A receptor, further highlighting the neuroprotective potential of $\alpha 3$ -GABA-A receptor-preferring compounds. However, the most promising activity in neural repair and regeneration was observed with compounds **4** and **20**, both of which were characterized by the desired functional profile: high efficacy at $\alpha 1$ and low efficacy at $\alpha 5$ GABA-A receptors. These molecules demonstrated neuroprotective effects when administered at a concentration of 1 μ M. It is important to note that many promising neuroprotective compounds that have shown efficacy *in vivo*, also exhibit efficacy at concentrations 1 μ M under *in vitro* OGD conditions.^{76,77} This is related to the harsh

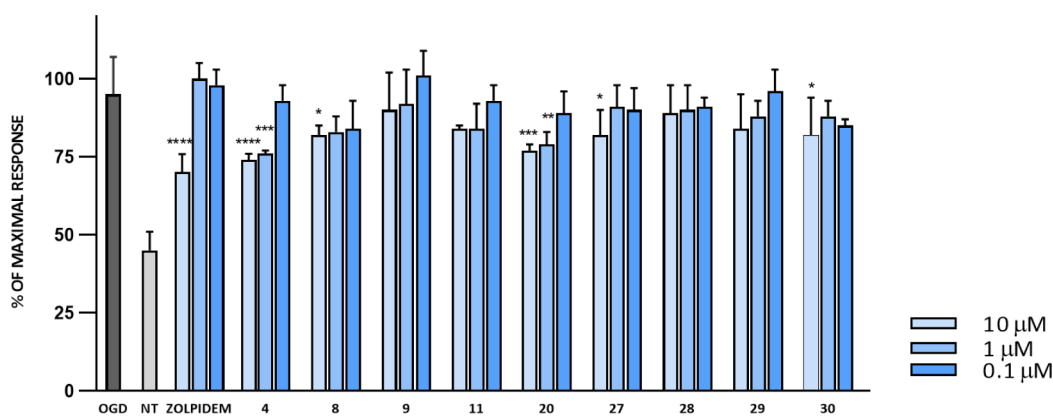


Figure 5. Neuronal death induced by OGD in N2A cells. After OGD exposure, the tested compounds at concentration 10 μM 1 μM and 0.1 μM were added. N2A cells were cultured under normoxic condition for reoxygenation for 24h. After this time the cells membrane damage was measured used multifunctional plate reader POLARstar Omega (BMG, Labtech). NT – no treated N2A cells, normal conditions without OGD. All values are expressed as mean with SD. Differences among groups were evaluated by One-Way ANOVA followed by posthoc analysis (Dunnnett's multiple comparison tests) and were considered statistically significant if $p < 0.05$ (* $p < 0.05$, ** $p < 0.01$, *** $p < 0.001$, **** $p < 0.0001$).

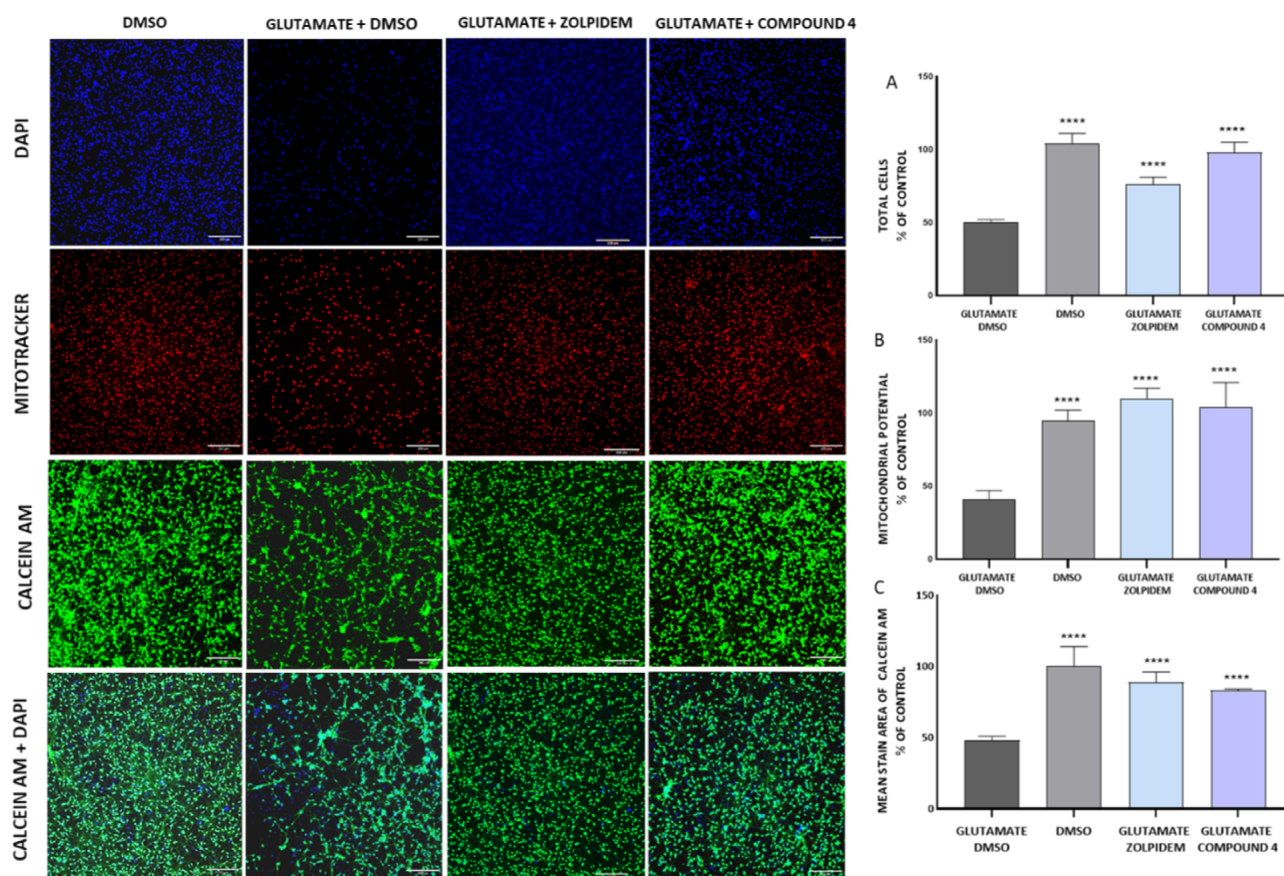


Figure 6. Representative images of neuroprotective effect of the tested compound on the iCell GABANeurons. Quantification assessed with High Content Screening (HCS). The cells were stained with (A) Hoechst 33342 to detect the nucleus (B) Mitotracker to detect mitochondrial potential (C) Calcein AM to highlight the outer membranes. The cells were pretreated with tested compound (10 μM) or vehicle (0.1% DMSO, v/v) for 1 h after this time the cells were incubated with glutamate (1 mM) for 3 h. Cells morphology assessment using a MultiWave Scoring module. The results of the experiment were imaged using 10 \times magnification with the ImageXpress Micro XLS (Molecular Devices). Scal bar: 200 μm . Statistical analysis: Way ANOVA followed by posthoc analysis (Dunnnett's multiple comparison tests), * $p < 0.05$, ** $p < 0.01$, *** $p < 0.001$, **** $p < 0.0001$.

conditions of OGD; energy deficits caused by ischemia affect ion channel activity, including GABA-A receptors, by disrupting ion pumps and leading to electrolyte imbalances,⁷⁸ which in turn necessitate higher compound concentrations for effective action.⁷⁹ Nevertheless, considering the overall pharmacological properties and physicochemical profiles of both compounds 4

and 20, compound 4 has emerged as the most promising candidate for further advanced studies.

Neuroprotective Studies of Compound 4 in GABA Neurons Derived from iPSCs. The neuroprotective activity of compound 4 was further tested in GABAergic neurons derived from induced pluripotent stem cells (iPSCs). We particularly focused

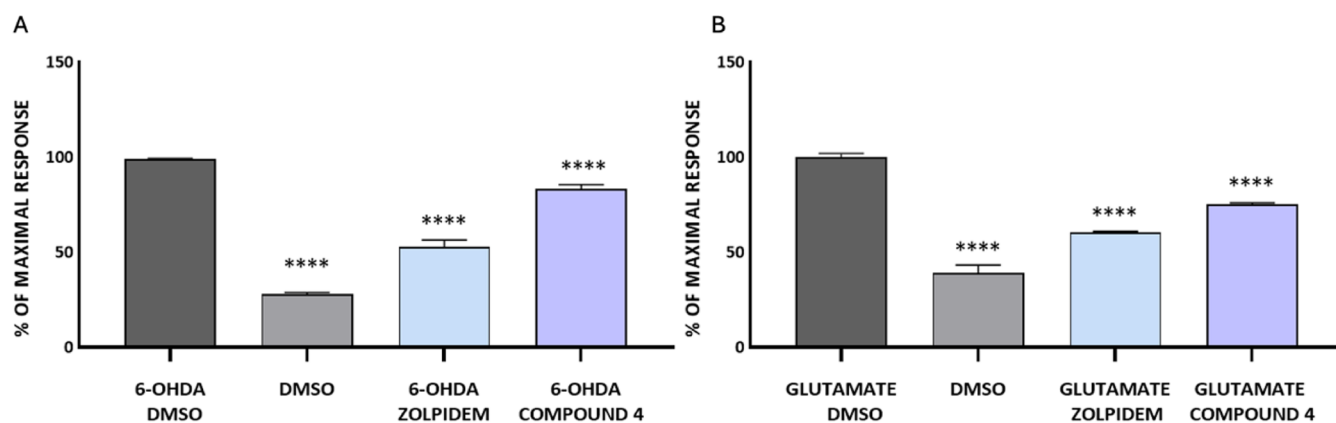


Figure 7. (A) Determination of intracellular calcium concentration. The cells were pretreated with tested compounds (10 μM) or vehicle (0.1% DMSO, v/v) for 1 h after this time the cells were incubated with glutamate (1 mM) for 3 h. Experiments were carried on with the ImageXpress Micro XLS (Molecular Devices). (B) Caspase-3/7 activity assay. After pretreatment with tested compounds (10 μM) or vehicle (0.5% DMSO, v/v) for 1 h, the cells were incubated with 6-OHDA in concentration 400 μM for 2 h. Experiments were carried on with multifunctional plate reader POLARstar Omega (BMG Labtech, Germany). Statistical analysis: Way ANOVA followed by posthoc analysis (Dunnett's multiple comparison tests), * $p < 0.05$, ** $p < 0.01$, *** $p < 0.001$, **** $p < 0.0001$.

on examining the ability of compound 4 to reduce mitochondrial dysfunction, regulate intracellular calcium levels, and decrease caspase 3 levels, as these activities have been previously associated with functional tissue repair and neuronal survival following stroke.^{80–82} The toxicity in iPSCs was induced with a high concentration of glutamate (1 mM), which resulted in cell death (Figure 6). Given that previous studies have shown that most neuroprotective compounds are active in the micromolar range under glutamate-induced toxicity assays,^{83,84} we selected 10 μM as the concentration to evaluate the efficacy of our compound 4 and used zolpidem as a positive reference. We observed that similarly to the reference zolpidem, treatment with compound 4 markedly improved the survival of GABA neurons, showing enhanced neuronal viability relative to the control group (Figure 6A,C) and prevented mitochondrial dysfunction, a pivotal element in ischemic cell death (Figure 6B). Both, compound 4 and zolpidem decreased intracellular calcium levels, a hallmark of excitotoxicity and subsequent neuronal damage (Figure 7A). Further analysis revealed that glutamate induced an increase in caspase-3, a key marker of apoptosis and axon degeneration, while treatment with zolpidem and compound 4 significantly reduced caspase-3 levels (Figure 7B).

Neurite Outgrowth Assay for Compound 4. There is strong evidence that modulation of GABA-ergic signaling plays a significant role in neurite growth and adult neurogenesis,^{11–14} processes which are essential for repairing neural circuits damaged by stroke.^{85,86} To further assess the capacity of compound 4 to foster neural repair and neuron outgrowth, we employed a multiparametric neurite outgrowth assay using high content screening (HCS) technology.⁸⁷ Toxicity was induced by the addition of a high concentration of glutamate (1 mM). Given that under these severe conditions, glutamate causes significant lesions and reduced cellular functionality, and that screening assays for compounds promoting neurite outgrowth in iPSCs using HCS are often conducted at 10 μM ,^{88,89} we selected to evaluate the efficacy of our compound at a concentration of 10 μM and used zolpidem as a positive reference. We envisioned that this approach would provide the necessary preliminary confirmation of our molecule's efficacy in *in vitro* assays, facilitating progression to more advanced *in vivo* studies.

In the assay we observed that glutamate added to GABAergic iPSCs induced significant neuronal loss, and treatment with

vehicle did not influence any of the neuronal outgrowth parameters (Figure 8A–F). In contrast, treatment with compound 4 had a positive impact on neuronal outgrowth as evidenced by several assay end points. We observed that compound 4 preserved 42% of total neurite outgrowth relative to untreated control neurons. This effect surpassed that of the reference drug zolpidem, which maintained only 16% of total neurite outgrowth (Figure 8A). Additionally, compound 4 showed 55% preservation of processes, while zolpidem exhibited 38%, indicating significant cellular growth under these conditions (Figure 8F). Moreover, a notable increase was observed in the mean number of neurite branches per cell (Figure 8C), where compound 4 preserved 27% more branching compared to control conditions. Overall, these results suggest that compound 4 promotes neurite outgrowth and protects neuronal architecture under excitotoxic stress. Beyond its neuroprotective properties, compound 4 actively promotes neurite regeneration and synaptic structure maintenance, both of which are critical for neuronal recovery and network functionality.

Extended ADME-Tox and Pharmacokinetic Studies of Compound 4. In the extended ADME-Tox studies for the lead molecule 4, we performed MDR1-MDCKII permeability assay in both directions (A-B and B-A) to evaluate the potential efflux by P-glycoprotein (Pgp) at the blood-brain barrier (BBB),⁹⁰ metabolic stability assay and cytotoxicity. Compound 4 demonstrated a significantly higher apical-to-basolateral (A-B) permeability value of $55.6 \pm 2.98 \times 10^{-6}$ cm/s compared to the lower basolateral-to-apical (B-A) permeability of $29.7 \pm 0.70 \times 10^{-6}$ cm/s, indicative of its reduced susceptibility to P-glycoprotein (Pgp) efflux (Table 5). In metabolic stability assay with human liver microsomes (HLM), the assessed half-life was 176 min, and intrinsic clearance (Cl_{int}) was 9.8 $\mu\text{L}/\text{mg}/\text{min}$ (Tables 5 and S2). The primary metabolic pathway was hydroxylation (Figures S1–S3). The evaluated rat plasma protein binding was 81.40% and brain tissue binding for compound 4 was 46.56% (Table 5). In the hepatotoxicity assay conducted on hepatoma HepG2 cells, compound 4, after a 48-h incubation period, exhibited only a slight decrease in cell viability at the highest tested concentration of 100 μM . Similar observations were made when evaluating neurotoxicity.

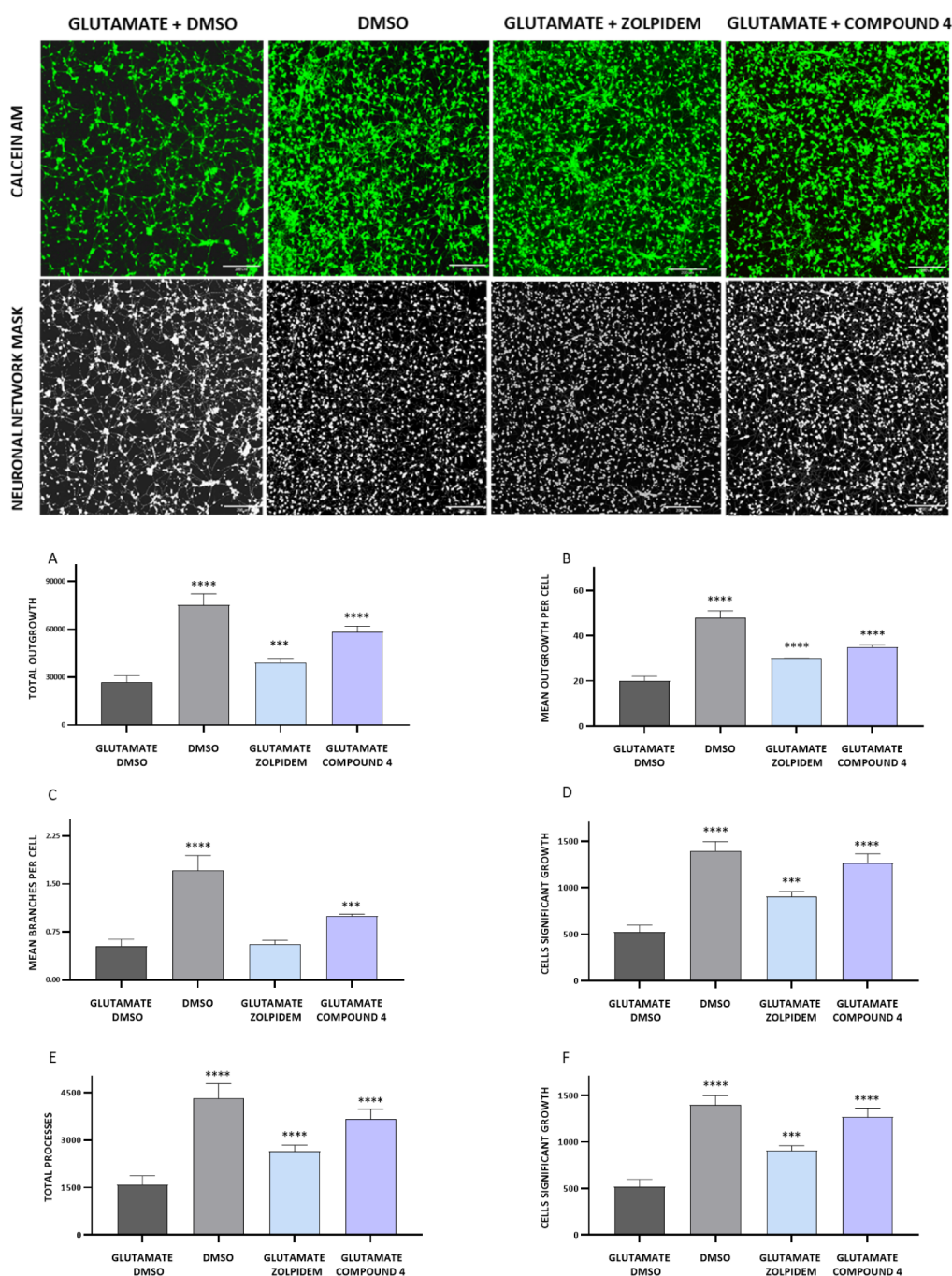


Figure 8. Representative images of neuroprotective effect of the tested compounds on the iCell GABANeurons. (A) Total length of skeletonized outgrowth in μm (corrected for diagonal lengths). (B) Average skeletonized outgrowth in μm corrected for diagonal lengths divided by the number of cells. (C) Total branches divided by number of cells (μm). (D) Number of cells in the image with outgrowth greater than the threshold length specified in the settings. (E) Number of outgrowths in the image that are connected to cell bodies. (F) Total processes divided by number of cells. The cells were pretreated with tested compound ($10\ \mu\text{M}$) or vehicle (0.1% DMSO, v/v) for 1 h. After this time the cells were incubated with glutamate ($1\ \text{mM}$) for 3 h. Quantification assessed with High Content Screening (HCS). Cells morphology assessment using a Neuron Outgrowth module. The results of experiment were image using $10\times$ magnification with the ImageXpress Micro XLS (Molecular Devices). Scal bar: $200\ \mu\text{m}$. Statistical analysis: Way ANOVA followed by posthoc analysis (Dunnett's multiple comparison tests), $*p < 0.05$, $**p < 0.01$, $***p < 0.001$, $****p < 0.0001$.

The pharmacokinetic profile of compound 4 was evaluated after its *i.p.* and *i.v.* administration in rats at a screening dose of $3\ \text{mg/kg}$. The pharmacokinetic parameters, derived through noncompartmental analysis, are displayed in Table 6, Figures S4 and S5. The peak concentration of compound 4 in both serum and brain was reached at the initial observation time-point (i.e., $t_{\text{max}} = 5\ \text{min}$) following *i.p.* and *i.v.* administration, signifying rapid absorption. The area under the concentration–

time curve (AUC_{0-t}) for brain tissue following administration of the compound 4 was $8229\ \text{ng}\cdot\text{min/mL}$ after *i.p.* administration and $15265\ \text{ng}\cdot\text{min/mL}$ after *i.v.* administration. The observed volume of distribution (V_z) was $0.383\ \text{L/kg}$, and clearance (Cl) was $5.56\ \text{mL/min/kg}$. The bioavailability (F) of the molecule was 23.8% . The calculated unbound plasma concentration ($C_{p,u}$) after *i.p.* administration was $837.13\ [\text{ng/mL}]$ and unbound brain concentration ($C_{b,u}$) was $117.30\ [\text{ng/g}]$. The

Table 5. *In Vitro* Extended ADME-Tox Parameters for Compound 4

<i>In Vitro</i> parameter	value
A-B permeability (MDR1-MDCKII, pH 7.4/7.4) (10^{-6} cm/s) \pm SD	55.6 \pm 2.98
B-A permeability (MDR1-MDCKII, pH 7.4/7.4) (10^{-6} cm/s) \pm SD	29.7 \pm 0.70
Metabolic stability HLM ^a	
$t_{0.5}$ [min]	176
Cl_{int} [μ L/mg/min]	9.8
Hepatotox ^b	>100 μ M
Neurotox ^c	>100 μ M
Plasma protein binding ^d	81.3971%
Brain tissue binding ^d	46.5625%

^aHLM-human liver microsomes. ^bThe IC_{50} values were determined after treating HepG2 cells with the test compound for 24 and 48 h, across three separate experiments. ^cThe IC_{50} values were determined after treating SH-SY5Y cells with the test compound for 24 h, across three separate experiments. ^dRat, concentration tested 10^{-5} M.

Table 6. Pharmacokinetic Parameters and Brain Uptake for Compound 4 After *i.v.* and *i.p.* Administration at a Dose of 3 mg/kg to Rats ($n = 6$)

Parameters	<i>i.p.</i>		<i>i.v.</i>		Zolpidem (plasma <i>i.p.</i>) ^a
	Plasma	Brain	Plasma	Brain	
$AUC_{0 \rightarrow t}$ [ng \times min/mL] [ng \times min/g] ^b	128 271	8229	538 253	15 265	2341
$t_{0.5}$ [min]	269.6	653.2	47.8	135.1	30.6
MRT [min]	50.9	102.5	39.7	65.5	27.6
C_{max} [ng/mL]/[ng/g]	4500	219.5	-	444.7	2341
C_{pu} [ng/mL]/ C_{bu} [ng/g] ^c	837.13	117.30	-	237.64	
t_{max} [min]	5	5	-	5	
V_d [L/kg]			0.383		0.104
Cl [mL/min/kg]			5.56		141 [mL/h]

^aZolpidem administrated *i.p.* at dose of 5 mg/kg.^{35,36} $t_{0.5}$ —terminal half life; C_{max} —maximum plasma concentration; t_{max} —time to reach C_{max} ; V_d —volume of distribution; Cl—clearance; MRT—mean residence time $F = 23.8\%$. ^bConcentration in brain AUC —area under the curve. ^cThe unbound plasma concentration: $C_{p,u} = 2482.75$ nM (*i.p.*). The unbound brain concentration: $C_{b,u} = 348.03$ nM (*i.p.*).

latter corresponds to a brain unbound concentration of 348.03 nM, which indicates sufficient exposure to cover cellular mechanistic target GABA-A, with a $K_i = 53.7$ nM (pK_i of 7.27). The clearance of compound 4 from plasma and brain proceeded slowly, exhibiting terminal $t_{0.5}$ of 269.6 and 653.2 min, respectively. These values were nearly nine times higher compared to the reference drug zolpidem, which has a reported half-life of 30.6 min in rats,³⁵ (2–3 h in human plasma).³⁷ The overall ADMET and PK profiles permitted us to evaluate the efficacy of compound 4 in pharmacodynamic studies.

Evaluation of the Efficacy of Compound 4 in Animal Model of Ischemia. Previous studies have demonstrated that low, sub-sedative doses of GABA-A positive allosteric modulators enhance neural plasticity and facilitate functional recovery poststroke, whereas higher doses induce sedation and may hamper functional recovery, possibly due to a decrease in BDNF levels.^{9,43,91} Moreover, previous studies have revealed that GABA-A receptor ligands may impair memory function only at sedative doses.⁹² Consequently, it was considered essential to determine the sedative threshold of compound 4 before proceeding with its evaluation in the ischemia animal model. At this stage of our investigation, it was critical to exclude any sedative effects or impairment of locomotor activity at the doses used in the MCAO model in rats, as such properties could limit its future therapeutic potential. Compound 4 administered *i.p.* at the doses of 3, 10, and 30 mg/kg, did not change locomotor activity in rats during 60 min observation in the open field test, compared to vehicle treated animals (Table 7). These results suggest that doses up to 30 mg/kg are safe with respect to potential sedative activity. It is important to note that

preferential $\alpha 1$ GABA-A ligands have been reported to reduce spontaneous locomotor activity across various dose ranges. The available studies indicate that zolpidem significantly suppresses locomotor activity at doses up to 10 mg/kg.⁹³ Other high-affinity α -1 GABA-A ligands significantly reduced locomotor activity at higher doses, such as 30 mg/kg,⁵⁷ while alpidem exhibited similar effects at doses ranging from 30 to 60 mg/kg.⁹⁴ While these diverse *in vivo* activities do not appear to correlate with *in vitro* binding potencies, literature data suggest that this feature may be attributed to a constellation of factors,⁶⁴ including specific pharmacokinetic profile of a compound, such as variations in regional distribution, ligand–receptor interaction kinetics, stabilization of preferred receptor conformations, and interaction of a ligand with GABA-A receptors that show specific subunit stoichiometry ($2:\alpha_1:2:\beta_{1-3}, 1:\gamma_{1-3}/3\alpha_1:2\beta_{1-3}/2\alpha_1:3\beta_{1-3}$).⁹⁵ In fact, zolpidem has been reported to interact with $\alpha 1$ -GABA-A receptors containing different subunit stoichiometries ($2:\alpha_1:2:\beta, 1:\gamma$ and $3\alpha_1:2\beta$), which may influence its pharmacological profile.^{11,95} Nevertheless, considering that the primary goal of the *in vivo* studies was to evaluate the therapeutic potential of compound 4 in enhancing stroke recovery, it was advanced to an animal model of stroke to obtain proof-of-concept at the preclinical level.

To evaluate the neuroprotective and the ability to enhance functional recovery after stroke, compound 4 was tested using the 90 min Middle Cerebral Artery Occlusion (90-MCAO) model in male Sprague–Dawley rats. This model induces ischemia followed by reperfusion, leading to tissue injury and significant neurological deficits.⁹⁶ Compound 4 was evaluated in a subchronic regimen at doses of 1.5 mg/kg and 3 mg/kg,

Table 7. Open Field Test in Rats Demonstrating the Influence of Compound 4 on Locomotor Activity^a

Treatment	Dose (mg/kg)	X ambulation ± SEM	Y ambulation ± SEM	Total distance (cm) ± SEM
Vehicle	0	155.71 ± 28.09	113.43 ± 12.80	5404 ± 895
Cmpd 4	3	133.00 ± 47.09 ns vs vehicle	114.00 ± 34.51 ns vs vehicle	6985 ± 1846 ns vs vehicle
	10	159.67 ± 13.76 ns vs vehicle	164.00 ± 16.28 ns vs vehicle	6888 ± 562 ns vs vehicle
	30	172.00 ± 43.20 ns vs vehicle F(3,1)=0.2039; ns	179.50 ± 46.04 ns vs vehicle F(3,21)=1.3340; ns	6347 ± 845 ns vs vehicle F(3,21)=0.4371; ns

^aThe data of open field studies were evaluated by an analysis of variance one-way ANOVA followed by Bonferroni's post hoc test (statistical significance set at $p < 0.05$, $n = 8$). ns—not significant.

administered *i.p.* once daily for 3 days, starting 1.5 h postreperfusion. On the third day of treatment, neurological deficits and stroke volume were assessed. Zolpidem was used as a positive reference drug in this model and was administered over a 3-day treatment period at a dose of 1.5 mg/kg, selected based on our previous experiments in animal studies and literature data.⁹¹ Administration of compound 4 at both doses significantly improved functional recovery, as evidenced by a reduction in neurological severity assessed using the Bederson score⁹⁷ (Figure 9A). Animals treated with compound 4

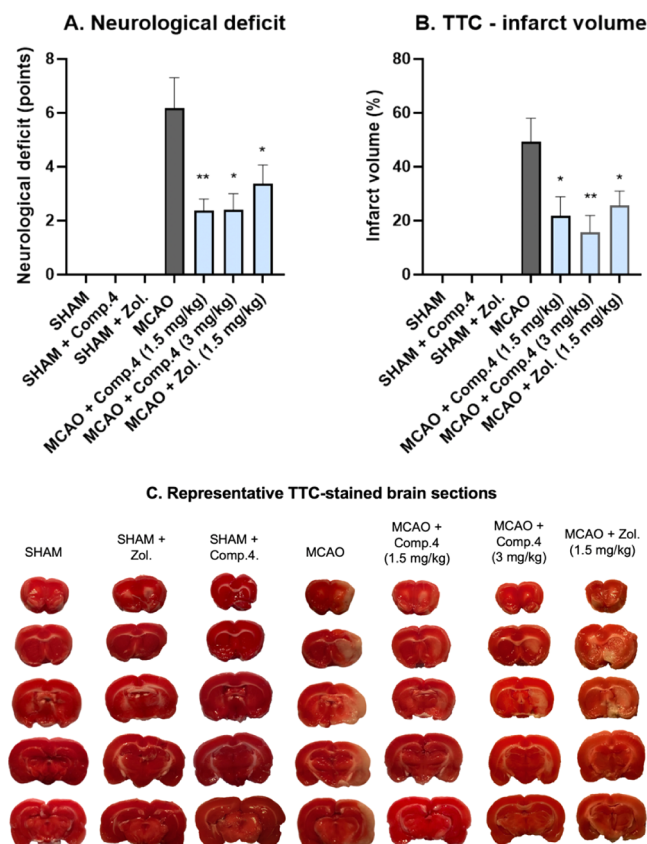


Figure 9. Effects of 3-day treatment (once daily for 3 days) with compound 4. A. The neurological deficits were evaluated following a 3-day treatment on the third day poststroke using with Bederson scale. Sham-operated animals exhibited no neurological deficits. The difference among ischemic groups was analyzed using a Mann–Whitney U test ($n = 8$), with statistical significance evaluated at $* p < 0.05$; $* p < 0.01$. B. Assessment of the lesion size following a 3-day treatment with compound 4 (1.5 mg/kg and 3 mg/kg) and zolpidem (1.5 mg/kg). The infarct volume in % of ipsilateral hemisphere is presented as the mean \pm SEM ($n = 6$). The difference between groups was evaluated using one-way ANOVA with Sidak's post hoc test. The statistical significance marked with $* p < 0.05$; $* p < 0.01$. C. Examples of TTC-stained coronal brain sections (2 mm) from each experimental group. Pale areas indicate the infarct. MCAO – middle cerebral artery occlusion.

improved neurological deficit, compared to the MCAO group. Improvements in neurological scores following treatment with compound 4 at both doses were slightly greater than those observed with the reference drug zolpidem. These results indicate the potential of compound 4 in the recovery of motor functions (Figure 9A). Furthermore, administration of compound 4 at 1.5 mg/kg and 3 mg/kg significantly reduced infarct volume, when compared to the MCAO group, as assessed by

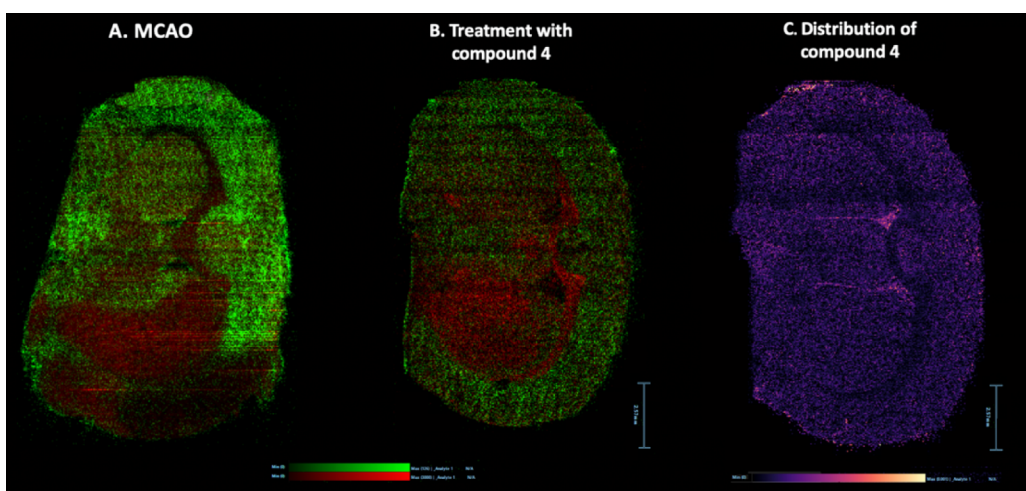


Figure 10. Representative images of DESI analysis. A. Brain tissue following stroke, detected ions using (−)-DESI-MSI red: $m/z = 89.0237$ (lactic acid), green: $m/z = 346.0550$ (AMP). B. Brain tissue following MCAO and treatment with 1.5 mg/kg of compound 4. C. Relative abundance and spatial distribution of the compound 4 ($m/z 338.1669$) using (+)-DESI-MSI in the sagittal rat brain sections following MCAO. Compound 4 was administrated *i.p.* at dose of 1.5 mg/kg, 1.5h after the reperfusion, brain tissue collected after 5 min. Scale bar: 2.7 mm (Statistical analysis Figure S11).

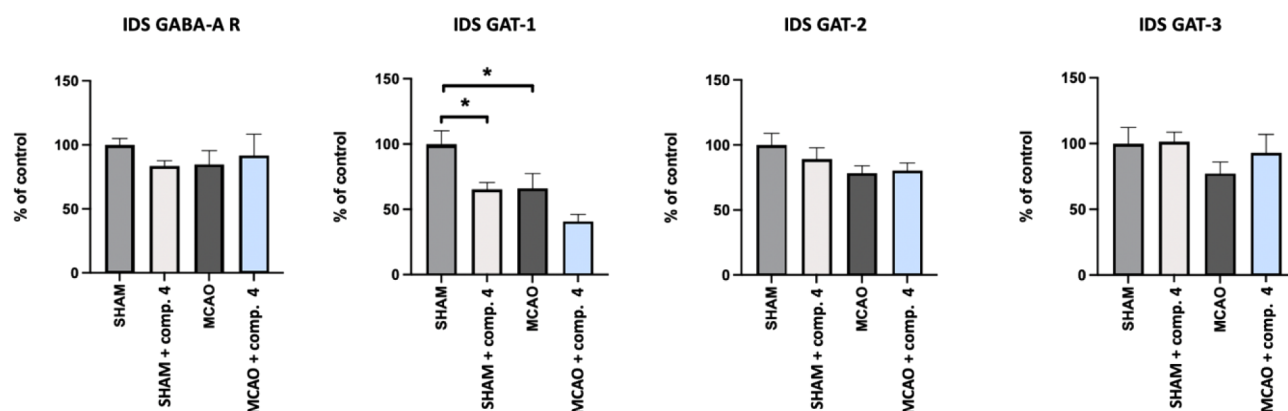


Figure 11. Protein levels of rat GAT-1, GAT-2, GAT-3 and $\alpha 1$ -GABA-A receptor 3 days following MCAO and after a 3-day treatment with compound 4 (1.5 mg/kg). IDS—ipsilateral dorsal striatum. Changes in groups are presented as % of control. Data are presented as the mean \pm SEM, one-way ANOVA, followed by Sidak's correction for post hoc comparisons; * $p < 0.05$. $n = 6$. For representative immunoblots and total protein, see Figures S6–S10.

triphenyl tetrazolium chloride (TTC) staining (Figure 9B,C). These effects were comparable to those induced by the positive control, zolpidem.

Apart from TTC staining, to evaluate the neuroprotective effects of compound 4, we employed Desorption Electrospray Ionization (DESI) mass spectrometry, to detect changes in the abundance of molecular markers present in stroke-affected and healthy tissues. In DESI images, we observed a marked decrease in adenosine monophosphate (AMP) a molecular marker of healthy tissue, particularly within the cortex (Figure 10A, green region). Alongside, we detected increased levels of lactic acid in stroke area, a hallmark of poststroke acidosis (Figure 10A, red marker). Treatment with compound 4 reduced lactic acid concentrations in the cortex (Figure 10B, red marker). The levels of lactic acid were lower in somatosensory cortex and we could detect the presence of AMP in this area, a marker of a healthy tissue (Figures 10B and S11—statistical analysis). These results further support the neuroprotective effects of compound 4 suggesting also that it can modulate early post stroke acidosis. Tissue acidosis serves as a sensitive metabolic marker of injury progression following cerebral ischemia and is a known factor that can exacerbate neuronal injury and impede recovery.⁹⁸ By

reducing acidosis, the compound 4 may help mitigate damage to neural tissues and support recovery processes. Next, we employed DESI to map compound's 4 distribution within the brain tissue following MCAO.⁹⁹ We observed that compound 4 exhibited uniform distribution across different regions of the brain (Figure 10C), suggesting that stroke did not influence the compounds regional distribution.⁹⁹

Given that stroke induces fluctuations in the abundance in the GABA transporters (GAT) which influences changes in GABAergic signaling, we measured the protein levels of GATs and $\alpha 1$ -GABA-A receptors in the dorsal striatum—a region significantly affected by ischemia—following MCAO and a three-day treatment with compound 4. The Western blot analyses revealed that stroke induced significant decrease in protein levels of GAT-1 in the MCAO group (Figure 11), which is in line with previous literature data.¹⁰⁰ The levels of GAT-2 and GAT-3 after the stroke were decreased however not significantly. Previous experimental data from stroke models have revealed that synaptically localized $\alpha 1$ -GABA-A receptors remain unchanged after stroke,⁷ or their abundance is only transiently altered.⁹ Consistent with these findings, we observed no change in $\alpha 1$ -GABA-A receptor levels after stroke (Figure 11).

Treatment with compound **4** did not influence the abundance of GABA-A receptors, suggesting that compound **4** modulates receptor function without causing potentially disruptive changes in the protein levels of the $\alpha 1$ -GABA-A receptor.

CONCLUSIONS

Currently, nearly half of stroke survivors do not recover sufficiently to gain an autonomous lifestyle.^{1,3} Ischemic stroke patients rely solely on physical rehabilitation as there are no effective pharmacological treatments available to promote recovery after stroke, highlighting a significant unmet medical need that demands novel approaches. Considering the beneficial role of phasic GABA signaling mediated by synaptic GABA-A receptors in poststroke recovery, we aimed to identify GABA-A ligands with a suitable subtype selectivity profile for stroke treatment—preferential activity at $\alpha 1$ -GABA-A receptors and negligible activity at extrasynaptic $\alpha 5$ -GABA-A receptors. With this aim we conducted SAR around three chemotypes, yielding the conclusion that imidazo[1,2-*a*]pyridine derivatives and 2-phenylimidazo[1,2-*b*]pyridazine bearing cyclic amide exerted the most promising affinities toward GABA-A receptor. Selected compounds were evaluated in terms of functional selectivity for synaptic type vs extrasynaptic type of GABA-A receptors, showing a pronounced preference toward synaptic type of $\alpha 1$ -GABA-A receptors and minimal efficacy at $\alpha 5$ -GABA-A receptors. When tested in the OGD model, several molecules demonstrated a promising ability to promote neuronal healing and neuronal survival. Among all compounds, we selected lead molecule **4**, characterized by the most prominent neuroprotective activity and superior ADMET properties within the entire library. The effects of compound **4** in certain assays outperformed the reference drug zolpidem in terms of neuroprotective activities. Moreover, compound **4** demonstrated an improved PK profile compared to zolpidem, with a $t_{0.5}$ in rats of 269 min, compared to zolpidem's $t_{0.5}$ of 30.6 min in rats. Further studies revealed that compound **4** is able to prevent mitochondrial dysfunction, reduce calcium overload, and decrease caspase 3 levels—features previously associated with functional tissue repair and neuronal survival following stroke.^{80,81} Given previous literature reports showing that GABA signaling promotes neurogenesis, we tested compound **4** in a neurite outgrowth assay and found that it enhanced overall neuronal growth and promoted healing of GABAergic iPSCs following excitotoxicity. Compound **4** was further tested in the MCAO model of ischemic stroke, characterized by transient ischemia followed by reperfusion, which induces pronounced neuronal damage and neurological dysfunction. We observed that compound **4**, administered once daily for 3 days at doses of 1.5 mg/kg and 3 mg/kg, induced neuroprotective and neuro-rehabilitative properties, significantly reducing lesion size and enhancing motor performance in animals following stroke. The overall efficacy of compound **4** implies its therapeutic potential in promoting functional recovery following ischemic stroke and warrants further investigation in advanced studies.

Experimental Section. Molecular Modeling. Using Maestro Schrödinger (Release 2017–2), the ligands' 3D structures were prepared and subsequently optimized using the LigPrep tool. Next, the C++ library ULYSSES was utilized to perform geometry optimization, free energy evaluation and calculation of deformation energy with semiempirical quantum chemical calculations on GFN2-xTB theory level and ALPB solvation model. The Human GABA-A receptor $\alpha 1\beta 2\gamma 2$ subtype complex bound with GABA and Zolpidem was

downloaded from the PDB database (PDB code: 8DD2).⁶⁰ Hydrogen atoms were introduced into the complex, disulfide bonds were regenerated, and the hydrogen bond network was fine-tuned using PROPKA at a pH of 7.4. The OPLS3 algorithm was utilized for the initial minimization, with a convergence criterion of 0.5 Å set for heavy atoms. Optimization of the entire complex was performed by applying the MM-GBSA method, which took into account the flexible residues of the protein within a 7 Å radius surrounding the Zolpidem molecule, and utilized the VSGB solvation model. To facilitate molecular docking, only chains D ($\alpha 1$ -subunit) and E ($\gamma 2$ -subunit) were selectively preserved, and a grid was created with the focus on the Zolpidem molecule. The grid was sized to accommodate ligands of comparable dimensions and encompassed rotations on all OH and SH groups. The docking procedure was performed using the XP protocol, considering the initial ligand conformations of rings that were prepared during the optimization phase. The inclusion of intramolecular hydrogen bonds had a positive impact on the final score, and the contribution of aromatic hydrogen bonds was also taken into consideration. For each ligand, the best result was retained and subsequently optimized using MM-GBSA in a manner similar to the predocking optimization of the complex.

Synthetic Procedures. General Information. Unless specified otherwise, all reagents were sourced from commercial suppliers and employed as received without additional purification. Reaction progress was tracked using TLC plates from Merck, coated with silica gel 60 F254 on aluminum backing, and visualized under UV light at 254 nm. Reaction mixtures were purified employing an automatic CombiFlash RF (Teledyne Isco) system utilizing RediSep R_f flash columns (silica gel 60, particle size 40–63 μ m) or RediSep Gold columns (silica gel 60, particle size 20–40 μ m). The UPLC–MS data were collected with the Waters ACQUITY UPLC (Waters Corporation, Milford, MA, USA) merged with a Waters tandem quadrupole mass spectrometer (TQD) (electrospray ionization (ESI) mode with TQD) according to the previously published protocols.¹⁰¹ All compounds are >95% pure by HPLC analysis. ¹H NMR, ¹³C NMR and ¹⁹F NMR spectra were recorded using JEOL JNM-ECZR 500 RS1 (ECZR version) at 500, 126, and 471 MHz or Varian Mercury spectrometer (Varian Inc., Palo Alto, CA, USA) at 300 MHz, 75 or 126 and 282 MHz. Chemical shifts (δ) are presented in parts per million (ppm), calibrated using the respective reference solvents: chloroform-*d*, methanol-*d*₄, or DMSO-*d*₆ as standards. All the spectra were analyzed using the ACD/Spectrum Processor 2017. Melting points were measured using a Büchi melting point apparatus and the values are reported as uncorrected.

2-(4-Fluorophenyl)-6-methylimidazo[1,2-*a*]pyridine (1). A solution of 5-methylpyridine-2-amine (1 eq, 9 mmol), a 2-bromo-1-(4-fluorophenyl)ethan-1-one (1 eq, 9 mmol) and sodium bicarbonate (1.5 eq, 13.5 mmol) w toluene (15 mL) was stirred for 1 h at 100 °C using the CEM-Discover system, which operates at 2.445 GHz and allows for continuous irradiation power adjustments from 0 to 200 W, as previously described. After that time, precipitate was filtered off and washed with petroleum ether, distilled water and diethyl ether and dried under reduced pressure to give beige solid with 91% yield. No further purification was needed. ¹H NMR (500 MHz, CHLOROFORM-*d*) δ 7.88 (dd, 3H, *J* = 5.4, 9.0 Hz), 7.69 (s, 1H), 7.50 (d, 1H, *J* = 9.2 Hz), 7.09 (t, 2H, *J* = 8.8 Hz), 7.00 (dd, 1H, *J* = 1.6, 9.2 Hz), 2.30 (s, 3H). ¹³C NMR (126 MHz, CHLOROFORM-*d*) δ 163.4 (d, *J* = 248.7 Hz), 146.59, 144.9,

130.3, 128.0, 127.7, 123.4, 122.2, 116.9 (d, $J = 20.9$ Hz), 115.8, 107.6, 21.4. (471 MHz, CHLOROFORM- d) $\delta = 114.4$ (s, 1F). Formula: $C_{14}H_{11}FN_2$; MS (ESI⁺) m/z 227.024 (M+H⁺).

2-(2-(4-Fluorophenyl)-6-methylimidazo[1,2-*a*]pyridin-3-yl)-2-hydroxyacetic Acid (2). A solution of (1) 2-(4-fluorophenyl)-6-methylimidazo[1,2-*a*]pyridine (1 eq, 8.2 mmol) and glyoxylic acid (2.6 eq, 21.3 mmol) in DCM (25 mL) was stirred for 16 h under the reflux. After this time, the crude mixture was concentrated under reduced pressure. Crude product was then crystallized from methanol, filtered and dried to give compound 2 as white powder with 90% yield. ¹H NMR (500 MHz, CHLOROFORM- d) δ 8.29–8.3 (s, 1H), 7.82–7.79 (s, 2H), 7.53–7.51 (d, 1H), 7.30 (t, 2H), 7.16–7.18 (m, 1H), 5.63 (s, 1H), 2.3 (s, 3H). ¹³C NMR (126 MHz, CHLOROFORM- d) δ 163.47, 161.52 (d, $J = 248.1$ Hz), 143.69, 142.76, 131.09, 128.85, 124.24, 121.90, 118.56, 116.77, 116.08, 115.91 (d, $J = 21.1$ Hz), 64.78, 18.45. ¹⁹F NMR (471 MHz, CHLOROFORM- d) $\delta = 114.12$ (s, 1F). Formula: $C_{16}H_{13}FN_2O_3$; MS (ESI⁺) m/z 301.214 (M+H⁺).

2-(2-(4-Fluorophenyl)-6-methylimidazo[1,2-*a*]pyridin-3-yl)acetic Acid (3). A solution of compound (2) (1 eq, 6 mmol) and Palladium on carbon (0.1 eq, 0.6 mmol) in formic acid (20 mL) was stirred for 16 h at 100 °C. After that time, reaction mixture was diluted with methanol and filtered through silica gel. Obtained filtrate was concentrated under reduced pressure to yellowish solid with 93% yield. No further purification was needed. ¹H NMR (500 MHz, DMSO- d_6) δ 8.23 (s, 1H), 8.16 (s, 1H), 7.81–7.78 (s, 2H), 7.46–7.44 (d, 1H), 7.25 (t, 2H), 7.10–7.08 (d, 1H), 3.93 (s, 2H), 2.26 (s, 3H). ¹³C NMR (126 MHz, DMSO- d_6) δ 171.90, 161.14 (d, $J = 248.08$ Hz), 143.29, 141.59, 131.74, 130.06, 127.83, 122.90 (d, $J = 3.6$ Hz), 121.47, 116.49, 115.99 (d, $J = 21.1$ Hz), 115.82 (d, $J = 19.31$ Hz), 31.63, 18.33. ¹⁹F NMR (DMSO- d_6 , 471 MHz) δ -114.99 (s, 1F). Formula: $C_{16}H_{13}FN_2O_2$; MS (ESI⁺) m/z 285.210 (M+H⁺).

General Procedure for the Preparation of Final Products (4–23). The intermediate acid (3) (1 eq, 0.7 mmol) was dissolved in anhydrous tetrahydrofuran previously dried over molecular sieves. The reaction mixture was first heated to 50 °C, then cooled to 10 °C, and 1,3-dicyclohexylcarbodiimide (CDI) (1.3 eq, 0.91 mmol) was slowly added and the resulting mixture was stirred for two hours at room temperature. After that time, an appropriately substituted amine (1.2 eq, 0.84 mmol) was added, and the mixture was stirred at 40 °C for 12 h. Next, the solvent was evaporated under reduced pressure, and the resultant precipitate was extracted three times using dichloromethane and water. The organic phase was washed with brine, then separated and dried over anhydrous sodium sulfate. The filtrate was concentrated under reduced pressure. The products were purified using flash chromatography, using (Et₂O/DCM/MeOH, 2.0/7.5/0.5, v/v/v) as eluent.

2-(4-Fluorophenyl)-6-methyl-3-(2-oxo-2-(pyrrolidin-1-yl)ethyl)imidazo[1,2-*a*]pyridin-1-ium 3-carboxy-2,3-dihydroxypropanoate (4). The title compound was obtained first as a free base by reacting intermediate acid 3 (0.7 mmol, 0.200 g) with pyrrolidine (0.84 mmol, 0.06g). Yield: 26%, white solid. The salt was prepared by stirring free base (1 equiv) with tartaric acid (1 equiv) in methanol for 1h and evaporating the solvent. ¹H NMR (500 MHz, METHANOL- d_4) δ 8.17 (s, 1H), 7.60 (dd, 2H, $J = 5.3, 8.9$ Hz), 7.56 (d, 1H, $J = 9.2$ Hz), 7.40 (dd, 1H, $J = 1.5, 9.2$ Hz), 7.23 (t, 2H, $J = 8.8$ Hz), 4.45 (s, 2H), 4.12 (s, 2H), 3.57 (t, 2H, $J = 6.8$ Hz), 3.44 (t, 2H, $J = 6.9$ Hz), 2.38 (s, 3H), 2.0–2.0 (m, 2H), 1.90 (quin, 2H, $J = 6.7$ Hz). ¹³C NMR (126 MHz, METHANOL- d_4) δ ppm 175.63, 168.77, 164.70 (d, $J = 247.6$

Hz), 143.53, 140.81, 132.46, 131.90 (d, $J = 8.4$ Hz), 129.40 (d, $J = 3.3$ Hz), 125.80, 124.55, 117.36, 117.10 (d, $J = 22.0$ Hz), 115.21, 73.82, 48.20, 47.55, 31.01, 27.17, 25.47, 18.29. ¹⁹F NMR (471 MHz, METHANOL- d_4) $\delta = 114.5$ (s, 1F). m.p.=213.4–214.5 °C (free base). Formula: $C_{20}H_{20}FN_3O_3$; MS (ESI⁺) m/z : 338.275 (M + H⁺).

2-(2-(4-Fluorophenyl)-6-methylimidazo[1,2-*a*]pyridin-3-yl)-1-morpholinoethan-1-one (5). The title compound was obtained using acid 3 (0.7 mmol, 0.200 g) and morpholine (0.84 mmol, 0.073g). Yield: 67%, white solid. ¹H NMR (300 MHz, CHLOROFORM- d) δ 8.02–8.01 (m, 1H), 7.61 (dd, 2H, $J = 5.4, 8.7$ Hz), 7.54 (dd, 1H, $J = 0.8, 9.2$ Hz), 7.16 (t, 2H, $J = 8.7$ Hz), 7.09 (dd, 1H, $J = 1.7, 9.1$ Hz), 4.06 (s, 2H), 3.59 (s, 4H), 3.38 (br d, 2H, $J = 5.1$ Hz), 3.29 (br d, 2H, $J = 4.9$ Hz), 2.37 (d, 3H, $J = 1.0$ Hz). ¹³C NMR (75 MHz, CHLOROFORM- d) δ ppm 166.72, 162.60 (d, $J = 247.7$ Hz), 144.24, 142.79, 130.70 (d, $J = 3.3$ Hz), 130.20 (d, $J = 7.7$ Hz), 127.92, 122.10 (d, $J = 5.0$ Hz), 116.72, 115.86 (d, $J = 21.6$ Hz), 113.27, 66.79, 66.41, 46.30, 42.41, 29.82, 18.48. ¹⁹F NMR (282 MHz, CHLOROFORM- d) δ ppm -113.82 (s, 1F). m.p.= 211.7–212.2 °C. Formula: $C_{20}H_{20}FN_3O_2$; MS (ESI⁺) m/z : 354,842 (M + H⁺).

2-(2-(4-Fluorophenyl)-6-methylimidazo[1,2-*a*]pyridin-3-yl)-1-thiomorpholinoethan-1-one (6). The title compound was obtained using acid 3 (0.7 mmol, 0.200 g) and thiomorpholine (0.84 mmol, 0.086g). Yield: 40%, white solid. ¹H NMR (500 MHz, DMSO- d_6) δ 8.07 (s, 1H), 7.64 (dd, 2H, $J = 5.6, 8.9$ Hz), 7.51 (d, 1H, $J = 9.2$ Hz), 7.29 (t, 2H, $J = 8.9$ Hz), 7.14 (dd, 1H, $J = 1.7, 9.2$ Hz), 4.19 (s, 2H), 3.80–3.90 (m, 4H), 2.61 (ddd, 4H, $J = 2.8, 5.0, 10.4$ Hz), 2.32 (s, 3H). ¹³C NMR (126 MHz, METHANOL- d_4) δ ppm 169.26, 164.40 (d, $J = 246.5$ Hz), 145.04, 143.13, 131.72 (d, $J = 8.1$ Hz), 130.50, 124.46, 123.9, 116.86 (d, $J = 21.9$ Hz), 116.76, 116.39, 50.03, 46.33, 30.32, 28.79, 28.36, 18.35. ¹⁹F NMR (471 MHz, METHANOL- d_4) δ ppm -115.6. m.p.=215.2–217.1 °C. Formula: $C_{20}H_{20}FN_3OS$; MS (ESI⁺) m/z : 370.138 (M + H⁺).

2-(2-(4-Fluorophenyl)-6-methylimidazo[1,2-*a*]pyridin-3-yl)-1-(piperazin-1-yl)ethan-1-one (7). The title compound was obtained using acid 3 (0.7 mmol, 0.200 g) and piperazine (0.84 mmol, 0.086g). Yield: 26%, white solid. ¹H NMR (300 MHz, CHLOROFORM- d) δ 7.9–8.1 (m, 2H), 7.6–7.7 (m, 2H), 7.53 (dd, 1H, $J = 0.9, 9.1$ Hz), 7.18 (br t, 2H, $J = 8.6$ Hz), 7.1–7.1 (m, 1H), 4.13 (s, 2H), 3.60 (br dd, 1H, $J = 4.5, 6.0$ Hz), 3.5–3.6 (m, 1H), 3.3–3.5 (m, 2H), 3.1–3.3 (m, 4H), 2.9–3.0 (m, 1H), 2.37 (s, 3H). ¹³C NMR (75 MHz, CHLOROFORM- d) δ ppm 166.78, 162.60 (d, $J = 248.2$ Hz), 160.75, 144.33 (d, $J = 1.7$ Hz), 142.84, 130.10 (d, $J = 8.3$ Hz), 128.03, 122.2 (d, $J = 6.1$ Hz), 116.8, 116.70 (d, $J = 21.6$ Hz), 112.83, 45.35, 42.59, 41.5, 39.86, 30.22, 18.46. ¹⁹F NMR (282 MHz, CHLOROFORM- d) $\delta = 113.30$ (s, 1 F). m.p.=219.4–220.3 °C. Formula: $C_{20}H_{21}FN_4O$; MS (ESI⁺) m/z 353.125 (M+H⁺).

2-(4-Fluorophenyl)-6-methyl-3-(2-oxo-2-(phenylamino)ethyl)imidazo[1,2-*a*]pyridin-1-ium 3-carboxy-2,3-dihydroxypropanoate (8). The title compound was obtained first as a free base by reacting intermediate acid 3 (0.7 mmol, 0.200 g) with aniline (0.84 mmol, 0.078g). Yield 55%, yellowish solid. Next, the salt was prepared by stirring free base (1 equiv) with tartaric acid (1 equiv) in methanol for 1h and evaporating the solvent. ¹H NMR (500 MHz, DMSO- d_6) δ 10.45 (s, 1H), 8.24 (s, 1H), 7.79 (dd, 2H, $J = 5.6, 8.8$ Hz), 7.6–7.6 (m, 2H), 7.49 (d, 1H, $J = 9.2$ Hz), 7.2–7.3 (m, 4H), 7.12 (dd, 1H, $J = 1.6, 9.2$ Hz), 7.03 (t, 1H, $J = 7.4$ Hz), 4.28 (s, 2H), 4.19 (s, 2H), 2.28 (s, 3H). ¹³C NMR (126 MHz, DMSO- d_6) δ ppm 173.71, 167.80, 162.20 (d, $J = 244.4$ Hz), 143.48, 142.28, 139.52, 131.61 (d, $J = 3.0$ Hz),

130.21 (d, $J = 8.2$ Hz), 129.34, 128.10, 124.02, 122.87, 121.74, 119.81, 116.55, 116.09 (d, $J = 21.4$ Hz), 115.52, 72.68, 32.12, 18.35. ^{19}F NMR (471 MHz, DMSO-d_6) δ -114.73 (s, 1F). m.p. = 232.5–233.0 °C (free base). Formula: $\text{C}_{22}\text{H}_{18}\text{FN}_3\text{O}$; MS (ESI^+) m/z 360.069 ($\text{M} + \text{H}^+$).

2-(4-Fluorophenyl)-3-(2-((2-fluorophenyl)amino)-2-oxoethyl)-6-methylimidazo[1,2-a]pyridin-1-ium 3-carboxy-2,3-dihydroxypropanoate (9). The title compound was obtained first as a free base by reacting intermediate acid 3 (0.7 mmol, 0.200 g) with 2-fluoroaniline (0.84 mmol, 0.093g). Yield 42%, yellowish solid. Next, the salt was prepared by stirring free base (1 equiv) with tartaric acid (1 equiv) in methanol for 1h and evaporating the solvent. ^1H NMR (500 MHz, METHANOL-d_4) δ 8.27 (s, 1H), 7.8–7.9 (m, 1H), 7.72 (dd, 2H, $J = 5.3, 8.8$ Hz), 7.57 (d, 1H, $J = 9.2$ Hz), 7.41 (dd, 1H, $J = 1.6, 9.2$ Hz), 7.24 (t, 2H, $J = 8.8$ Hz), 7.1–7.2 (m, 3H), 4.47 (s, 2H), 4.27 (s, 2H), 2.39 (s, 3H). ^{13}C NMR (126 MHz, METHANOL-d_4) δ ppm 174.02, 168.31, 163.20 (d, $J = 247.6$ Hz), 155.60, 153.64, 142.29, 139.93, 130.84, 130.43 (d, $J = 8.4$ Hz), 128.0 (d, $J = 3.4$ Hz), 126.12 (d, $J = 7.8$ Hz), 125.50 (d, $J = 11.8$ Hz), 124.42 (d, $J = 21.7$ Hz), 124.10 (d, $J = 3.7$ Hz), 122.80, 115.64, 115.47, 115.20 (d, $J = 19.8$ Hz), 113.98, 72.3, 30.6, 16.8. ^{19}F NMR (471 MHz, METHANOL-d_4) δ -114.57 (s, 1F), -127.52 (s, 1F). m.p. = 231.5–233.1 °C (free base). Formula: $\text{C}_{22}\text{H}_{17}\text{F}_2\text{N}_3\text{O}$; MS (ESI^+) m/z 378.186 ($\text{M} + \text{H}^+$).

N-(3-Fluorophenyl)-2-(2-(4-fluorophenyl)-6-methylimidazo[1,2-a]pyridin-3-yl)acetamide (10). The title compound was obtained using acid 3 (0.7 mmol, 0.200 g) and 3-fluoroaniline (0.84 mmol, 0.093g). Yield: 56%, white solid. ^1H NMR (500 MHz, DMSO-d_6) δ 8.25–8.22 (m, 1H), 7.82–7.74 (m, 2H), 7.64–7.59 (m, 1H), 7.58–7.51 (m, 1H), 7.43–7.28 (m, 4H), 7.13 (dd, 1H, $J = 1.4$ and 9.2 Hz), 6.94–6.87 (m, 1H), 4.19 (s, 2H), 2.28 (s, 3H). ^{13}C NMR (126 MHz, DMSO-d_6) δ 168.20, 162.67 (d, $J = 241.4$ Hz), 162.22 (d, $J = 244.4$ Hz), 143.57, 142.39, 141.07, 131.58 (d, $J = 3.0$ Hz), 131.03, 130.95, 130.20 (d, $J = 7.8$ Hz), 128.19, 122.78, 121.77, 116.52, 116.04 (d, $J = 21.1$ Hz), 115.47, 114.99, 110.51 (br d, $J = 21.1$ Hz), 106.74, 106.53, 32.11, 18.33. ^{19}F NMR (DMSO-d_6 , 471 MHz) δ -114.91 (s, 1F), -111.92 (s, 1F). m.p. = 214.9–216.0 °C. Formula: $\text{C}_{22}\text{H}_{17}\text{F}_2\text{N}_3\text{O}$; MS (ESI^+) m/z 378.391 ($\text{M} + \text{H}^+$).

2-(4-Fluorophenyl)-3-(2-((4-fluorophenyl)amino)-2-oxoethyl)-6-methylimidazo[1,2-a]pyridin-1-ium 3-carboxy-2,3-dihydroxypropanoate (11). The title compound was obtained first as a free base by reacting intermediate acid 3 (0.7 mmol, 0.200 g) with and 4-fluoroaniline (0.84 mmol, 0.093g). Yield: 44%, yellowish solid. Next, the salt was prepared by stirring free base (1 equiv) with tartaric acid (1 equiv) in methanol for 1h and evaporating the solvent to obtain final salt. ^1H NMR (500 MHz, METHANOL-d_4) δ 8.27 (s, 1H), 7.72 (dd, 2H, $J = 5.3, 8.8$ Hz), 7.6–7.6 (m, 3H), 7.42 (br d, 1H, $J = 9.2$ Hz), 7.26 (t, 2H, $J = 8.8$ Hz), 7.06 (t, 2H, $J = 8.8$ Hz), 4.49 (s, 2H), 4.22 (s, 2H), 2.41 (s, 3H). ^{13}C NMR (126 MHz, METHANOL-d_4) δ ppm 174.2, 167.7, 163.2 (d, $J = 247.4$ Hz), 159.5 (d, $J = 242.3$ Hz), 142.4 (t, $J = 5.3$ Hz), 134.5 (d, $J = 2.8$ Hz), 130.7, 130.4 (d, $J = 8.2$ Hz), 124.3, 122.8, 121.8 (d, $J = 8.1$ Hz), 115.5 (d, $J = 22.2$ Hz), 115.0 (d, $J = 22.6$ Hz), 114.1, 72.4, 30.8, 18.0. ^{19}F NMR (471 MHz, METHANOL-d_4) δ -114.65 (s, 1F), -120.06 (s, 1F). m.p. = 255.9–257.1 °C (free base). Formula: $\text{C}_{22}\text{H}_{17}\text{F}_2\text{N}_3\text{O}$; MS (ESI^+) m/z 378.053 ($\text{M} + \text{H}^+$).

3-(2-((2-Chlorophenyl)amino)-2-oxoethyl)-2-(4-fluorophenyl)-6-methylimidazo[1,2-a]pyridin-1-ium 3-carboxy-2,3-dihydroxypropanoate (12). The title compound was obtained first as a free base by reacting intermediate acid 3

(0.7 mmol, 0.200 g) with and 2-chloroaniline (0.84 mmol, 0.107g). Yield: 37%, yellowish solid. Next, the salt was prepared by stirring free base (1 equiv) with tartaric acid (1 equiv) in methanol for 1h and evaporating the solvent. ^1H NMR (500 MHz, CHLOROFORM-d) δ 8.28 (dd, 1H, $J = 1.6, 8.7$ Hz), 7.8–7.8 (m, 2H), 7.75 (dd, 2H, $J = 5.4, 8.9$ Hz), 7.57 (d, 1H, $J = 9.2$ Hz), 7.25 (s, 1H), 7.2–7.2 (m, 1H), 7.16 (t, 2H, $J = 8.6$ Hz), 7.12 (dd, 1H, $J = 1.7, 9.2$ Hz), 7.01 (dt, 1H, $J = 1.4, 7.7$ Hz), 4.17 (s, 2H), 2.35 (s, 3H). ^{13}C NMR (126 MHz, CHLOROFORM-d) δ 172.42, 167.56 (d, $J = 244.5$ Hz), 149.08, 148.31, 145.92, 139.15, 136.85 (d, $J = 3.0$ Hz), 135.41, 135.4, 135.28, 132.55, 128.69, 126.82, 124.56, 122.84, 121.61, 120.41 (d, $J = 21.7$ Hz), 119.46, 27.44, 18.80. ^{19}F NMR (471 MHz, METHANOL-d_4) δ -113.65 (s, 1F). m.p. = 213.9–215.2 °C (free base). Formula: $\text{C}_{22}\text{H}_{17}\text{ClFN}_3\text{O}$; MS (ESI^+) m/z 394.101 ($\text{M} + \text{H}^+$).

N-(3-Chlorophenyl)-2-(2-(4-fluorophenyl)-6-methylimidazo[1,2-a]pyridin-3-yl)acetamide (13). The title compound was obtained using acid 3 (0.7 mmol, 0.200 g) and 3-chloroaniline (0.84 mmol, 0.103g). Yield: 46%, yellowish solid. ^1H NMR (500 MHz, CHLOROFORM-d) δ 9.05 (m, 1H), 8.96 (s, 1H), 8.06 (m, 2H), 7.63 (t, 1H), 7.61 (m, 1H), 7.41–7.34 (m, 3H), 7.10 (m, 2H), 7.05 (d, 1H, $J = 7.35$ Hz), 4.11 (s, 2H), 2.27–2.24 (m, 3H); ^{13}C NMR (126 MHz, CHLOROFORM-d) δ 172.40, 167.58 (d, $J = 244.5$ Hz), 149.01, 148.31, 145.85, 139.12, 136.84 (d, $J = 3.02$ Hz), 135.43, 135.32, 135.27, 132.57, 128.60, 126.85, 124.51, 122.88, 121.65, 120.43 (d, $J = 21.72$ Hz), 119.41, 27.28, 18.55; ^{19}F NMR (471 MHz, CHLOROFORM-d) δ -113.10 (s, 1F). m.p. = 206.8–208.1 °C. Formula: $\text{C}_{22}\text{H}_{17}\text{ClFN}_3\text{O}$; MS (ESI^+) m/z 394.105 ($\text{M} + \text{H}^+$).

N-(4-Chlorophenyl)-2-(2-(4-fluorophenyl)-6-methylimidazo[1,2-a]pyridin-3-yl)acetamide (14). The title compound was obtained using acid 3 (0.7 mmol, 0.200 g) and 4-chloroaniline (0.84 mmol, 0.103g). Yield: 23%, yellowish solid. ^1H NMR (500 MHz, CHLOROFORM-d) δ 8.16–8.13 (m, 1H), 7.85–7.82 (m, 1H), 7.75–7.72 (m, 2H), 7.57–7.52 (m, 1H), 7.47–7.45 (m, 1H), 7.42–7.39 (m, 2H), 7.26–7.23 (m, 2H), 7.18–7.15 (m, 1H), 4.19–4.14 (m, 2H), 2.41–2.38 (m, 3H). ^{13}C NMR (126 MHz, CHLOROFORM-d) δ 167.58 (d, $J = 244.5$ Hz), 149.01, 145.86, 139.13, 136.85 (d, $J = 3.0$ Hz), 135.52, 135.29, 132.58, 129.90 (d, $J = 7.8$ Hz), 129.18, 128.73, 123.30, 121.47, 120.95, 117.10, 116.11 (d, $J = 21.73$ Hz), 33.71, 18.54. ^{19}F NMR (471 MHz, CHLOROFORM-d) δ -112.32 (s, 1F). m.p. = 208.6–211.2 °C. Formula: $\text{C}_{22}\text{H}_{17}\text{ClFN}_3\text{O}$; MS (ESI^+) m/z 394.105 ($\text{M} + \text{H}^+$).

2-(2-(4-Fluorophenyl)-6-methylimidazo[1,2-a]pyridin-3-yl)-N-(O-tolyl)acetamide (15). The title compound was obtained using acid 3 (0.7 mmol, 0.200 g) and 2-methylaniline (0.84 mmol, 0.090g). Yield: 41%, yellowish solid. ^1H NMR (500 MHz, ACETONE-d_6) δ 8.23 (s, 1H), 7.96–7.89 (m, 2H), 7.64–7.57; (m, 1H), 7.43 (d, 1H, $J = 9.2$ Hz), 7.23–7.11 (m, 5H), 7.06–6.99 (m, 1H), 4.28 (s, 2H), 2.33–2.31 (m, 3H), 2.23 (s, 3H). ^{13}C NMR (126 MHz, ACETONE-d_6) δ 167.11, 161.24 (d, $J = 244.4$ Hz), 143.78, 142.96, 136.52, 131.73 (d, $J = 3.0$ Hz), 131.21, 130.38, 130.10 (d, $J = 7.8$ Hz), 127.33, 126.09, 125.31, 124.47, 122.19, 121.60, 116.51, 115.18 (d, $J = 21.7$ Hz), 114.69, 31.91, 17.39, 17.37. ^{19}F NMR (471 MHz, ACETONE-d_6) δ -113.17 (s, 1F). m.p. = 214.8–215.6 °C. Formula: $\text{C}_{23}\text{H}_{20}\text{FN}_3\text{O}$; MS (ESI^+) m/z 394.105 ($\text{M} + \text{H}^+$).

2-(2-(4-Fluorophenyl)-6-methylimidazo[1,2-a]pyridin-3-yl)-N-(M-tolyl)acetamide (16). The title compound was obtained using acid 3 (0.7 mmol, 0.200 g) and 3-methylaniline (0.84 mmol, 0.090g). Yield: 46%, yellowish solid. ^1H NMR (500 MHz, CHLOROFORM-d) δ 7.80 (s, 1H), 7.71 (dd, 2H, $J = 5.4,$

8.7 Hz), 7.57 (s, 1H), 7.52 (d, 1H, $J = 9.2$ Hz), 7.29 (s, 1H), 7.1–7.2 (m, 5H), 6.94 (d, 1H, $J = 7.3$ Hz), 4.10 (s, 2H), 2.36 (s, 3H), 2.30 (s, 3H). ^{13}C NMR (126 MHz, CHLOROFORM- d) δ ppm 166.5, 162.7 (d, $J = 248.0$ Hz), 144.5, 144.0, 139.1, 137.1, 130.0 (d, $J = 3.3$ Hz), 129.8 (d, $J = 8.2$ Hz), 128.9, 128.4, 125.7, 123.0, 120.9, 120.8, 117.2, 116.9, 115.9 (d, $J = 21.4$ Hz), 112.5, 33.6, 21.4, 18.4. ^{19}F NMR (471 MHz, CHLOROFORM- d) δ –113.30 (s, 1F). m.p. = 203.1–205.2 °C. Formula: $\text{C}_{23}\text{H}_{20}\text{FN}_3\text{O}$; MS (ESI $^+$) m/z 374.196 (M+H $^+$).

2-(2-(4-Fluorophenyl)-6-methylimidazo[1,2-*a*]pyridin-3-yl)-*N*-(*p*-tolyl)acetamide (17). The title compound was obtained using acid 3 (0.7 mmol, 0.200 g) and 4-methylaniline (0.84 mmol, 0.090 g). Yield: 35%, brownish solid. ^1H NMR (500 MHz, CHLOROFORM- d) δ 7.79 (s, 1H), 7.70–7.65 (m, 2H), 7.46 (d, 1H, $J = 9.2$ Hz), 7.30 (d, 2H, $J = 8.3$ Hz), 7.10–7.05 (m, 5H), 4.05 (s, 2H), 2.34–2.32 (m, 3H), 2.31–2.26 (m, 3H). ^{13}C NMR (126 MHz, CHLOROFORM- d) δ 166.64, 162.79 (d, $J = 248.1$ Hz), 144.48, 143.96, 139.08, 134.74 (d, $J = 3.0$ Hz), 129.92 (d, $J = 8.4$ Hz), 129.60, 128.58, 125.68, 123.12, 121.11, 120.41, 116.87, 115.99 (d, $J = 21.7$ Hz), 112.73, 33.54, 20.95, 18.52. ^{19}F NMR (471 MHz, CHLOROFORM- d) δ –115.2 (s, 1F). m.p. = 203.9–205.0 °C. Formula: $\text{C}_{23}\text{H}_{20}\text{FN}_3\text{O}$; MS (ESI $^+$) m/z 374.249 (M+H $^+$).

2-(2-(4-Fluorophenyl)-6-methylimidazo[1,2-*a*]pyridin-3-yl)-*N*-(2-methoxyphenyl)acetamide (18). The title compound was obtained using acid 3 (0.7 mmol, 0.200 g) and 2-methoxyaniline (0.84 mmol, 0.103 g). Yield: 25%, yellowish solid. ^1H NMR (500 MHz, ACETONE- d_6) δ 8.26–8.22 (m, 1H), 7.93 (br s, 1H), 7.84 (s, 1H), 7.75–7.73 (m, 2H), 7.56 (d, 1H, $J = 9.2$ Hz), 7.16–7.08 (m, 3H), 7.01–6.97 (m, 1H), 6.93–6.88 (m, 1H), 6.79–6.73 (m, 1H), 4.10 (s, 2H), 3.60 (s, 3H), 2.14 (s, 3H). ^{13}C NMR (126 MHz, ACETONE- d_6) δ 166.32, 162.81 (d, $J = 247.5$ Hz), 148.06, 144.49, 143.84, 130.21, 130.14, 128.53, 127.91, 126.91, 124.53, 122.94, 121.07, 120.02, 115.87 (d, $J = 21.1$ Hz), 114.16, 113.02, 110.07, 55.63, 29.79, 18.48. ^{19}F NMR (471 MHz, ACETONE- d_6) δ –114.42 (s, 1F). m.p. = 170.9–172.1 °C. Formula: $\text{C}_{23}\text{H}_{20}\text{FN}_3\text{O}_2$; MS (ESI $^+$) m/z 390.266 (M+H $^+$).

2-(4-Fluorophenyl)-3-(2-((3-methoxyphenyl)amino)-2-oxoethyl)-6-methylimidazo[1,2-*a*]pyridin-1-ium 3-carboxy-2,3-dihydroxypropanoate (19). The title compound was obtained first as a free base by reacting intermediate acid 3 (0.7 mmol, 0.200 g) with 3-methoxyaniline (0.84 mmol, 0.103 g). Yield 29%, yellowish solid. Next, the salt was prepared by stirring free base (1 equiv) with tartaric acid (1 equiv) in methanol for 1h and evaporating the solvent. ^1H NMR (500 MHz, METHANOL- d_4) δ 8.36 (s, 1H), 7.71 (dd, 2H, $J = 5.2, 8.8$ Hz), 7.65 (d, 1H, $J = 9.2$ Hz), 7.54 (dd, 1H, $J = 1.3, 9.2$ Hz), 7.3–7.3 (m, 3H), 7.2–7.2 (m, 1H), 7.07 (dd, 1H, $J = 1.1, 8.1$ Hz), 6.67 (ddd, 1H, $J = 0.8, 2.5, 8.3$ Hz), 4.49 (s, 2H), 4.23 (s, 2H), 3.74 (s, 3H), 2.43 (s, 3H). ^{13}C NMR (126 MHz, METHANOL- d_4) δ ppm 173.74, 167.41, 163.50 (d, $J = 248.3$ Hz), 160.26, 141.28, 139.39, 138.17, 132.33, 130.49 (d, $J = 8.7$ Hz), 129.35, 126.65 (d, $J = 2.4$ Hz), 125.38, 123.36, 116.21, 115.80 (d, $J = 21.9$ Hz), 113.13, 111.91, 109.63, 105.67, 100.00, 72.20, 54.34, 51.40, 30.74, 16.84. ^{19}F NMR (471 MHz, METHANOL- d_4) δ –113.63 (s, 1F). m.p. = 192.0–195.3 °C (free base). Formula: $\text{C}_{23}\text{H}_{20}\text{FN}_3\text{O}_2$; MS (ESI $^+$) m/z 390.157 (M+H $^+$).

2-(2-(4-Fluorophenyl)-6-methylimidazo[1,2-*a*]pyridin-3-yl)-*N*-(4-methoxyphenyl)acetamide (20). The title compound was obtained using acid 3 (0.7 mmol, 0.200 g) and 4-methoxyaniline (0.84 mmol, 0.103 g). Yield: 43%, beige solid. ^1H NMR (500 MHz, CHLOROFORM- d) δ 7.81 (s, 1H), 7.69

(dd, 2H, $J = 5.4, 8.7$ Hz), 7.61 (s, 1H), 7.48 (d, 1H, $J = 9.2$ Hz), 7.35 (d, 2H, $J = 9.0$ Hz), 7.13 (t, 2H, $J = 8.7$ Hz), 7.09 (dd, 1H, $J = 1.6, 9.2$ Hz), 6.83 (d, 2H, $J = 9.0$ Hz), 4.09 (s, 2H), 3.77 (s, 3H), 2.36 (s, 3H). ^{13}C NMR (126 MHz, CHLOROFORM- d) δ ppm 166.5, 162.7 (d, $J = 248.0$ Hz), 156.8, 144.4, 144.0, 130.2, 129.9 (d, $J = 3.1$ Hz), 129.8 (d, $J = 8.1$ Hz), 128.4, 123.0, 122.2, 120.9, 116.8, 115.9 (d, $J = 21.6$ Hz), 114.1, 112.5, 55.4, 33.4, 18.4. ^{19}F NMR (471 MHz, CHLOROFORM- d) δ –113.42 (s, 1F). m.p. = 206.8–208.1 °C. Formula: $\text{C}_{23}\text{H}_{20}\text{FN}_3\text{O}_2$; MS (ESI $^+$) m/z 390.432 (M+H $^+$).

2-(4-Fluorophenyl)-6-methyl-3-(2-oxo-2-((2-(trifluoromethyl)phenyl)amino)ethyl)imidazo[1,2-*a*]pyridin-1-ium 3-carboxy-2,3-dihydroxypropanoate (21). The title compound was obtained first as a free base by reacting intermediate acid 3 (0.7 mmol, 0.200 g) with 2-trifluoromethylaniline (0.84 mmol, 0.135 g). Yield 34%, pale orange solid. Next, the salt was prepared by stirring free base (1 equiv) with tartaric acid (1 equiv) in methanol for 1h and evaporating the solvent. ^1H NMR (500 MHz, DMSO- d_6) δ 10.12 (s, 1H), 8.18 (s, 1H), 7.83 (br dd, 2H, $J = 5.7, 8.5$ Hz), 7.73 (d, 1H, $J = 7.4$ Hz), 7.67 (t, 1H, $J = 7.6$ Hz), 7.4–7.6 (m, 3H), 7.26 (br t, 2H, $J = 8.8$ Hz), 7.14 (dd, 1H, $J = 1.4, 9.2$ Hz), 4.24 (s, 2H), 4.21 (s, 2H), 2.30 (s, 3H). ^{13}C NMR (126 MHz, DMSO- d_6) δ ppm 173.73, 169.06, 162.25 (d, $J = 248.1$ Hz), 143.53, 142.46, 135.67, 133.65, 131.60 (d, $J = 3.0$ Hz), 131.00, 130.2 (d, $J = 8.1$ Hz), 128.09, 127.63, 126.89, 125.20, 122.77, 121.62, 116.60, 115.90 (d, $J = 21.4$ Hz), 115.10, 100.00, 72.60, 31.43, 18.30. ^{19}F NMR (471 MHz, DMSO- d_6) δ –59.20 (s, 3F), –114.78 (s, 1F). m.p. = 210.9–212.9 °C. Formula: $\text{C}_{22}\text{H}_{17}\text{FN}_3\text{O}$; MS (ESI $^+$) m/z 428.213 (M+H $^+$).

2-(2-(4-Fluorophenyl)-6-methylimidazo[1,2-*a*]pyridin-3-yl)-*N*-(3-(trifluoromethyl)phenyl)acetamide (22). The title compound was obtained using acid 3 (0.7 mmol, 0.200 g) and 3-trifluoromethylaniline (0.84 mmol, 0.135 g). Yield: 54%, pale yellow solid. ^1H NMR (500 MHz, CHLOROFORM- d) δ 9.77 (s, 1H), 8.96 (d, 1H, $J = 7.2$ Hz), 7.93–7.91 (m, 1H), 7.77–7.76 (m, 2H), 7.63–7.60 (m, 2H), 7.48–7.45 (m, 1H), 7.31–7.28 (m, 1H), 7.10–7.07 (m, 3H), 4.05–3.98 (m, 2H), 3.49–3.44 (m, 3H). ^{13}C NMR (126 MHz, CHLOROFORM- d) δ 167.39, 162.71 (d, $J = 248.1$ Hz), 144.25, 143.78, 138.39, 131.42 (d, $J = 32.0$ Hz), 129.92, 129.85, 129.60, 128.61, 123.91 (q, $J = 272.1$ Hz), 123.22 (d, $J = 16.3$ Hz), 122.76, 121.27 (d, $J = 3.6$ Hz), 121.12, 117.06 (d, $J = 3.6$ Hz), 116.35, 115.84 (d, $J = 21.1$ Hz), 112.71, 33.11, 18.46. ^{19}F NMR (471 MHz, CHLOROFORM- d) δ –62.71 (s, 3F), –113.21 (s, 1F). m.p. = 210.9–213.0 °C. Formula: $\text{C}_{23}\text{H}_{17}\text{F}_4\text{N}_3\text{O}$; MS (ESI $^+$) m/z 428.213 (M+H $^+$).

2-(2-(4-Fluorophenyl)-6-methylimidazo[1,2-*a*]pyridin-3-yl)-*N*-(4-(trifluoromethyl)phenyl)acetamide (23). The title compound was obtained using acid 3 (0.7 mmol, 0.200 g) and 4-trifluoromethylaniline (0.84 mmol, 0.135 g). Yield: 44%, beige solid. ^1H NMR (500 MHz, CHLOROFORM- d) δ 8.04–8.00 (m, 1H), 7.79–7.77 (m, 1H), 7.67–7.61 (m, 2H), 7.60–7.56 (m, 2H), 7.54–7.49 (m, 3H), 7.14–7.09 (m, 3H), 4.13–4.07 (m, 2H), 2.37–2.31 (m, 3H). ^{13}C NMR (126 MHz, CHLOROFORM- d) δ 166.97, 162.84 (d, $J = 248.1$ Hz), 144.55, 144.00, 140.48, 129.99, 129.91, 129.84, 128.83, 126.37 (d, $J = 3.6$ Hz), 123.28, 122.77, 120.96, 119.81, 116.81, 116.05 (d, $J = 21.7$ Hz), 112.36, 33.46, 18.53. ^{19}F NMR (471 MHz, CHLOROFORM- d) δ –62.44 (s, 3F), –113.81 (s, 1F). m.p. = 228.1–229.2 °C. Formula: $\text{C}_{23}\text{H}_{17}\text{F}_4\text{N}_3\text{O}$; MS (ESI $^+$) m/z 428.337 (M+H $^+$).

2-(4-Fluorophenyl)-6-methylimidazo[1,2-*b*]pyridazine (24). A mixture of 2-bromo-1-(4-fluorophenyl)ethan-1-one (1.0 eq, 45.8 mmol, 9.94 g), sodium bicarbonate (1.5 eq, 68.7 mmol,

5.76 g) and 6-methylpyridazine-3-amine (1.0 eq, 45.8 mmol, 5.0 g) in toluene (50 mL) was heated for 12 h at 110 °C. After this time, the reactor was cooled to room temperature and depressurized. The reaction mixture was extracted three times with ethyl acetate and water. The organic phase was washed with brine, separated and dried over anhydrous sodium sulfate. The organic phase was concentrated under reduced pressure and purified using flash column chromatography using Hex/EtOAc (7/3, v/v) as eluent to provide compound 24 as yellow solid with 67% of yield. ¹H NMR (500 MHz, CHLOROFORM-*d*) δ 8.20 (m, 1H), 8.12 (m, 1H), 7.67 (d, 1H, *J* = 9.2 Hz), 7.11 (t, 2H, *J* = 8.8 Hz), 7.05 (dd, 2H, *J* = 1.3, 9.1 Hz), 2.32 (s, 3H). ¹³C NMR (126 MHz, CHLOROFORM-*d*) δ 163.92 (d, *J* = 248.7 Hz), 149.32 (d, *J* = 23.9 Hz), 145.13, 138.46, 134.16 (d, *J* = 3.9 Hz), 127.12, 126.96, 116.94 (d, *J* = 3.1 Hz), 112.37, 109.23, 22.08. ¹⁹F NMR (471 MHz, CHLOROFORM-*d*) δ -112.12 (s, 1F). Formula: C₁₃H₁₀FN₃; MS (ESI⁺) *m/z* 228.242 (M+H⁺).

2-(2-(4-Fluorophenyl)-6-methylimidazo[1,2-*b*]pyridazin-3-yl)acetic Acid (26). A solution of 2-(4-fluorophenyl)-6-methylimidazo[1,2-*b*]pyridazine (1.0 eq, 22 mmol, 5.0 g) and glyoxalic acid (2.6 eq, 57 mmol, 4.235 g) in dichloromethane was heated at 60 °C for 12 h. After this time, the solvent was evaporated under reduced pressure and the reaction mixture was extracted three times with dichloromethane and water. The organic phase was washed with brine, dried over anhydrous sodium sulfate, concentrated under reduced pressure. The intermediate 2-(2-(4-fluorophenyl)-6-methylimidazo[1,2-*b*]pyridazin-3-yl)-2-hydroxyacetic acid (25) was used directly to the next step without further purification. To a solution of an intermediate 25 (1. eq, 5 mmol, 1.5 g) in dry toluene (15 mL), iodine (1. eq, 5 mmol, 1.269 g) and triphenylphosphine (2.6 eq, 13 mmol, 3.410 g) were added and the resulting mixture was heated at 80 °C for 12 h. Next, the solvent was concentrated and the reaction mixture was extracted three times with ethyl acetate and aqueous solution of Na₂S₂O₃. The organic phase was rinsed with brine, separated and dried over anhydrous sodium sulfate, concentrated under reduced pressure and purified by flash chromatography using DCM/MeOH (6/4, v/v) as eluent to give 26 as beige solid with 32% of yield. ¹H NMR (500 MHz, CHLOROFORM-*d*) δ 10.24 (s, 1H), 8.16 (m, 1H), 8.04 (m, 2H), 7.15 (m, 1H), 6.92 (m, 2H), 4.26 (s, 2H), 2.08 (s, 3H). ¹³C NMR (126 MHz, CHLOROFORM-*d*) δ 170.22, 163.96 (d, *J* = 247.9 Hz), 148.41, 140.92, 136.13, 131.87, 130.12, 126.91, 122.90, 117.94, 115.92 (d, *J* = 21.1 Hz), 35.13, 21.34. ¹⁹F NMR (471 MHz, CHLOROFORM-*d*) δ -117.12 (s, 1F). Formula: C₁₅H₁₂FN₃O₂; MS (ESI⁺) *m/z* 286.332 (M+H⁺).

General Procedure for the Preparation of Final Amides (27-37). A mixture of 2-[2-(4-fluorophenyl)-6-methylimidazo[1,2-*b*]pyridazin-3-yl]acetic acid (26) (1.0 eq, 0.35 mmol), TBTU (2.0 eq, 0.7 mmol) and DIPEA (0.25 eq, 0.09 mmol) in DCM (3 mL) was stirred for 5 min at room temperature. After this time, an appropriately substituted amine (1.2 equiv) was added. The reaction was heated in a microwave reactor for 5 min at 30 °C (frequency: 2.45 GHz, 200 W). After this time, the reaction mixture was washed two times with water. The organic phase was washed with brine, then separated and dried over anhydrous sodium sulfate, concentrated under reduced pressure and purified via flash column chromatography using (Et₂O/DCM/MeOH, 2.0/7.5/0.5, v/v/v) as eluent.

3-(2-(Dimethylamino)-2-oxoethyl)-2-(4-fluorophenyl)-6-methylimidazo[1,2-*b*]pyridazin-1-ium 3-carboxy-2,3-dihydroxypropanoate (27). The title compound was obtained using acid 26 (0.35 mmol, 0.100 g) and dimethylamine (0.42

mmol, 0.21 mL as 2 M solution in THF). Yield: 30%, pale orange solid. Next, the salt was prepared by stirring free base (1 equiv) with tartaric acid (1 equiv) in methanol for 1 h and evaporating the solvent. ¹H NMR (500 MHz, METHANOL-*d*₄) δ 7.89 (d, 1H, *J* = 9.3 Hz), 7.82 (dd, 2H, *J* = 5.4, 8.9 Hz), 7.5–7.6 (m, 2H), 7.28 (t, 2H, *J* = 8.0 Hz), 7.21 (t, 2H, *J* = 8.8 Hz), 7.18 (d, 1H, *J* = 9.2 Hz), 7.1–7.1 (m, 1H), 4.51 (s, 2H), 4.23 (s, 2H), 2.57 (s, 3H). ¹³C NMR (126 MHz, METHANOL-*d*₄) δ ppm 173.52, 168.26, 163.03 (d, *J* = 246.8 Hz), 153.08, 142.19, 138.42, 137.63, 130.00 (d, *J* = 8.4 Hz), 129.60 (d, *J* = 3.3 Hz), 128.54, 124.04, 123.58, 120.24, 119.87, 119.34, 115.40 (d, *J* = 21.9 Hz), 72.14, 31.02, 20.39. ¹⁹F NMR (471 MHz, METHANOL-*d*₄) δ -115.62 (s, 1F). m.p. = 183.4–184.0 °C (free base). Formula: C₁₇H₁₇FN₄O; MS (ESI⁺) *m/z* 313.246 (M + H⁺).

2-(4-Fluorophenyl)-6-methyl-3-(2-oxo-2-(pyrrolidin-1-yl)ethyl)imidazo[1,2-*b*]pyridazin-1-ium 3-carboxy-2,3-dihydroxypropanoate (28). The title compound was obtained using acid 26 (0.35 mmol, 0.100 g) and pyrrolidine (0.42 mmol, 0.03 g). Yield: 35%, white solid. Next, the salt was prepared by stirring free base (1 equiv) with tartaric acid (1 equiv) in methanol for 1 h and evaporating the solvent. ¹H NMR (500 MHz, METHANOL-*d*₄) δ 7.89 (d, 1H, *J* = 9.3 Hz), 7.76 (dd, 2H, *J* = 5.3, 8.9 Hz), 7.2–7.3 (m, 3H), 4.51 (s, 2H), 4.17 (s, 2H), 3.74 (t, 2H, *J* = 6.8 Hz), 3.45 (t, 2H, *J* = 6.9 Hz), 2.57 (s, 3H), 2.05 (quin, 2H, *J* = 6.8 Hz), 1.9–2.0 (m, 2H). ¹³C NMR (126 MHz, METHANOL-*d*₄) δ ppm 173.48, 167.98, 163.10 (d, *J* = 247.0 Hz), 153.19, 141.53, 137.31, 130.02 (d, *J* = 8.2 Hz), 129.37 (d, *J* = 3.1 Hz), 123.32, 120.44, 119.94, 115.40 (d, *J* = 21.9 Hz), 72.13, 47.10, 46.05, 29.29, 25.75, 24.08, 20.41. ¹⁹F NMR (471 MHz, METHANOL-*d*₄) δ -115.24 (s, 1F). m.p. = 174.8–175.1 °C (free base). Formula: C₁₉H₁₉FN₄O; MS (ESI⁺) *m/z* 339.141 (M + H⁺).

2-(4-Fluorophenyl)-6-methyl-3-(2-morpholino-2-oxoethyl)imidazo[1,2-*b*]pyridazin-1-ium 3-carboxy-2,3-dihydroxypropanoate (29). Therefore, it was resynthesized in our study and investigated in terms of *in vitro* pharmacology. The title compound was obtained using acid 26 (0.35 mmol, 0.100 g) and morpholine (0.42 mmol, 0.037 g). Yield: 23%, beige solid. Next, the salt was prepared by stirring free base (1 equiv) with tartaric acid (1 equiv) in methanol for 1 h and evaporating the solvent. ¹H NMR (500 MHz, DMSO-*d*₆) δ 7.98 (d, 1H, *J* = 9.2 Hz), 7.79 (dd, 2H, *J* = 5.6, 8.9 Hz), 7.28 (t, 2H, *J* = 8.9 Hz), 7.11 (d, 1H, *J* = 9.2 Hz), 4.29 (s, 2H), 4.18 (s, 2H), 3.71 (br d, 2H, *J* = 4.4 Hz), 3.65 (br d, 2H, *J* = 4.4 Hz), 3.55 (br d, 2H, *J* = 5.2 Hz), 3.46 (br d, 2H, *J* = 5.1 Hz), 2.49 (s, 3H). ¹³C NMR (126 MHz, DMSO-*d*₆) δ ppm 173.66, 167.45, 162.40 (d, *J* = 244.7 Hz), 152.35, 142.02, 137.32, 131.30 (d, *J* = 3.0 Hz), 129.92 (d, *J* = 8.2 Hz), 125.10, 120.33, 119.65, 116.15 (d, *J* = 21.4 Hz), 72.69, 66.87, 66.81, 46.49, 42.61, 28.38, 21.9. ¹⁹F NMR (471 MHz, DMSO-*d*₆) δ -114.35 (s, 1F). m.p. = 169.8–172.0 °C. Formula: C₁₉H₁₉FN₄O₂; MS (ESI⁺) *m/z* 355.171 (M + H⁺).

2-(2-(4-Fluorophenyl)-6-methylimidazo[1,2-*b*]pyridazin-3-yl)-1-thiomorpholinoethan-1-one (30). The title compound was obtained using acid 26 (0.35 mmol, 0.100 g) and thiomorpholine (0.42 mmol, 0.043 g). Yield: 43%, white solid. ¹H NMR (CHLOROFORM-*d*, 500 MHz) δ 7.8–7.8 (m, 3H), 7.13 (t, 2H, *J* = 8.7 Hz), 6.92 (d, 1H, *J* = 9.2 Hz), 4.12 (s, 2H), 3.7–3.8 (m, 4H), 3.6–3.7 (m, 4H), 2.55 (s, 3H). ¹³C NMR (126 MHz, CDCl₃, δ): 167.53, 162.90 (d, *J* = 247.47 Hz), 151.90, 143.22, 137.52, 130.1 (d, *J* = 8.4 Hz), 124.72, 119.28, 119.07, 115.72 (d, *J* = 21.73 Hz), 67.05, 66.85, 46.70, 42.64, 28.25, 21.96. ¹⁹F NMR (471 MHz, METHANOL-*d*₄) δ

–115.31 (m, 1F). m.p.= 195.7–197.2 °C. Formula: C₁₉H₁₉FN₄OS; MS (ESI⁺) *m/z* 371.188 (M + H⁺).

2-(4-Fluorophenyl)-6-methyl-3-(2-oxo-2-(phenylamino)ethyl)imidazo[1,2-*b*]pyridazin-1-ium 3-carboxy-2,3-dihydroxypropanoate (31). The title compound was obtained using acid **26** (0.35 mmol, 0.100 g) and aniline (0.42 mmol, 0.039 g). Yield: 40%, beige solid. Next, the salt was prepared by stirring free base (1 equiv) with tartaric acid (1 equiv) in methanol for 1h and evaporating the solvent. ¹H NMR (500 MHz, METHANOL-*d*₄) δ 7.91 (d, 1H, *J* = 9.3 Hz), 7.85 (dd, 2H, *J* = 5.4, 8.9 Hz), 7.5–7.6 (m, 2H), 7.31 (t, 2H, *J* = 8.0 Hz), 7.24 (t, 2H, *J* = 8.8 Hz), 7.21 (d, 1H, *J* = 9.2 Hz), 7.1–7.1 (m, 1H), 4.54 (s, 2H), 4.26 (s, 2H), 2.60 (s, 3H). ¹³C NMR (126 MHz, METHANOL-*d*₄) δ ppm 173.52, 168.26, 163.03 (d, *J* = 246.8 Hz), 153.08, 142.19, 138.42, 137.63, 130.00 (d, *J* = 8.4 Hz), 129.60 (d, *J* = 3.3 Hz), 128.54, 124.04, 123.58, 120.24, 119.87, 119.34, 115.40 (d, *J* = 21.9 Hz), 72.14, 31.02, 20.39. ¹⁹F NMR (471 MHz, METHANOL-*d*₄) δ –115.40 (s, 1F). m.p.= 215.2–217.1 °C. Formula: C₂₁H₁₇FN₄O; MS (ESI⁺) *m/z* 361.292 (M + H⁺).

***N*-(2-Fluorophenyl)-2-(2-(4-fluorophenyl)-6-methylimidazo[1,2-*b*]pyridazin-3-yl)acetamide (32).** The title compound was obtained using acid **26** (0.35 mmol, 0.100 g) and 2-fluoroaniline (0.42 mmol, 0.047 g). Yield: 27%, yellowish solid. ¹H NMR (500 MHz, CHLOROFORM-*d*) δ 9.32 (br s, 1H), 8.38 (dt, 1H, *J* = 1.4, 8.2 Hz), 8.11–8.05 (m, 2H), 7.90 (d, 1H, *J* = 9.5 Hz), 7.27–7.25 (m, 2H), 7.13–7.06 (m, 4H), 4.19 (s, 2H), 2.74–2.71 (s, 3H). ¹³C NMR (126 MHz, CHLOROFORM-*d*) δ 167.22 163.11 (d, *J* = 247.5 Hz), 153.06, 152.96, 143.65, 137.72, 130.44, 130.34, 125.59, 124.73 (d, *J* = 3.6 Hz), 124.18 (d, *J* = 7.8 Hz), 121.37, 119.29, 117.88, 115.92 (d, *J* = 21.7 Hz), 114.79, 114.62, 33.97, 21.75. ¹⁹F NMR (471 MHz, CHLOROFORM-*d*) δ –130.74 (s, 1F), –113.38 (s, 1F). m.p.= 180.3–182.0 °C. Formula: C₂₁H₁₆F₂N₄O; MS (ESI⁺) *m/z* 379.235 (M + H⁺).

***N*-(3-Fluorophenyl)-2-(2-(4-fluorophenyl)-6-methylimidazo[1,2-*b*]pyridazin-3-yl)acetamide (33).** The title compound was obtained using acid **26** (0.35 mmol, 0.100 g) and 3-fluoroaniline (0.42 mmol, 0.047 g). Yield: 37%, yellowish solid. ¹H NMR (500 MHz, CHLOROFORM-*d*) δ 9.13–9.10 (m, 1H), 8.05–8.02 (m, 2H), 7.92 (d, 1H, *J* = 9.2 Hz), 7.42 (td, 1H, *J* = 2.3, 11.0 Hz), 7.25–7.22 (m, 3H), 7.18–7.15 (m, 1H), 7.03 (d, 1H, *J* = 9.2 Hz), 6.79 (dt, 1H, *J* = 2.3, 8.3 Hz), 4.24–4.22 (m, 2H), 2.84–2.71 (s, 3H). ¹³C NMR (126 MHz, CHLOROFORM-*d*) δ 167.04, 163.16 (d, *J* = 248.1 Hz), 163.09 (d, *J* = 245.06 Hz), 152.52, 143.87, 137.85, 130.35 (d, *J* = 8.5 Hz), 130.22 (d, *J* = 9.0 Hz), 125.81, 119.12, 117.93 (d, *J* = 6.6 Hz), 115.98 (d, *J* = 21.1 Hz), 114.78 (d, *J* = 2.41 Hz), 111.12, 111.01, 107.23, 107.04, 33.88, 22.05. ¹⁹F NMR (471 MHz, CHLOROFORM-*d*) δ –113.8 (s, 1F), –111.3 (s, 1F). m.p.=184.9–185.1 °C. Formula: C₂₁H₁₆F₂N₄O; MS (ESI⁺) *m/z* 379.321 (M + H⁺).

***N*-(4-Fluorophenyl)-2-(2-(4-fluorophenyl)-6-methylimidazo[1,2-*b*]pyridazin-3-yl)acetamide (34).** The title compound was obtained using acid **26** (0.35 mmol, 0.100 g) and 4-fluoroaniline (0.42 mmol, 0.047 g). Yield: 41%, brownish solid. ¹H NMR (500 MHz, CHLOROFORM-*d*) δ 8.88 (s, 1H), 8.08–8.03 (m, 2H), 7.93 (d, 1H, *J* = 9.5 Hz), 7.44–7.41 (m, 2H), 7.26–7.21 (m, 2H), 7.03–7.00 (m, 3H), 4.15 (s, 2H), 2.75–2.71 (s, 3H). ¹³C NMR (126 MHz, CHLOROFORM-*d*) δ 166.91, 163.0 (d, *J* = 248.1 Hz), 159.21 (d, *J* = 243.9 Hz), 152.47, 143.85, 137.80, 134.07 (d, *J* = 3.0 Hz), 132.21, 132.15, 130.31 (d, *J* = 7.8 Hz), 129.45 (d, *J* = 3.0 Hz), 128.68,

128.59, 125.71, 121.31 (d, *J* = 7.8 Hz), 119.13, 118.14, 115.83 (t, *J* = 21.7 Hz), 115.7 (d, *J* = 21.7 Hz), 33.66, 22.07. ¹⁹F NMR (471 MHz, CHLOROFORM-*d*) δ –117.75 (s, 1F), –113.19 (s, 1F). m.p.= 183.5–184.1 °C. Formula: C₂₁H₁₆F₂N₄O; MS (ESI⁺) *m/z* 379.345 (M + H⁺).

2-(2-(4-Fluorophenyl)-6-methylimidazo[1,2-*b*]pyridazin-3-yl)-*N*-(2-methoxyphenyl)acetamide (35). The title compound was obtained using acid **26** (0.35 mmol, 0.100 g) and 2-methoxyaniline (0.42 mmol, 0.052 g). Yield: 43%, white solid. ¹H NMR (500 MHz, CHLOROFORM-*d*) δ 8.95–8.94 (m, 1H), 8.31 (dd, 1H, *J* = 1.6, 8.2 Hz), 8.13 (s, 2H), 7.88 (d, 1H, *J* = 9.2 Hz), 7.25–7.24 (m, 2H), 7.03–7.00 (m, 2H), 6.98–6.94 (m, 1H), 6.83 (dd, 1H, *J* = 1.4, 8.0 Hz), 4.23 (s, 2H), 3.79 (s, 3H), 2.70 (s, 3H). ¹³C NMR (126 MHz, CHLOROFORM-*d*) δ 166.91, 163.03 (d, *J* = 247.5 Hz), 152.17, 148.10, 143.52, 137.73, 130.24 (d, *J* = 8.5 Hz), 129.75 (d, *J* = 3.02 Hz), 127.67, 125.24, 124.09, 121.20, 120.41, 118.99, 118.47, 115.87 (d, *J* = 21.7 Hz), 110.19, 55.76, 33.82, 21.93. ¹⁹F NMR (471 MHz, CHLOROFORM-*d*) δ –113.51 (s, 1F). m.p.= 162.6–163.1 °C. Formula: C₂₂H₁₉FN₄O₂; MS (ESI⁺) *m/z* 391.199 (M + H⁺).

2-(2-(4-Fluorophenyl)-6-methylimidazo[1,2-*b*]pyridazin-3-yl)-*N*-(3-methoxyphenyl)acetamide (36). The title compound was obtained using acid **26** (0.35 mmol, 0.100 g) and 3-methoxyaniline (0.42 mmol, 0.052 g). Yield: 40%, white solid. ¹H NMR (500 MHz, CHLOROFORM-*d*) δ 8.92 (s, 1H), 8.05–8.04 (m, 2H), 7.90 (d, 1H, *J* = 9.2 Hz), 7.27 (t, 1H, *J* = 2.1 Hz), 7.25 (m, 1H), 7.23–7.21 (m, 2H), 7.01 (d, 1H, *J* = 9.2 Hz), 6.96–6.93 (m, 1H), 6.62 (ddd, 1H, *J* = 0.7, 2.4, 8.3 Hz), 4.10 (s, 2H), 3.85–3.84 (m, 3H), 2.71 (s, 3H). ¹³C NMR (126 MHz, CHLOROFORM-*d*) δ 166.93, 163.10 (d, *J* = 248.1 Hz), 160.28, 152.38, 143.84, 139.27, 137.70, 132.13, 130.31 (d, *J* = 7.8 Hz), 129.85, 129.52 (d, *J* = 3.0 Hz), 128.59, 125.67, 119.03, 118.19, 115.94 (d, *J* = 21.7 Hz), 111.66, 110.17, 105.43, 55.40, 33.94, 22.05. ¹⁹F NMR (471 MHz, CHLOROFORM-*d*) δ –113.21 (s, 1F). m.p.= 169.3–169.7 °C. Formula: C₂₂H₁₉FN₄O₂; MS (ESI⁺) *m/z* 391.337 (M + H⁺).

2-(2-(4-Fluorophenyl)-6-methylimidazo[1,2-*b*]pyridazin-3-yl)-*N*-(4-methoxyphenyl)acetamide (37). The title compound was obtained using acid **26** (0.35 mmol, 0.100 g) and 3-methoxyaniline (0.42 mmol, 0.052 g). Yield: 21%, yellowish solid. ¹H NMR (CHLOROFORM-*d*, 500 MHz) δ 8.71 (s, 1H), 8.13–8.10 (m, 2H), 7.91 (d, 1H, *J* = 9.2 Hz), 7.40–7.33 (m, 2H), 7.24–7.23 (m, 2H), 7.01 (d, 1H, *J* = 9.5 Hz), 6.86–6.84 (m, 2H), 4.15 (s, 2H), 3.72 (s, 3H), 2.71 (s, 3H). ¹³C NMR (126 MHz, CHLOROFORM-*d*) δ 166.69, 163.12 (d, *J* = 247.5 Hz), 156.44, 152.35, 143.79, 137.79, 131.17, 130.33 (d, *J* = 8.4 Hz), 129.54 (d, *J* = 3.0 Hz), 125.66, 121.32, 118.99, 118.40, 115.93 (d, *J* = 21.7 Hz), 114.29, 55.52, 33.63, 22.01. ¹⁹F NMR (471 MHz, CHLOROFORM-*d*) δ –113.31 (s, 1F). m.p.= 197.3–197.8 °C. Formula: C₂₂H₁₉FN₄O₂; MS (ESI⁺) *m/z* 391.139 (M + H⁺).

2-(2-(4-Fluorophenyl)-6-methylimidazo[1,2-*a*]pyridazin-3-yl)-*N,N*-dimethylacetamide (40). A solution of 5-methylpyridazin-2-amine (1 eq, 4.6 mmol, 1 g) and 2-bromo-1-(4-fluorophenyl)ethan-1-one (1 eq, 4.6 mmol, 2 g) in acetonitrile (30 mL) was stirred at 80 °C overnight. Subsequently, the acetonitrile was evaporated, and the crude mixture diluted with dichloromethane was washed twice with a sodium carbonate (saturated solution) and dried over sodium sulfate. The solvent was then evaporated, and the resultant product **38** was isolated after the purification by column chromatography (Hexane: EtOAc, 7/3, v/v). Yield 56% yield, brownish solid. The product's spectra were consistent with those previously

reported.¹⁰² Next, a mixture of compound **38** (1 eq, 2.22 mmol, 0.5 g), *N,N*-dimethyl-2-oxoacetamide (2.5 eq, 5.55 mmol, 0.561 g), and acetic acid (0.5 mL) in toluene (2 mL) was stirred at 60 °C for 1 h in a CEM-Discover system at a frequency of 2.445 GHz with continuous irradiation power ranging from 0 to 200 W. The system was cooled and depressurized, and the reaction mixture was washed twice with dichloromethane and water, dried over sodium sulfate, and the solvent evaporated. The resulting intermediate (**39**) was used directly in the subsequent step without purification. Thus, **39** was combined with phosphorus tribromide (2.6 eq, 0.8 mmol, 0.08 mL) in THF (2 mL) and irradiated at 45 °C for 45 min in the CEM-Discover system (frequency: 2.445 GHz, power from 0 to 200 W). After cooling, the mixture was treated with hexane, water, and aqueous sodium bicarbonate (saturated solution), extracted with ethyl acetate, dried over sodium sulfate, and the solvent evaporated. Purification through column chromatography (DCM: MeOH, 9S/5, v/v) yielded the final product (**40**) as a pale-yellow oil with a 37% yield. ¹H NMR (500 MHz, METHANOL-*d*₄) δ 8.5–8.5 (m, 1H), 8.45 (d, 1H, *J* = 2.3 Hz), 7.6–7.6 (m, 2H), 7.20 (t, 2H, *J* = 8.9 Hz), 4.19 (s, 2H), 3.16 (s, 3H), 2.98 (s, 3H), 2.38 (s, 3H).¹³ C NMR (126 MHz, METHANOL-*d*₄) δ ppm 169.1, 163.0 (d, *J* = 246.9 Hz), 152.8, 147.1, 143.2, 130.8, 130.2 (d, *J* = 7.8 Hz), 129.7 (d, *J* = 3.0 Hz), 118.8, 115.4 (d, *J* = 22.3 Hz), 114.0, 36.5, 34.8, 28.4, 13.9. Formula: C₁₇H₁₇FN₄O; MS (ESI⁺) *m/z* 313.246 (M + H⁺).

Radioligand Binding and Functional Studies. *Determination of Affinity for GABA-A Receptor.* The study was acquired according to the earlier protocols,^{69,101} performed in duplicates. The rats' brains were homogenized and prepared accurately according to the previous protocol. The assay was performed directly on 96-well microplates, which enclosed 50 mM Tris-HCl buffer (pH 7.4) in a total volume of 300 μL. Reaction mix included 240 μL of the brain tissue suspension, 30 μL of [3H]-muscimol, and 30 μL solution of tested compounds (administered at concentrations: 10⁻¹⁰–10⁻⁵ M). To establish possible nonspecific binding, 100 μM GABA was added. The 96-well microplates enclosing the reaction mix were incubated for 10 min at 0 °C, followed by rapid filtration over glass fiber filters FilterMate B (PerkinElmer, USA) with the use of the Harvester-96 MACH III FM (Tomtec, USA). The filter mats were gently dried using a microwave and inserted to a plastic bag (PerkinElmer, USA). Next, they were soaked in 10 mL of Ultima Gold MV liquid scintillation cocktail (PerkinElmer, USA). Afterward, the radioactivity present on the filter was quantified using a MicroBeta TriLux 1450 scintillation counter (PerkinElmer, USA). *K_i* values were estimated according to the Cheng and Prusoff equation. The statistical analysis was performed using (GraphPad Prism, version 4.0, San Diego, CA, USA).

Electrophysiological Studies. To determine the interaction of tested molecules with hERG channel, a method previously described was used.^{69,101} The PAM assay at α1β2γ2 GABA-A receptors was performed on HEK293 cells with a stable expression of the human α1β3γ2 GABA-A receptor according to previously described protocols.^{69,101} The α2/β3/γ2 GABA-A, α3/β3/γ2 GABA-A, and α5/β3/γ2 GABA-A IonFlux PAM assays were performed at Eurofins Discovery according to well-established protocols, which can be found on the company's Web site at www.eurofinsdiscoveryservices.com.

ADMET and Thermodynamic Solubility. *PAMPA.* Pre-coated PAMPA Plate System Gentest was obtained from Corning, (Tewksbury, MA, USA). It consists of 96-well receiver

filter plate that has been pre-coated with structured layers of phospholipids and a matched donor microplate. The stock solutions of tested compounds and reference drugs were diluted in the PBS buffer (pH 7.4) to the final concentration 100 μM. The compounds were applied into the donor wells (200 μL) and incubated (5 h) at RT. By using the UPLC-MS spectrometry (Waters ACQUITY TQD system with the TQ Detector, Waters, Milford, USA) with an internal standard the exact quantity of molecules that penetrated from donor to acceptor wells through phospholipid membrane was estimated. The permeability coefficients (*P_e*, cm/s) were calculated using the formula provided by the PAMPA Plate System manufacturer.¹⁰³

Thermodynamic Solubility in Phosphate Buffer pH = 7.4.

All the quantitative measurements were recorded on Waters Alliance e2695 Separations Module (Waters, Milford, CT, USA) containing a 2998 Photodiode Array (PDA) detector (Waters, Milford, CT, USA) and the Chromolith SpeedROD RP-18e 50–4.6 mm column (Merck, KGaA, Darmstadt, Germany). The conditions were as the following: temperature of the column: 30 °C; eluents: eluent A (water/0.1% formic acid), eluent B (MeCN/0.1% formic acid). The analysis was performed at a flow rate of 0.5 mL/min, with a gradient from 0 to 100% B over 3 min. Each sample was injected in a volume of 10 μL and analyzed in triplicate. The calibration curve was obtained by measuring the AUC for each compound at various concentrations, ranging from 2 to 0.250 mg/mL, dissolved in methanol. The spectra were analyzed at the maximum absorbance wavelength for each compound. The tested compounds (2 mg) were dissolved in 1 mL of Dulbecco's phosphate-buffered saline (DPBS) and agitated continuously at 20 °C for 24 h. Subsequently, the solutions were filtered through a cellulose acetate syringe filter (pore size: 0.22 μm) and transferred to a chromatographic HPLC to measure the AUC. Solubility, given in mg/mL, was calculated using the calibration curves.

Metabolic Stability. In Eppendorf tubes, the following were placed: potassium phosphate buffer (pH 7.4), working solution of the compound under investigation, and human liver microsomes (final concentration 0.4 mg/mL, Sigma-Aldrich). The resulting mixture was incubated with shaking in a thermoblock at 37 °C for 15 min. Subsequently, the NADPH regeneration system (Sigma-Aldrich) was added to the incubation mixture. The samples were then incubated with shaking at 37 °C over various time intervals (5, 15, 30, 60, 90, 120, 150, 180, 210, and 240 min). A control experiment was conducted in parallel, where phosphate buffer was added in place of the regeneration fraction. After the designated incubation time, an internal standard (levallorphan, Sigma-Aldrich) was added to the samples. Then, 70% perchloric acid (Sigma-Aldrich) was added to each sample, followed by centrifugation for 10 min at 4 °C at 6000 rpm. Subsequently, the supernatant from each sample was collected and subjected to LC-MS/MS analysis. Each sample was analyzed in duplicate.

A-B and B-A permeability (MDR1-MDCKII) assay was performed by Eurofins Pharma Discovery Services according to previously reported methods.¹⁰⁴ **Plasma protein binding** assay was performed by Eurofins Pharma Discovery Services according to previously reported methods.¹⁰⁵ **Brain tissue binding** assay was performed by Eurofins Pharma Discovery Services according to well-established protocols, which can be found on the company's Web site at www.eurofinsdiscoveryservices.com.

Cytotoxicity. Neurotoxicity was assessed using human neuroblastoma cells (SH-SY5Y) obtained from American Type Culture Collection (ATCC). The cells were cultured in Dulbecco's Modified Eagle's Medium—high glucose, (DMEM, Thermo Fisher) supplemented with 10% fetal bovine serum (Thermo Fisher), with added 100 IU/ml penicillin (Merck) and 100 $\mu\text{g}/\text{mL}$ streptomycin (Merck). The cells were cultured in flasks with an area of 75 cm^2 (Nunc), and incubated at 37 °C, 5% CO_2 . For the test of compounds with the SH-SY5Y cells line, neuronal cells were seeded on 96-well culture plate (Falcon) at a density of 2×10^4 cells per well for measurement caspase-3/7 activity. The cells were grown for 24 h in the incubator (37 °C, 5% CO_2) before performing experiments. Cell viability was evaluated using Presto Blue reagent (ThermoFisher), according to the manufacturer procedures. Following 24 h of incubation with the tested molecule, PrestoBlue reagent was added to a microplate well in an amount equal to one tenth of the remaining medium volume. The resulting mixture was incubated for 15 min at 37 °C, and the fluorescence intensity (EX 530; EM 580 nm) was measured in the plate reader POLARstar Omega, (BMG Labtech). The results (viability values) are provided as a percentage of live cells with respect to DMSO (control sample). The results of the experiment were imaged using 10 \times magnification with the ImageXpress Micro XLS (Molecular Devices). Hepatotoxicity asses was performed as previously described.⁵⁰

In Vitro Pharmacology. Cell Preparation. The mouse neuroblastoma cells (N2A) were cultured in Dulbecco's Modified Eagle's Medium—high glucose, (DMEM, GlutaMx ThermoFisher) supplemented with 10% fetal bovine serum heat inactivated (ThermoFisher), with added 100 IU/ml penicillin (Merck) and 100 $\mu\text{g}/\text{mL}$ streptomycin (Merck). The cells were cultured in flasks with an area of 175 cm^2 (Nunc), and incubated at 37 °C, 5% CO_2 . For the test of compounds with the N2A cells line, neuronal cells were seeded on 96-well culture plate (Falcon) at a density of 3×10^4 cells per well for measurement cell membrane damage in OGD models and 2×10^4 cells per well for measurement toxicity of tested compounds. The cells were grown for 24 h in the incubator (37 °C, 5% CO_2) before performing experiments. Human induced pluripotent stem cell iPSC-derived GABAergic neurons (iCell GABANeurons) were purchased from FUJIFILM Cellular Dynamics. iCell GABA-Neurons were plated at a density of 3.5×10^4 cells per well in 96-well plates (BlackView, Plate, PerkinElmer) coated with poly L-ornithine (0,01%) and laminin (3.3 $\mu\text{g}/\text{mL}$) (Merck) in the iCell Neurons Maintenance Medium (Cellular Dynamics International) at 37 °C and 5% CO_2 . The cells were maintained according to the manufacturer's instructions. Media were changed every 3 days until the day of the assay. iCell GABANeurons were allowed to form neuronal networks in 96-plates for 8 days. After this time, the neuroprotective effect of the tested compound in response to neuronal damage with glutamate was checked. **Preparation of the solutions of the tested compounds.** Stock solutions of tested molecules were prepared in the concentration of 10^{-2} M. Minimum 1 mg of each tested compound was weighed and dissolved in appropriate volume of dimethyl sulfoxide. Serial dilutions were prepared in DMSO and then the diluted compounds were transferred to PBS, mixed and put to medium with adherent cells. Before assays eventual precipitation or opalescence was checked. **Oxygen—glucose deprivation (OGD) model.** The N2A cells were incubated in serum and glucose-free MEM media (ThermoFisher) after two washes with HBSS buffer (Thermo-

Fisher) and transferred into the anaerobic chamber (MIC-101) with an atmosphere of 0.5% CO_2 and 99.5% N_2 . The MIC-101 chamber was placed in an incubator at 37 °C for 4 h. After OGD exposure, the tested compounds were added and N2A cells were continued to be cultured in DMEM containing glucose and serum (ThermoFisher) under normoxic condition for reoxygenation for 24. Control cell cultures were not deprived of oxygen and glucose and always placed in norm-oxygenated DMEM containing glucose. The assessment of cell membrane damage. **Cell membrane damage after OGD was measured** using the bioluminescent ToxiLight bioassay (Lonza), a cytotoxicity highly sensitive assay. After 24 h of treatments, 5 μL of the clear fluid above a sediment was transferred into 384-well plate (PerkinElmer). Then 20 μL of the Adenylate Kinase Detection Reagent (AKDR) was added. The luminescence was measured after 10 min of incubation with a plate reader POLARstar Omega, (BMG Labtech). The results are expressed as a percentage of control (OGD), which corresponds to the percentage of dead cells with respect to the control sample. **Neurotoxicity induced by glutamate.** The iCell GABANeurons were pretreated with tested compound at a concentration of 10 μM or vehicle (0.1% DMSO, v/v) for 1 h. After this time the cells were incubated with glutamate (1 mM) for 3 h. The cells were stained with Hoechst 33342,¹⁰⁶ Mitotracker to detect mitochondrial potential or Calcein AM.¹⁰⁷ The mitochondrial membrane potential of cells was measured with the use of the MitoTracker probes contain a mildly thiol-reactive chloromethyl moiety (ThermoFisher). The fluorescent dye, stains mitochondria in live cells and its accumulation is dependent upon membrane potential. After end of treatments, medium was removed and cells were incubated with DMEM FluoroBrite (ThermoFisher) contain 100 nM Mitotracker and 2 $\mu\text{g}/\text{mL}$ Hoechst 33342. The results are expressed as a percentage of control (DMSO). The fluorescence intensity was measured in the ImageXpress Micro XLS (Molecular Devices). **The concentration of intracellular Ca^{2+}** were tested using the homogeneous cell-based assays with calcium Fluo-4 Direct Calcium Assay Kits (ThermoFisher). After end of incubation with tested compounds, the supernatant was removed and cells were incubated with Fluo-4/AM (1 μM) in DMEM FluoroBrite (ThermoFisher) for 1 h at 37 °C. The results are expressed as a percentage of control (DMSO). The fluorescence intensity was measured in the ImageXpress Micro XLS (Molecular Devices). **Caspase-3/7 activity assay.** After pretreatment with tested compounds (50 μM) or vehicle (0.5% DMSO, v/v) for 1 h, the iCell GABANeurons were incubated with 6-OHDA in concentration 400 μM for 2 h. The activity of caspase 3/7 were measured using Caspase-Glo 3/7 (Promega). The assay provides a luminogenic caspase-3/7 substrate, which contains the tetrapeptide sequence DEVD (Asp—Glu—Val—Asp) in reagent optimized for caspase activity, luciferase activity and cell lysis. After the incubation, to the tested compounds, 100 μL of Caspase-Glo 3/7 reagent were added to the assay plates. The whole content was incubated for 1 h at 22 °C. The results are expressed as a percentage of control (6-OHDA). Luminescence were measured in a multifunction plate reader (POLARstar Omega, BMG Labtech). **Neurite outgrowth assay.** After inducing neurotoxicity on iCell GABANeurons with glutamate (1 mM) described above, neuronal networks were visualized with labeled calcein AM (ThermoFisher). Image analysis was performed using the MetaXpress software Neurite Outgrowth Application Module in Image High Content Screening System. Following incubation of the cells with test compounds, medium

was removed and cells were incubated with DMEM FluoroBrite (ThermoFisher) contain 0,5 μM Calcein AM and 2 $\mu\text{g}/\text{mL}$ Hoechst 33342. The Calcein AM signal was used to measure neurite outgrowth, cell viability, and a variety of morphology parameters. Hoechst 33342 was utilized to measure total cell count and nuclear shape. After a 1h incubation the images were acquired using the ImageXpress Micro XLS (Molecular Devices).

Pharmacokinetic Study. A group of 72 adult male rats (Wistar, 200–220 g) were used in the experiment. The animals were purchased from the Animal House at the Faculty of Pharmacy, Jagiellonian University Medical College, Krakow, Poland. During the habituation period, groups of 4 rats were housed in a plastic cage (253 mm \times 166 mm \times 148 mm) under controlled conditions, including room temperature (22 ± 2 °C), humidity ($55 \pm 10\%$), and full-spectrum cold white light (350–400 lx). The light/dark cycle was 12 h, with lights on at 7:00 a.m. and off at 7:00 p.m. The rats had free access to standard laboratory pellets and tap water. The tested compound was dissolved in saline were administered by intravenous (*i.v.*) and intraperitoneal (*i.p.*) route at a dose of 3 mg/kg. Blood samples were collected at 0 min (predose), 5 min, 15 min, 30 min, 60 min, 120 min, 240 and 480 min after compound administration. The blood and brain samples were collected under general anesthesia induced by *i.p.* injection of 50 mg/kg ketamine plus 8 mg/kg xylazine. The blood samples were taken into heparinized tubes, immediately centrifuged at 3000xg for 10 min, and plasma was collected. The plasma and brain samples were immediately frozen at -80 °C. All experimental procedures were carried out in accordance with EU Directive 2010/63/EU and approved by the I Local Ethics Committee for Experiments on Animals of the Jagiellonian University in Krakow, Poland (approval number: 83/2018). Pharmacokinetic parameters were calculated by a noncompartmental approach from the average concentration values, using Phoenix WinNonlin software (Certara, Princeton, NJ 08540 USA). First order elimination rate constant (λ_z) was calculated by linear regression of time versus log concentration as previously described.¹⁰¹ The LC/ESI-MS/MS experiments were performed on an ABSciex (Concord, Ontario, Canada) API 3200 triple quadrupole mass spectrometer equipped with an electrospray (ESI) ionization interface. This instrument was coupled to Elite LaChrom (Merck, Germany) HPLC system. Data acquisition and processing were accomplished using ABSciex Analyst 1.5.2 data collection and integration software as previously described.¹⁰¹ Statistical analysis for *in vitro* pharmacology studies was performed using GraphPad Prism 8.0. All values are expressed as mean with SD. Differences among groups were evaluated by One-Way ANOVA followed by posthoc analysis (Dunnett's multiple comparison tests) and were considered statistically significant if $p < 0.05$ (* $p < 0.05$, ** $p < 0.01$, *** $p < 0.001$, **** $p < 0.0001$).

In Vivo Pharmacology. Open Field Test. The experiments were performed on male Sprague–Dawley rats (260–320g) obtained from an accredited animal facility at the Jagiellonian University Medical College, Poland. The animals were housed in group of two in controlled environment (ambient temperature 21 ± 2 °C; relative humidity 50–60%; 12-h light/dark cycles (lights on at 8:00). Standard laboratory food (LSM-B) and filtered water were freely available. Animals were assigned randomly to treatment groups. The experiments were performed between 9:00 and 14:00 on separate groups of animals. All animals were used only once. Procedures involving animals and their care were conducted in accordance with

current European Community and Polish legislation on animal experimentation. Additionally, all efforts were made to minimize animal suffering and to use only the number of animals necessary to produce reliable scientific data. The animals were housed in pairs in a controlled environment (ambient temperature 21 ± 2 °C; relative humidity $55 \pm 10\%$, 12-h light/dark cycles, with luminosities on at 8:00 a.m.). Animals had access to standard laboratory food (LSM-B) and tap water ad libitum. The groups of animals ($n = 8$) were randomly assigned to treatment conditions, and experiments were conducted between 9:00 a.m. and 2:00 p.m. on separate sets of animals. Each animal was used only a single time. Efforts were made to minimize animal suffering and to use only the number of animals necessary to obtain reliable scientific data. The experimental protocols and procedures described in this work were approved by the I Local Ethics Commission in Cracow (no 794/2023) and complied with the European Communities Council Directive of 24 November 1986 (86/609/EEC) and were in accordance with the 1996 NIH Guide for the Care and Use of Laboratory Animals. The tested compound was dissolved in saline immediately before administration to the animals in a volume of 2 mL/kg. Compound 4 was administered intraperitoneally (*i.p.*) 60 min before testing. Control animals received the vehicle (0.9% NaCl) according to the same schedule. The study was conducted in a dimly lit room using the Motor Monitor System (Campden Instruments, Ltd., UK), which comprised four Smart Frame Open Field stations (40 \times 40 \times 38 cm) with 16 \times 16 beams. These stations were located in soundproof and faintly lit (40 lx) chambers and connected to a PC software by a control unit. Thirty minutes before testing, individual animals injected intraperitoneally (*i.p.*) with either vehicle or drug were gently transferred into the observation chambers to avoid hyperactivity due to the novel environment. The ambulations (in X and Y axes) and the total distance (in cm) traversed by a rat for 60 min were recorded by an automated Motor Monitor System. The data from open field studies were evaluated by one-way ANOVA followed by Bonferroni's post hoc test (statistical significance set at $p < 0.05$).

Model of Focal Cerebral Ischemia. All experiments were performed on male Sprague–Dawley rats (280–320 g purchased from an accredited animal facility at the Jagiellonian University Medical College, Poland). The animals were randomly allocated into the following groups: sham, MCAO, sham+tested compound, MCAO+ tested compound ($n = 8$). The compound was administrated *i.p.* 1,5 h after the reperfusion (3h from the ischemia onset, once daily for 3 days). The animals were maintained on a normal day-night cycle at 22 ± 2 °C with free access to food and water. The experimental protocols were performed in accordance with the Guide for the Care and Use of Laboratory Animals published by the National Institutes of Health and were approved by the First Local Ethics Committee at Jagiellonian University in Krakow (permit no: 486/2021). 90 min MCAO was induced following a protocol similar to Longa et al. (1989).¹⁰⁸ Surgical procedures were executed under a stereoscopic microscope (Leica, A60F, Germany). To maintain physiological body temperature, a heating blanket (Homeothermic Blanket System, Harvard Apparatus) was used. Arterial occlusion was verified with a laser speckle contrast analysis system (PeriCam HR PSI, Perimed, Sweden), considering a minimum of 70% reduction in blood flow in the MCA region as indicative of a successful occlusion. Anesthesia was induced with 5% isoflurane and maintained with 2.5% isoflurane. The surgery involved exposing the left external carotid artery (ECA), internal

carotid artery (ICA), and common carotid artery (CCA). Initially, branches of the ECA were coagulated, followed by the application of microvascular clips to the ECA, ICA, and CCA. A silicone-coated filament (Doccol, USA) was then inserted into the ECA and advanced until a significant blood flow reduction was observed. The clip on the CCA was then removed, and the incision was closed with silk sutures. The occlusion was maintained for 90 min, after which the filament was removed to restore blood flow, and the wound was closed again. In the sham-operated group, the same procedure was performed without inserting the filament. The mortality rate for MCAO was 6.3% at the 24-h time point, with an optimal occlusion success rate of 92.1%. The treatment did not affect the mortality rate in the sham group, while in the stroke group, the mortality rate was 2.78%, indicating a reduction compared to the vehicle-treated stroke animals. Random assignment of animals to treatment groups was ensured using a random number generator to minimize bias. Exclusion criteria were based on survival and physiological parameters, excluding animals that did not survive the surgery or showed extreme baseline parameter outliers. Specifically, animals with less than 70% reduction in CBF during occlusion or inconsistent CBF recovery during reperfusion were excluded to maintain the model's accuracy and consistency.

Neurological Deficit Assessment. Neurological deficits were evaluated following a 3-day treatment on the third day poststroke using a 10-point grading system described by Phillips et al. (2000),¹⁰⁹ as previously detailed in our studies (Krzyzanowska et al., 2016,¹¹⁰ Krzyzanowska et al., 2017).¹¹¹ The assessment scored various neurological symptoms: 4 points for no resistance when pushed in a contralateral direction, 3 points for circling behavior in a contralateral direction, 2 points for contralateral shoulder adduction, and 1 point for contralateral forelimb flexion. A score of zero indicated no neurological deficits, while 10 indicated maximum severity. Each group consisted of $n = 8$ animals, and evaluations were performed by a blinded observer.

Infarct Volume Evaluation. Infarct volume was assessed using TTC staining. Following a 3-day treatment on the third day post-MCAO or sham procedure, animals ($n = 6$) were decapitated, and their brains were immediately extracted and sectioned using a brain matrix (Harvard Apparatus, USA). Coronal sections, 2 mm thick, were stained with a 1% solution of 2,3,5-triphenyltetrazolium chloride (TTC) dye (Sigma-Aldrich, USA) in 0.01 M phosphate-buffered saline (Sigma-Aldrich, USA) at 37 °C for 10 min in the dark. The sections were then fixed in 10% phosphate-buffered formalin (Sigma-Aldrich, USA) for 30 min at 4 °C. The stained and fixed slices were photographed using a surgical microscope with a camera (Flexacam C1, Leica, Germany) by a blinded investigator. Infarct volume was determined using NIH ImageJ software (National Institutes of Health, version 8.0), with the white areas corresponding to the infarcted regions outlined and multiplied by the thickness of the brain section. Infarct volume was expressed as a percentage of the brain ipsilateral hemisphere volume.

Western Blotting. The striatum from the left (ipsilateral) hemisphere was immediately removed after decapitation (3 days after SHAM or MCAO surgery) and homogenized in 2% SDS containing 1 mM PMSF (phenylmethylsulfonyl fluoride), 1 mM Na_3VO_4 (sodium orthovanadate) and a protease-phosphatase inhibitors cocktail (Sigma-Aldrich, USA), using a Bead Ruptor Elite homogenizer (Omni International, USA). The samples were denatured for 10 min at 95 °C and centrifuged for 10 min at

4 °C (10 000 g). The protein concentration was quantified in each sample by a BCA Protein Assay Kit (Thermo Scientific, USA) and adjusted to 30 $\mu\text{g}/10 \mu\text{L}$. Next, the proteins were separated in stain-free gradient (4–15%) polyacrylamide gels (Bio-Rad, USA) and transferred to PVDF membranes (Bio-Rad, USA) using a Trans-Blot Turbo Transfer System (Bio-Rad, USA). After several washes and blocking nonspecific binding sites, the membranes were incubated with selected antibodies. The list of antibodies used within the study is summarized in Table S3. The signals were developed using the ECL method (Western Bright Quantum, Advansta, USA) and imaged by a G:BOX Imaging System (Syngene, USA). Gene Tools software (Syngene, USA) was used to analyze protein expression with total protein normalization. For a list of antibodies used in Western blotting, refer to Table S3.

DESI Analyses. Rat Brain Tissue Preparation. Rats were decapitated after MCAO procedure or MCAO and compound's administration (10 min after the compound's 4 administration). Brains were swiftly excised from the skulls, flash-frozen using gaseous CO_2 , and then sectioned into 10 μm coronal slices using a cryostat. Tissue sections were mounted on microscope slides and then preserved in sealed containers at $-80 \text{ }^\circ\text{C}$. The experimental protocols and procedures described in this work were approved by the I Local Ethics Commission in Cracow (no 878/2024) and complied with the European Communities Council Directive of 24 November 1986 (86/609/EEC) and were in accordance with the 1996 NIH Guide for the Care and Use of Laboratory Animals.

Desorption Electrospray Ionization (DESI) Imaging. DESI imaging was performed on Waters Synapt XS mass spectrometer equipped with a Waters DESI XS imaging ion source with heated transfer line (HTL). The solvent spray consisted of methanol–water–formic acid (98:2:0.01, v/v/v) mixture with 200 ng/mL Leu-enkephalin as mass reference compound dispensed with a flow of 4 $\mu\text{L}/\text{min}$ and the nitrogen nebulizer gas was set to a pressure of 0.1 MPa. Each mass spectrum was measured for 236 ms with pixel size 50 $\mu\text{m} \times 50 \mu\text{m}$. The spray-to-inlet and spray-to-sample distance were optimized to approximately 6 mm and 2 mm respectively with a spray angle of approximately 75°. The spray potential was 0.7 kV for positive ion mode and -0.7 kV for negative ion mode, and the mass-to-charge (m/z) scan range was set between 100 and 1000 for all measurements. Cone potential was set to 40 V, and HTL temperature to 250 °C. In both positive and negative ion mode, measurements were performed on brain sections from three different rat brains, $n = 3$, and a typical representative were used for the images in the figures.

Data Analysis of DESI Imaging. The RAW files were analyzed using Waters HDI v. 1.6. Images were generated for the m/z values of interest with a m/z window of $\pm 0.01 \text{ Da}$ and mass resolution of 20 000 (fwhm). For Figure 10 images A and B, semiquantitative data for changes in the abundance of the lactate and AMP are given on Figure 10. This has been done by dividing the summed intensity of the ion in the analyzed square area of 1 mm^2 , equivalent to 400 pixels, with the summed intensity of the same ion in a reference area of the same shape and size on the contralateral to the stroke site of the cortex, showing no signs of ischemia. The data are presented as intensity ratio, mean \pm SD, $n = 3$ animals as previously reported.¹¹² The chosen areas were: for A— normal cortex, normal striatum, ischemic cortex, ischemic striatum and necrotic cortex, for B— normal cortex, normal striatum, cortex above ischemic striatum and ischemic striatum. Statistical analysis was performed using one-way

ANOVA and posthoc Tukey's HSD test. Figure showing semiquantitative analysis is presented in the supporting info (Figure S12).

■ ASSOCIATED CONTENT

SI Supporting Information

The Supporting Information is available free of charge at <https://pubs.acs.org/doi/10.1021/acs.jmedchem.4c01578>.

Molecular formula strings (CSV)

Homology (docking) model of the binding modes for compounds **6**, **20**, **37**, and zolpidem (ZIP)

Calculated physicochemical properties and CNS MPO scores for the final compounds (Table S1), metabolic stability studies of compound **4** in HLM (Table S2, Figures S1–S3), pharmacokinetic evaluation of compound **4** (Figures S4–S5), representative immunoblots (S6–S10), semiquantitative analysis of lactate and AMP following DESI analysis (Figure S11), the results obtained from docking specific compounds to the transmembrane binding site of zolpidem, which is located between the TMD interfaces of $\beta 2/\alpha 1$ subunits (Figure S12), list of antibodies used for Western blotting (Table S3), and representative NMR and LCMS spectra of selected final compounds (PDF)

■ AUTHOR INFORMATION

Corresponding Author

Monika Marcinkowska – Department of Medicinal Chemistry, Faculty of Pharmacy, Jagiellonian University Medical College, Kraków 30-688, Poland; Center for the Development of Therapies for Civilization and Age-Related Diseases, Jagiellonian University Medical College, Krakow 31-066, Poland; orcid.org/0000-0002-4948-6617; Email: monika.marcinkowska@uj.edu.pl

Authors

Barbara Mordyl – Department of Pharmacobiology, Faculty of Pharmacy, Jagiellonian University Medical College, Kraków 30-688, Poland

Nikola Fajkis-Zajczkowska – Department of Medicinal Chemistry, Faculty of Pharmacy, Jagiellonian University Medical College, Kraków 30-688, Poland

Katarzyna Szafrńska – Department of Medicinal Chemistry, Faculty of Pharmacy, Jagiellonian University Medical College, Kraków 30-688, Poland; Doctoral School of Medical and Health Sciences, Jagiellonian University Medical College, Krakow 31-530, Poland

Agata Siwek – Department of Pharmacobiology, Faculty of Pharmacy, Jagiellonian University Medical College, Kraków 30-688, Poland; Center for the Development of Therapies for Civilization and Age-Related Diseases, Jagiellonian University Medical College, Krakow 31-066, Poland

Monika Głuch-Lutwin – Department of Pharmacobiology, Faculty of Pharmacy, Jagiellonian University Medical College, Kraków 30-688, Poland

Pawel Żmudzki – Department of Medicinal Chemistry, Faculty of Pharmacy, Jagiellonian University Medical College, Kraków 30-688, Poland; Center for the Development of Therapies for Civilization and Age-Related Diseases, Jagiellonian University Medical College, Krakow 31-066, Poland; orcid.org/0000-0003-3594-1241

Jakub Jończyk – Department of Medicinal Chemistry, Faculty of Pharmacy, Jagiellonian University Medical College, Kraków 30-688, Poland

Tadeusz Karcz – Department of Technology and Biotechnology of Drugs, Jagiellonian University Medical College, Kraków 30-688, Poland

Karolina Słoczyńska – Department of Pharmaceutical Biochemistry, Jagiellonian University Medical College, Kraków 30-688, Poland

Elżbieta Pękala – Department of Pharmaceutical Biochemistry, Jagiellonian University Medical College, Kraków 30-688, Poland

Bartosz Pomierny – Center for the Development of Therapies for Civilization and Age-Related Diseases, Jagiellonian University Medical College, Krakow 31-066, Poland; Department of Toxicological Biochemistry, Jagiellonian University Medical College, Kraków 30-688, Poland

Weronika Krzyżanowska – Department of Toxicological Biochemistry, Jagiellonian University Medical College, Kraków 30-688, Poland

Jakub Jurczyk – Doctoral School of Medical and Health Sciences, Jagiellonian University Medical College, Krakow 31-530, Poland; Department of Toxicology, Jagiellonian University Medical College, Kraków 30-688, Poland

Alicja Skórkowska – Center for the Development of Therapies for Civilization and Age-Related Diseases, Jagiellonian University Medical College, Krakow 31-066, Poland; Department of Toxicological Biochemistry, Jagiellonian University Medical College, Kraków 30-688, Poland

Aleksandra Salach – Department of Clinical Pharmacy, Faculty of Pharmacy, Jagiellonian University Medical College, Kraków 30-688, Poland

Magdalena Jastrzębska-Więsek – Department of Clinical Pharmacy, Faculty of Pharmacy, Jagiellonian University Medical College, Kraków 30-688, Poland; orcid.org/0000-0002-5388-1214

Maria Walczak – Department of Toxicology, Jagiellonian University Medical College, Kraków 30-688, Poland; orcid.org/0000-0002-5670-9866

Maciej Tadeusz Gawlik – Department of Toxicology, Jagiellonian University Medical College, Kraków 30-688, Poland; orcid.org/0000-0002-0808-4603

Magdalena Smolik – Department of Toxicology, Jagiellonian University Medical College, Kraków 30-688, Poland

Marcin Kolaczkowski – Department of Medicinal Chemistry, Faculty of Pharmacy, Jagiellonian University Medical College, Kraków 30-688, Poland

Complete contact information is available at:

<https://pubs.acs.org/doi/10.1021/acs.jmedchem.4c01578>

Author Contributions

[†]B.M. and N.F.-Z. contributed equally as first authors. The manuscript was written through the contribution of all authors. All authors have given approval to the final version of the manuscript.

Notes

The authors declare no competing financial interest.

■ ACKNOWLEDGMENTS

This research was funded by National Science Centre, Poland grant: 2018/30/E/NZ7/00247. The publication was created with the use of equipment cofinanced by the qLIFE Priority

Research Area under the program “Excellence Initiative—Research University” (no. 06/IDUB/2019/94) at Jagiellonian University (Software for ACD/Spectrus Processor 2017). DESI imaging was performed with the use of research infrastructure financed by the European Union with the Smart Growth Operation Programme, POIR 4.2 project no. POIR.04.02.00–00-D023/20. The Figure 1 and TOC graphic were created with biorender.com. The MetaXpress software Neurite Outgrowth Application Module in the Image High Content Screening System was purchased with support from a grant under the Priority Research Area qLIFE as part of the Strategic Programme Excellence Initiative at Jagiellonian University. We thank MSc Emilia Sługocka for very helpful discussions regarding computational studies.

■ ABBREVIATIONS

6-OHDA, 6-hydroxydopamine; 90-MCAO, 90 min Middle Cerebral Artery Occlusion; A-B, apical-to-basolateral; ACD/Laboratories, Advanced Chemistry Development; ADME-Tox, administration-distribution-metabolism-excretion-toxicity; AKDR, Adenylate Kinase Detection Reagent; ALPB, analytical linearized Poisson–Boltzmann model; AMP, adenosine monophosphate; AUC, area under the curve; AUC_{0-t} , area under the concentration–time curve; Å, ångström; B-A, basolateral-to-apical; BBB, blood-brain barrier; BCA, bicinchoninic acid; br, broad; °C, degrees Celsius; C++, C-plus-plus programming language; CBF, cerebral blood flow; CCA, common carotid artery; CDI, 1,1'-carbonyldiimidazole; CF_3 , tetrafluoromethyl; CH_3COOH , ethanol; CHO, chinese hamster ovary; CL/F, apparent clearance; Cl_{int} , intrinsic clearance; C_{max} , maximum plasma concentration; CNS, central nervous system; CO_2 , carbon dioxide; Compd, compound; cryo-EM, cryogenic electron microscopy; d, doublet; Da, Dalton; DCM, dichloromethane; dd, doublet of doublets; DESI, Desorption Electrospray Ionization; DIPEA, diisopropylethylamine; DMEM, Dulbecco's Modified Eagle's Medium; DMSO, dimethylsulfoxide; DPBS, Dulbecco's phosphate-buffered saline; DSTR, dorsal striatum; dt, doublet of triplets; dtd, doublet of triplets of doublets; ΔE_{def} , deformation energy; ECA, external carotid artery; ECL, electrochemiluminescence; EEC, European Economic Community; ESL, electrospray ionization; Eq, equivalent; Et_2O , diethyl ether; EU, European Union; FDA, Federal Drug Agency; fwhm, full width at high maximum; GABA, gamma-aminobutyric acid; GABA-AR, γ -aminobutyric acid receptor type A; GAT-3/4, GABA transporter; GHz, gigahertz; HBSS, Hanks' balanced salt solution; HCOOH, formic acid; HCS, High Content Screening; HEK293, human embryonic kidney cells; HepG2, hepatoma G2 cell line; hERG, human *Ether-à-go-go*-Related Gene; His, histidine; HLMs, human liver microsomes; HPLC, high performance liquid chromatography; HTL, heated transfer line; I_2 , molecular iodine; IC_{50} , half maximal inhibitory concentration; ICA, internal carotid artery; IDS, ipsilateral dorsal striatum; i.e., id est; i.p., intraperitoneal; iPSCs, induced pluripotent stem cells; IU, international units; J , coupling constant; K_i , inhibitory constant; kg, kilogram; kV, kilovolt; L, liter; lx, lux; m, multiplet; M, mole; MCAO, middle cerebral artery occlusion; MDR1-MDCKII, Madin-Darby canine kidney cell line transfected by human MDR1 gene; Me, methyl; MeCN, acetonitrile; MEM, minimum essential media; MeOH, methanol; mg, milligram; MHz, megahertz; min, minute; mL, millilitre; mm, millimetre; mM, millimole; mmol, millimole; MM-GSA, Molecular Mechanics, General Born surface area; m.p., melting point;

MPa, megapascal; MPO, multiparameter optimization; MRT, mean residence time; ms, millisecond; MS, mass spectrometry; MSI, mass spectrometry imaging; MW, microwaves; m/z , mass-to-charge ratio; μL , microliter; μm , micrometer; μM , micromole; n, number; N_2 , molecular nitrogen; N2A, mouse neuroblastoma cells; bNaCl, sodium chloride; vNa_2CO_{3aq} , aqueous solution of sodium carbonate; $NaHCO_3$, sodium hydroxycarbonate; $vNa_2S_2O_3$, sodium thiosulfate; Na_3VO_4 , sodium orthovanadate; ND, not determined; ng, nanogram; NIH, National Institutes of Health; nM, nanomole; NMR, nuclear magnetic resonance; ns, not significant; OCH₃, methoxy; OGD, oxygen-glucose deprivation; OH, hydroxyl; OPLS3, optimized potential for liquid simulations; PAMPA, parallel artificial membrane permeability assay; PAMs, positive allosteric modulators; PBr_3 , phosphorus tribromide; PBS, phosphate buffered saline; PDA, Photodiode Array; PDB, Protein Data Bank; Pd/C, 10% palladium on carbon; P_e , permeability; Pgp, P-glycoprotein; pH, negative decimal logarithm of proton concentration; Phe, phenylalanine; pIC_{50} , negative decimal logarithm of half maximal inhibitory concentration; PK, pharmacokinetics; pK_i , negative decimal logarithm of inhibitory constant; p.m., post meridiem; PMSF, phenylmethylsulfonyl fluoride; ppm, part per million; PPh_3 , triphenylphosphine; PROPKA, protein pK_a ; PVF, polyvinylidene difluoride; q, quartet; QM, quantum mechanicsquintet; rpm, rotations per minute; RT, room temperature; s, singlet; SAR, structure–activity relationship; SD, standard deviation; SEM, standard error of mean; Ser, serine; SH, thiol; SH-SY5Y, bone marrow human neuroblastoma cell line; t, triplet; TBTU, 2-(1H-Benzotriazole-1-yl)-1,1,3,3-tetramethylammonium tetrafluoroborate; THF, tetrahydrofuran; Thr, threonine; TLC, thin layer chromatography; $t_{0.5}$, terminal half-life; t_{max} , time to reach C_{max} ; Tris-HCl, Tris(hydroxymethyl)aminomethane hydrochloride; TTC, triphenyl tetrazolium chloride; Tyr, tyrosine; TQD, tandem quadrupole; R_f , Retention factor; UPLC–MS, Ultra Performance Liquid Chromatography Mass Spectrometry; UV, ultraviolet light; V, volt; VSGB, solvation model; V_d/F , apparent volume of distribution; V_z/F , apparent volume of distribution; W, Watt

■ REFERENCES

- (1) Krishnamurthi, R. V.; deVeber, G.; Feigin, V. L.; Barker-Collo, S.; Fullerton, H.; Mackay, M. T.; O'Callahan, F.; Lindsay, M. P.; Kolk, A.; Lo, W.; Shah, P.; Linds, A.; Jones, K.; Parmar, P.; Taylor, S.; Norrving, B.; Mensah, G. A.; Moran, A. E.; Naghavi, M.; Forouzanfar, M. H.; Nguyen, G.; Johnson, C. O.; Vos, T.; Murray, C. J. L.; Roth, G. A. for the GBD 2013 Stroke Panel Experts Group. Stroke Prevalence, Mortality and Disability-Adjusted Life Years in Children and Youth Aged 0–19 Years: Data from the Global and Regional Burden of Stroke 2013. *Neuroepidemiology* **2015**, *45* (3), 177–189.
- (2) Feigin, V. L.; Brainin, M.; Norrving, B.; Martins, S.; Sacco, R. L.; Hacke, W.; Fisher, M.; Pandian, J.; Lindsay, P. World Stroke Organization (WSO): Global Stroke Fact Sheet 2022. *Int. J. Stroke* **2022**, *17* (1), 18–29.
- (3) Lawrence, E. S.; Coshall, C.; Dundas, R.; Stewart, J.; Rudd, A. G.; Howard, R.; Wolfe, C. D. A. Estimates of the Prevalence of Acute Stroke Impairments and Disability in a Multiethnic Population. *Stroke* **2001**, *32* (6), 1279–1284.
- (4) Hubbard, I. J.; Parsons, M. W.; Neilson, C.; Carey, L. M. Task-specific Training: Evidence for and Translation to Clinical Practice. *Occup. Ther. Int.* **2009**, *16* (3–4), 175–189.
- (5) Kim, J. S. tPA Helpers in the Treatment of Acute Ischemic Stroke: Are They Ready for Clinical Use? *J. Stroke* **2019**, *21* (2), 160–174.
- (6) Clarkson, A. N.; Huang, B. S.; MacIsaac, S. E.; Mody, I.; Carmichael, S. T. Reducing Excessive GABA-Mediated Tonic

Inhibition Promotes Functional Recovery after Stroke. *Nature* **2010**, *468* (7321), 305–309.

(7) Jaenisch, N.; Liebmann, L.; Guenther, M.; Hübner, C. A.; Frahm, C.; Witte, O. W. Reduced Tonic Inhibition after Stroke Promotes Motor Performance and Epileptic Seizures. *Sci. Rep.* **2016**, *6* (1), 26173.

(8) Luscher, B.; Fuchs, T.; Kilpatrick, C. L. GABAA Receptor Trafficking-Mediated Plasticity of Inhibitory Synapses. *Neuron* **2011**, *70* (3), 385–409.

(9) Hiu, T.; Farzampour, Z.; Paz, J. T.; Wang, E. H. J.; Badgely, C.; Olson, A.; Micheva, K. D.; Wang, G.; Lemmens, R.; Tran, K. V.; Nishiyama, Y.; Liang, X.; Hamilton, S. A.; O'Rourke, N.; Smith, S. J.; Huguenard, J. R.; Bliss, T. M.; Steinberg, G. K. Enhanced Phasic GABA Inhibition during the Repair Phase of Stroke: A Novel Therapeutic Target. *Brain* **2016**, *139* (2), 468–480.

(10) Paparella, I.; Vandewalle, G.; Stagg, C. J.; Maquet, P. An Integrated Measure of GABA to Characterize Post-Stroke Plasticity. *NeuroImage Clin.* **2023**, *39*, 103463.

(11) Maric, D.; Liu, Q.-Y.; Maric, I.; Chaudry, S.; Chang, Y.-H.; Smith, S. V.; Sieghart, W.; Fritschy, J.-M.; Barker, J. L. GABA Expression Dominates Neuronal Lineage Progression in the Embryonic Rat Neocortex and Facilitates Neurite Outgrowth via GABA_A Autoreceptor/Cl⁻ Channels. *J. Neurosci.* **2001**, *21* (7), 2343–2360.

(12) Bordey, A. Enigmatic GABAergic Networks in Adult Neurogenic Zones. *Brain Res. Rev.* **2007**, *53* (1), 124–134.

(13) Wang, D. D.; Kriegstein, A. R. Defining the Role of GABA in Cortical Development. *J. Physiol.* **2009**, *587* (9), 1873–1879.

(14) Sernagor, E. GABAergic Control of Neurite Outgrowth and Remodeling during Development and Adult Neurogenesis: General Rules and Differences in Diverse Systems. *Front Cell Neurosci.* **2010**, *4*, 1579.

(15) Reyes-Haro, D.; Cisneros-Mejorado, A.; Arellano, R. O. Therapeutic Potential of GABAergic Signaling in Myelin Plasticity and Repair. *Front. Cell Dev. Biol.* **2021**, *9*, 662191.

(16) Owens, D. F.; Kriegstein, A. R. Is There More to Gaba than Synaptic Inhibition? *Nat. Rev. Neurosci.* **2002**, *3* (9), 715–727.

(17) Farrant, M.; Nusser, Z. Variations on an Inhibitory Theme: Phasic and Tonic Activation of GABAA Receptors. *Nat. Rev. Neurosci.* **2005**, *6* (3), 215–229.

(18) Mortensen, M.; Patel, B.; Smart, T. G. GABA Potency at GABAA Receptors Found in Synaptic and Extrasynaptic Zones. *Front Cell Neurosci.* **2012**, *6*, 1.

(19) Glykys, J.; Mody, I. Hippocampal Network Hyperactivity After Selective Reduction of Tonic Inhibition in GABA_A Receptor A5 Subunit-Deficient Mice. *J. Neurophysiol.* **2006**, *95* (5), 2796–2807.

(20) Olsen, R. W.; Sieghart, W. GABAA Receptors: Subtypes Provide Diversity of Function and Pharmacology. *Neuropharmacology* **2009**, *56* (1), 141–148.

(21) Jacob, T. C. Neurobiology and Therapeutic Potential of A5-GABA Type A Receptors. *Front. Mol. Neurosci.* **2019**, *12*, 179.

(22) Orfila, J. E.; Grewal, H.; Dietz, R. M.; Strnad, F.; Shimizu, T.; Moreno, M.; Schroeder, C.; Yonchek, J.; Rodgers, K. M.; Dingman, A.; Bernard, T. J.; Quillinan, N.; Macklin, W. B.; Traystman, R. J.; Herson, P. S. Delayed Inhibition of Tonic Inhibition Enhances Functional Recovery Following Experimental Ischemic Stroke. *J. Cereb. Blood Flow Metab.* **2019**, *39* (6), 1005–1014.

(23) He, W.-M.; Ying-Fu, L.; Wang, H.; Peng, Y.-P. Delayed Treatment of A5 GABAA Receptor Inverse Agonist Improves Functional Recovery by Enhancing Neurogenesis after Cerebral Ischemia-Reperfusion Injury in Rat MCAO Model. *Sci. Rep.* **2019**, *9* (1), 2287.

(24) Pace, M.; Falappa, M.; Machado, P.; Facchin, L.; Hermann, D. M.; Bassetti, C. L. Poststroke Administration of the GABA_A α5 Antagonist S44819 Promotes Recovery of Peripheral Limb Fine Motor Skills After Permanent Distal Middle Cerebral Artery Occlusion in Rats. *Clin. Transl. Neurosci.* **2020**, *4*, 2514183X20948306.

(25) Chabriat, H.; Bassetti, C. L.; Marx, U.; Audoli-Inthavong, M.-L.; Sors, A.; Lambert, E.; Watzet, M.; Hermann, D. M.; Althaus, K.; Amaro, S.; Bae, H.-J.; Bak, Z.; Barbarini, L.; Bassi, P.; Bazan, R.; Bereczki, D.; Berkowicz, T.; Berrouschot, J.; Blacquiere, D.; Brola, W.; Butcher, K.;

Cardona, P.; Cha, J.-K.; Cloud, G.; Cohen, D.; Cordonnier, C.; Csanyi, A.; Czlonkowska, A.; Davis, S.; Dawson, J.; De Klippel, N.; Denier, C.; Desfontaines, P.; Diener, H.-C.; Dioszeghy, P.; Dippel, D. W.; Dorado, L.; Folyovich, A.; Freitas, G. R.; Friedrich, M. A.; Fryze, W.; Gagliardi, R. J.; Gottschal, M.; Grimley, R.; Grond, M.; Gröschel, K.; Hosseini, H.; Hwang, Y.; Kallmuenzer, B.; Khan, U.; Kim, J. S.; Kleinig, T.; Koves, A.; Lago Martin, A.; Lasek-Bal, A.; Lembo, G.; Lemmens, R.; Lindert, R.; Porcello Marrone, L. C.; Martinez Zabaleta, M.; Mas, J.-L.; Masjuan Vallejo, J.; Mazighi, M.; Minelli, C.; Mistri, A.; Molina, C.; Monicé Alvarez, F.; Cabral Moro, C. H.; Mulleners, W.; Nabavi, D.; Neau, J.-P.; O'Brien, B.; Ovary, C.; Panczel, G.; Park, M. S.; Phan, T.; Ragab, S.; Rejdak, K.; Rodriguez De Freitas, G.; Roffe, C.; Roquer Gonzalez, J.; Rover, L.; Sampaio Silva, G.; Schellinger, P.; Segura Martin, T.; Shaw, L.; Sibon, I.; Skoda, O.; Smadja, D.; Sobolewski, P.; Soda, H.; Sprigg, N.; Swiat, M.; Szapary, L.; Szedegi, N.; Toni, D.; Valikovics, A.; Vanhooren, G.; Vecsei, L.; Wein, T.; Wong, A.; Ximenez Carrillo, A. Safety and Efficacy of GABAA A5 Antagonist S44819 in Patients with Ischaemic Stroke: A Multicentre, Double-Blind, Randomised, Placebo-Controlled Trial. *Lancet Neurol.* **2020**, *19* (3), 226–233.

(26) Autret, K.; Arnould, A.; Mathieu, S.; Azouvi, P. Transient Improvement of Poststroke Apathy with Zolpidem: A Single-Case, Placebo-Controlled Double-Blind Study. *Case Rep.* **2013**, *2013* (feb08 1), bcr2012007816–bcr2012007816.

(27) Nyakale, N.; Clauss, R.; Nel, W.; Sathegke, M. Clinical and Brain SPECT Scan Response to Zolpidem in Patients after Brain Damage. *Arzneimittelforschung* **2010**, *60* (4), 177–181.

(28) Sutton, J. A.; Clauss, R. P. A Review of the Evidence of Zolpidem Efficacy in Neurological Disability after Brain Damage Due to Stroke, Trauma and Hypoxia: A Justification of Further Clinical Trials. *Brain Inj.* **2017**, *31* (8), 1019–1027.

(29) Langer, S. Z.; Faure-Halley, C.; Seeburg, P.; Graham, D.; Arbilla, S. The Selectivity of Zolpidem and Alpidem for the A1-Subunit of the GABAA Receptor. *Eur. Neuropsychopharmacol.* **1992**, *2* (3), 232–234.

(30) Pritchett, D. B.; Lüddens, H.; Seeburg, P. H. Type I and Type II GABA_A-Benzodiazepine Receptors Produced in Transfected Cells. *Science* **1989**, *245* (4924), 1389–1392.

(31) Owen, R. M.; Blakemore, D. C.; Cao, L.; Flanagan, N.; Fish, R.; Gibson, K. R.; Gurrell, R.; Huh, C. W.; Kammonen, J.; Mortimer-Cassen, E.; et al. Design and Identification of a Novel, Functionally Subtype Selective GABA_A Positive Allosteric Modulator (PF-06372865). *J. Med. Chem.* **2019**, *62*, 5773–5796.

(32) Szabó, G.; Éliás, O.; Erdélyi, P.; Potor, A.; Túrós, G. I.; Károlyi, B. I.; Varró, G.; Vaskó, A. G.; Bata, I.; Kapus, G. L.; Dohányos, Z.; Bobok, A. A.; Fodor, L.; Thán, M.; Vastag, M.; Komlódi, Z.; Soukupné Kedves, R. É.; Makó, É.; Süveges, B.; Greiner, I. Multiparameter Optimization of Naphthyridine Derivatives as Selective A5-GABA_A Receptor Negative Allosteric Modulators. *J. Med. Chem.* **2022**, *65* (11), 7876–7895.

(33) Maramai, S.; Benchekroun, M.; Ward, S. E.; Atack, J. R. Subtype Selective γ-Aminobutyric Acid Type A Receptor (GABA_A R) Modulators Acting at the Benzodiazepine Binding Site: An Update. *J. Med. Chem.* **2020**, *63* (7), 3425–3446.

(34) Rowlett, J. K.; Platt, D. M.; Lelas, S.; Atack, J. R.; Dawson, G. R. Different GABA_A Receptor Subtypes Mediate the Anxiolytic, Abuse-Related, and Motor Effects of Benzodiazepine-like Drugs in Primates. *Proc. Natl. Acad. Sci. U. S. A.* **2005**, *102* (3), 915–920.

(35) Trenque, T.; Bustany, P.; Lamiable, D.; Legros, S.; Choisy, H. Pharmacokinetics and Brain Distribution of Zolpidem in the Rat after Acute and Chronic Administration. *J. Pharm. Pharmacol.* **2011**, *46* (7), 611–613.

(36) Durand, A.; Thénot, J. P.; Bianchetti, G.; Morselli, P. L. Comparative Pharmacokinetic Profile of Two Imidazopyridine Drugs: Zolpidem and Alpidem. *Drug Metab. Rev.* **1992**, *24* (2), 239–266.

(37) Salvà, P.; Costa, J. Clinical Pharmacokinetics and Pharmacodynamics of Zolpidem: Therapeutic Implications. *Clin. Pharmacokinet.* **1995**, *29* (3), 142–153.

(38) Badillo, S. P. J.; Jamora, R. D. G. Zolpidem for the Treatment of Dystonia. *Front. Neurol.* **2019**, *10*, 779.

(39) Berson, A.; Descatoire, V.; Sutton, A.; Fau, D.; Maulny, B.; Vadrot, N.; Feldmann, G.; Berthon, B.; Tordjmann, T.; Pessayre, D.

- Toxicity of Alpidem, a Peripheral Benzodiazepine Receptor Ligand, but Not Zolpidem, in Rat Hepatocytes: Role of Mitochondrial Permeability Transition and Metabolic Activation. *J. Pharmacol. Exp. Ther.* **2001**, *299* (2), 793–800.
- (40) Ramerstorfer, J.; Furtmüller, R.; Vogel, E.; Huck, S.; Sieghart, W. The Point Mutation γ 2F77I Changes the Potency and Efficacy of Benzodiazepine Site Ligands in Different GABAA Receptor Subtypes. *Eur. J. Pharmacol.* **2010**, *636* (1–3), 18–27.
- (41) Daniele, A.; Panza, F.; Greco, A.; Logroscino, G.; Seripa, D. Can a Positive Allosteric Modulation of GABAergic Receptors Improve Motor Symptoms in Patients with Parkinson's Disease? The Potential Role of Zolpidem in the Treatment of Parkinson's Disease. *Parkinson's Dis.* **2016**, *2016*, 2531812.
- (42) Cohen, S. I.; Duong, T. T. Increased Arousal in a Patient with Anoxic Brain Injury After Administration of Zolpidem. *Am. J. Phys. Med. Rehabil.* **2008**, *87* (3), 229–231.
- (43) Oh, M.-K.; Yoon, K. J.; Lee, Y.-T.; Chae, S. W.; Choi, H. Y.; Shin, H. S.; Park, Y. H.; Chun, S.-W.; Park, Y. S. Effect of Zolpidem on Functional Recovery in a Rat Model of Ischemic Stroke. *J. Int. Med. Res.* **2018**, *46* (1), 249–257.
- (44) Zhu, S.; Noviello, C. M.; Teng, J.; Walsh, R. M.; Kim, J. J.; Hibbs, R. E. Structure of a Human Synaptic GABAA Receptor. *Nature* **2018**, *559* (7712), 67–72.
- (45) Olsen, R. W. GABAA Receptor: Positive and Negative Allosteric Modulators. *Neuropharmacology* **2018**, *136*, 10–22.
- (46) Zheng, X.; Wang, C.; Zhai, N.; Luo, X.; Liu, G.; Ju, X. In Silico Screening of Novel A1-GABAA Receptor PAMs towards Schizophrenia Based on Combined Modeling Studies of Imidazo [1,2-a]-Pyridines. *IJMS* **2021**, *22* (17), 9645.
- (47) Serra, M.; Madau, P.; Chessa, M. F.; Caddeo, M.; Sanna, E.; Trapani, G.; Franco, M.; Liso, G.; Purdy, R. H.; Barbaccia, M. L.; Biggio, G. 2-Phenyl-imidazo[1,2-a]Pyridine Derivatives as Ligands for Peripheral Benzodiazepine Receptors: Stimulation of Neurosteroid Synthesis and Anticonflict Action in Rats. *Br. J. Pharmacol.* **1999**, *127* (1), 177–187.
- (48) Kalgutkar, A. S. Designing around Structural Alerts in Drug Discovery. *J. Med. Chem.* **2020**, *63* (12), 6276–6302.
- (49) Marcinkowska, M.; Kolaczowski, M.; Kamiński, K.; Bucki, A.; Pawłowski, M.; Siwek, A.; Karcz, T.; Starowicz, G.; Słoczyńska, K.; Pękala, E.; Wesołowska, A.; Samochowiec, J.; Mierzejewski, P.; Bienkowski, P. 3-Aminomethyl Derivatives of 2-Phenylimidazo[1,2-a]-Pyridine as Positive Allosteric Modulators of GABAA Receptor with Potential Antipsychotic Activity. *ACS Chem. Neurosci.* **2017**, *8* (6), 1291–1298.
- (50) Marcinkowska, M.; Fajkis-Zajęczkowska, N.; Szafrńska, K.; Jończyk, J.; Siwek, A.; Mordyl, B.; Karcz, T.; Latacz, G.; Kolaczowski, M. 2-(4-Fluorophenyl)-1 H -Benzo[d]Imidazole as a Promising Template for the Development of Metabolically Robust, α 1 β 2 γ 2GABA-A Receptor-Positive Allosteric Modulators. *ACS Chem. Neurosci.* **2023**, *14* (6), 1166–1180.
- (51) Wager, T. T.; Hou, X.; Verhoest, P. R.; Villalobos, A. Central Nervous System Multiparameter Optimization Desirability: Application in Drug Discovery. *ACS Chem. Neurosci.* **2016**, *7* (6), 767–775.
- (52) Lalo, R.; Zekja, I.; Kamberi, F. Association of Cardiovascular Disease Risk and Health-Related Behaviors in Stroke Patients. *IJERPH* **2023**, *20* (4), 3693.
- (53) Pollard, C. E.; Valentin, J.; Hammond, T. G. Strategies to Reduce the Risk of Drug-induced QT Interval Prolongation: A Pharmaceutical Company Perspective. *Br. J. Pharmacol.* **2008**, *154* (7), 1538–1543.
- (54) Lapchak, P. A.; Zhang, J. H. The High Cost of Stroke and Stroke Cytoprotection Research. *Transl. Stroke Res.* **2017**, *8* (4), 307–317.
- (55) Cavalluzzi, M. M.; Imbrici, P.; Gualdani, R.; Stefanachi, A.; Mangiatori, G. F.; Lentini, G.; Nicolotti, O. Human Ether-à-Go-Go-Related Potassium Channel: Exploring SAR to Improve Drug Design. *Drug Discovery Today* **2020**, *25* (2), 344–366.
- (56) El Harchi, A.; Hancox, J. C. hERG Agonists Pose Challenges to Web-Based Machine Learning Methods for Prediction of Drug-hERG Channel Interaction. *J. Pharmacol. Toxicol. Methods* **2023**, *123*, 107293.
- (57) Selli, S.; Bruni, F.; Costagli, C.; Costanzo, A.; Guerrini, G.; Ciciani, G.; Gratteri, P.; Besnard, F.; Costa, B.; Montali, M.; Martini, C.; Fohlin, J.; De Siena, G.; Aiello, P. M. A Novel Selective GABA_A A1 Receptor Agonist Displaying Sedative and Anxiolytic-like Properties in Rodents. *J. Med. Chem.* **2005**, *48* (21), 6756–6760.
- (58) Falco, J. L.; Palomer, A.; Guglietta, A. *Imidazo [1,2-b]Pyridazines, Their Processes of Preparation and Their Use as Gaba Receptor Ligands*. WO 2,007,110,437 A1, 2006.
- (59) Fajkis, N.; Marcinkowska, M.; Gryzłó, B.; Krupa, A.; Kolaczowski, M. Study on a Three-Step Rapid Assembly of Zolpidem and Its Fluorinated Analogues Employing Microwave-Assisted Chemistry. *Molecules* **2020**, *25* (14), 3161.
- (60) Zhu, S.; Sridhar, A.; Teng, J.; Howard, R. J.; Lindahl, E.; Hibbs, R. E. Structural and Dynamic Mechanisms of GABAA Receptor Modulators with Opposing Activities. *Nat. Commun.* **2022**, *13* (1), 4582.
- (61) Jain, A.; Purohit, C. S.; Verma, S.; Sankaramakrishnan, R. Close Contacts between Carbonyl Oxygen Atoms and Aromatic Centers in Protein Structures: $\Pi \cdots \pi$ or Lone-Pair $\cdots \pi$ Interactions? *J. Phys. Chem. B* **2007**, *111* (30), 8680–8683.
- (62) Egli, M.; Sarkhel, S. Lone Pair–Aromatic Interactions: To Stabilize or Not to Stabilize. *Acc. Chem. Res.* **2007**, *40* (3), 197–205.
- (63) Menezes, F.; Popowicz, G. M. ULYSSES: An Efficient and Easy to Use Semiempirical Library for C⁺⁺. *J. Chem. Inf. Model.* **2022**, *62* (16), 3685–3694.
- (64) Sieghart, W.; Savić, M. M. International Union of Basic and Clinical Pharmacology. CVI: GABA_A Receptor Subtype- and Function-Selective Ligands: Key Issues in Translation to Humans. *Pharmacol. Rev.* **2018**, *70* (4), 836–878.
- (65) Ain, Q. U.; Owen, R. M.; Omoto, K.; Torella, R.; Bulusu, K. C.; Pryde, D. C.; Glen, R. C.; Fuchs, J. E.; Bender, A. Analysis of Differential Efficacy and Affinity of GABA_A (A1/A2) Selective Modulators. *Mol. Pharmaceutics* **2016**, *13* (11), 4001–4012.
- (66) Stadler, M.; Monticelli, S.; Seidel, T.; Luger, D.; Salzer, I.; Boehm, S.; Holzer, W.; Schwarzer, C.; Urban, E.; Khom, S.; et al. Design, Synthesis, and Pharmacological Evaluation of Novel B2/3 Subunit-Selective γ -Aminobutyric Acid Type A (GABA_A) Receptor Modulators. *J. Med. Chem.* **2019**, *62* (1), 317–341.
- (67) Falk-Petersen, C. B.; Tsonkov, T. M.; Nielsen, M. S.; Harpsøe, K.; Bundgaard, C.; Frølund, B.; Kristiansen, U.; Gloriam, D. E.; Wellendorph, P. Discovery of a New Class of Orthosteric Antagonists with Nanomolar Potency at Extrasynaptic GABAA Receptors. *Sci. Rep.* **2020**, *10* (1), 10078.
- (68) Petroski, R. E.; Pomeroy, J. E.; Das, R.; Bowman, H.; Yang, W.; Chen, A. P.; Foster, A. C. Indiplon Is a High-Affinity Positive Allosteric Modulator with Selectivity for A1 Subunit-Containing GABA_A Receptors. *J. Pharmacol. Exp. Ther.* **2006**, *317* (1), 369–377.
- (69) Marcinkowska, M.; Mordyl, B.; Siwek, A.; Gluch-Lutwin, M.; Karcz, T.; Gawalska, A.; Sapa, M.; Bucki, A.; Szafrńska, K.; Pomierny, B.; et al. Dual Molecules Targeting 5-HT₆ and GABA-A Receptors as a New Approach to Combat Depression Associated with Neuroinflammation. *ACS Chem. Neurosci.* **2023**, *14*, 1474–1489.
- (70) Di, L.; Kerns, E. H.; Fan, K.; McConnell, O. J.; Carter, G. T. High Throughput Artificial Membrane Permeability Assay for Blood–Brain Barrier. *Eur. J. Med. Chem.* **2003**, *38* (3), 223–232.
- (71) Kerns, E.; Di, L.; Carter, G. In Vitro Solubility Assays in Drug Discovery. *CDM* **2008**, *9* (9), 879–885.
- (72) Wang, Y.; Li, M.; Qian, S.; Zhang, Q.; Zhou, L.; Zuo, Z.; Lee, B.; Toh, M.; Ho, T. Zolpidem Mucoadhesive Formulations for Intranasal Delivery: Characterization, In Vitro Permeability, Pharmacokinetics, and Nasal Ciliotoxicity in Rats. *J. Pharm. Sci.* **2016**, *105* (9), 2840–2847.
- (73) Green, A. R.; Hainsworth, A. H.; Jackson, D. M. GABA Potentiation: A Logical Pharmacological Approach for the Treatment of Acute Ischaemic Stroke. *Neuropharmacology* **2000**, *39* (9), 1483–1494.
- (74) García-Santos, G.; Herrera, F.; Martín, V.; Rodríguez-Blanco, J.; Antolín, I.; Fernández-Marí, F.; Rodríguez, C. Antioxidant Activity and

Neuroprotective Effects of Zolpidem and Several Synthesis Intermediates. *Free Radical Res.* **2004**, *38* (12), 1289–1299.

(75) Yousefsani, B. S.; Akbarizadeh, N.; Pourahmad, J. The Antioxidant and Neuroprotective Effects of Zolpidem on Acrylamide-Induced Neurotoxicity Using Wistar Rat Primary Neuronal Cortical Culture. *Toxicol. Rep.* **2020**, *7*, 233–240.

(76) Zhang, H.; Yu, P.; Lin, H.; Jin, Z.; Zhao, S.; Zhang, Y.; Xu, Q.; Jin, H.; Liu, Z.; Yang, W.; Zhang, L. The Discovery of Novel ACA Derivatives as Specific TRPM2 Inhibitors That Reduce Ischemic Injury Both In Vitro and In Vivo. *J. Med. Chem.* **2021**, *64* (7), 3976–3996.

(77) Du, E.; Jia, X.; Li, X.; Zhang, B.; Zhai, Y.; Qin, F. Neuroprotective Effect of Ciclopirox Olamine in Retinal Ischemia/Reperfusion Injury. *BMC Mol. Cell Biol.* **2024**, *25* (1), 22.

(78) Kakee, A.; Takanaga, H.; Terasaki, T.; Naito, M.; Tsuruo, T.; Sugiyama, Y. Efflux of a Suppressive Neurotransmitter, GABA, across the Blood–Brain Barrier. *J. Neurochem.* **2001**, *79* (1), 110–118.

(79) Ionescu, M. I.; Grigoras, I.-F.; Ionescu, R.-B.; Chitimus, D. M.; Haret, R. M.; Ianosi, B.; Ceanga, M.; Zagrean, A.-M. Oxytocin Exhibits Neuroprotective Effects on Hippocampal Cultures under Severe Oxygen–Glucose Deprivation Conditions. *CIMB* **2024**, *46* (6), 6223–6236.

(80) Sorrentino, V.; Menzies, K. J.; Auwerx, J. Repairing Mitochondrial Dysfunction in Disease. *Annu. Rev. Pharmacol. Toxicol.* **2018**, *58* (1), 353–389.

(81) Unnisa, A.; Greig, N. H.; Kamal, M. A. Inhibition of Caspase 3 and Caspase 9 Mediated Apoptosis: A Multimodal Therapeutic Target in Traumatic Brain Injury. *Curr. Neuropharmacol.* **2023**, *21* (4), 1001–1012.

(82) Chung, J.-W.; Ryu, W.-S.; Kim, B. J.; Yoon, B.-W. Elevated Calcium after Acute Ischemic Stroke: Association with a Poor Short-Term Outcome and Long-Term Mortality. *J. Stroke* **2015**, *17* (1), 54.

(83) Sun, H.; Wei, S.; Gong, Y.; Ding, K.; Tang, S.; Sun, W.; Yuan, C.; Huang, L.; Liu, Z.; Chen, C.; Yao, L. Neuroprotective Effects of Cordycepin Inhibit Glutamate-Induced Apoptosis in Hippocampal Neurons. *Cell Stress Chaperones* **2024**, *29* (1), 10–20.

(84) Bayón-Cordero, L.; Ochoa-Bueno, B. I.; Ruiz, A.; Ozalla, M.; Matute, C.; Sánchez-Gómez, M. V. GABA Receptor Agonists Protect From Excitotoxic Damage Induced by AMPA in Oligodendrocytes. *Front. Pharmacol.* **2022**, *13*, 897056.

(85) Alia, C.; Cangì, D.; Massa, V.; Salluzzo, M.; Vignozzi, L.; Caleo, M.; Spalletti, C. Cell-to-Cell Interactions Mediating Functional Recovery after Stroke. *Cells* **2021**, *10* (11), 3050.

(86) Romaus-Sanjurjo, D.; Ledo-García, R.; Fernández-López, B.; Hanslik, K.; Morgan, J. R.; Barreiro-Iglesias, A.; Rodicio, M. C. GABA Promotes Survival and Axonal Regeneration in Identifiable Descending Neurons after Spinal Cord Injury in Larval Lampreys. *Cell Death Dis.* **2018**, *9* (6), 663.

(87) Arruda, G. L. M.; Vigerelli, H.; Bufalo, M. C.; Longato, G. B.; Veloso, R. V.; Zambelli, V. O.; Picolo, G.; Cury, Y.; Morandini, A. C.; Marques, A. C.; Sciani, J. M. Box Jellyfish (Cnidaria, Cubozoa) Extract Increases Neuron's Connection: A Possible Neuroprotector Effect. *Biomed Res. Int.* **2021**, *2021*, 1–12.

(88) Clarke, K. E.; Tams, D. M.; Henderson, A. P.; Roger, M. F.; Whiting, A.; Przyborski, S. A. A Robust and Reproducible Human Pluripotent Stem Cell Derived Model of Neurite Outgrowth in a Three-Dimensional Culture System and Its Application to Study Neurite Inhibition. *Neurochem. Int.* **2017**, *106*, 74–84.

(89) Petrova, V.; Snavely, A. R.; Splaine, J.; Zhen, S.; Singh, B.; Pandey, R.; Chen, K.; Cheng, A.; Hermawan, C.; Barrett, L. B.; Smith, J. A.; Woolf, C. J. Identification of Novel Neuroprotectants against Vincristine-Induced Neurotoxicity in iPSC-Derived Neurons. *Cell. Mol. Life Sci.* **2024**, *81* (1), 315.

(90) Di, L.; Kerns, E. H.; Bezar, I. F.; Petusky, S. L.; Huang, Y. Comparison of Blood–Brain Barrier Permeability Assays: In Situ Brain Perfusion, MDR1-MDCKII and PAMPA-BBB. *J. Pharm. Sci.* **2009**, *98* (6), 1980–1991.

(91) Mierzejewski, P.; Kolaczowski, M.; Marcinkowska, M.; Wesolowska, A.; Samochowiec, J.; Pawlowski, M.; Bienkowski, P.

Antipsychotic-like Effects of Zolpidem in Wistar Rats. *Eur. J. Pharmacol.* **2016**, *773*, 51–58.

(92) Sanger, D. J.; Benavides, J.; Perrault, G.; Morel, E.; Cohen, C.; Joly, D.; Zivkovic, B. Recent Developments in the Behavioral Pharmacology of Benzodiazepine (ω) Receptors: Evidence for the Functional Significance of Receptor Subtypes. *Neurosci. Biobehav. Rev.* **1994**, *18* (3), 355–372.

(93) Crestani, F.; Martin, J. R.; Möhler, H.; Rudolph, U. Mechanism of Action of the Hypnotic Zolpidem in Vivo. *Br. J. Pharmacol.* **2000**, *131* (7), 1251–1254.

(94) Zivkovic, B.; Morel, E.; Joly, D.; Perrault, G.; Sanger, D.; Lloyd, K. Pharmacological and Behavioral Profile of Alpidem as an Anxiolytic. *Pharmacopsychiatry* **1990**, *23* (S 3), 108–113.

(95) Che Has, A. T.; Absalom, N.; Van Nieuwenhuijzen, P. S.; Clarkson, A. N.; Ahring, P. K.; Chebib, M. Zolpidem Is a Potent Stoichiometry-Selective Modulator of A1 β GABAA Receptors: Evidence of a Novel Benzodiazepine Site in the A1-A1 Interface. *Sci. Rep.* **2016**, *6* (1), 28674.

(96) Kleinschnitz, C.; Fluri, F.; Schuhmann, M. Animal Models of Ischemic Stroke and Their Application in Clinical Research. *Drug Des., Dev. Ther.* **2015**, 3445.

(97) Bederson, J. B.; Pitts, L. H.; Tsuji, M.; Nishimura, M. C.; Davis, R. L.; Bartkowski, H. Rat Middle Cerebral Artery Occlusion: Evaluation of the Model and Development of a Neurologic Examination. *Stroke* **1986**, *17* (3), 472–476.

(98) Tóth, O. M.; Menyhart, Á.; Frank, R.; Hantosi, D.; Farkas, E.; Bari, F. Tissue Acidosis Associated with Ischemic Stroke to Guide Neuroprotective Drug Delivery. *Biology* **2020**, *9* (12), 460.

(99) Wu, Q.; Yan, R.; Sun, J. Probing the Drug Delivery Strategies in Ischemic Stroke Therapy. *Drug Delivery* **2020**, *27* (1), 1644–1655.

(100) Frahm, C.; Haupt, C.; Weinandy, F.; Siegel, G.; Bruehl, C.; Witte, O. W. Regulation of GABA Transporter mRNA and Protein after Photothrombotic Infarct in Rat Brain. *J. Comp. Neurol.* **2004**, *478* (2), 176–188.

(101) Marcinkowska, M.; Mordyl, B.; Fajkis-Zajackowska, N.; Siwek, A.; Karcz, T.; Gawalska, A.; Bucki, A.; Zmudzki, P.; Partyka, A.; Jastrzębska-Więsek, M.; Pomierny, B.; Walczak, M.; Smolik, M.; Pytka, K.; Mika, K.; Kotańska, M.; Kolaczowski, M. Hybrid Molecules Combining GABA-A and Serotonin 5-HT6 Receptors Activity Designed to Tackle Neuroinflammation Associated with Depression. *Eur. J. Med. Chem.* **2023**, *247*, 115071.

(102) Myadaraboina, S.; Alla, M.; Sattanapu, V.; Bommena, V. R.; Adlagatta, A. Structure Activity Relationship Studies of Imidazo[1,2-a]Pyrazine Derivatives against Cancer Cell Lines. *Eur. J. Med. Chem.* **2010**, *45* (11), 5208–5216.

(103) Chen, X.; Murawski, A.; Patel, K.; Crespi, C. L.; Balimane, P. V. A Novel Design of Artificial Membrane for Improving the PAMPA Model. *Pharm. Res.* **2008**, *25* (7), 1511–1520.

(104) Horio, M.; Chin, K. V.; Currier, S. J.; Goldenberg, S.; Williams, C.; Pastan, I.; Gottesman, M. M.; Handler, J. Transepithelial Transport of Drugs by the Multidrug Transporter in Cultured Madin-Darby Canine Kidney Cell Epithelia. *J. Biol. Chem.* **1989**, *264* (25), 14880–14884.

(105) Banker, M. J.; Clark, T. H.; Williams, J. A. Development and Validation of a 96-Well Equilibrium Dialysis Apparatus for Measuring Plasma Protein Binding. *J. Pharm. Sci.* **2003**, *92* (5), 967–974.

(106) Naito, H.; Kidoya, H.; Sakimoto, S.; Wakabayashi, T.; Takakura, N. Identification and Characterization of a Resident Vascular Stem/Progenitor Cell Population in Preexisting Blood Vessels: Endothelial Side Population and Angiogenesis. *EMBO J.* **2012**, *31* (4), 842–855.

(107) Ramirez, C. N.; Antczak, C.; Djaballah, H. Cell Viability Assessment: Toward Content-Rich Platforms. *Expert Opin. Drug Discovery* **2010**, *5* (3), 223–233.

(108) Longa, E. Z.; Weinstein, P. R.; Carlson, S.; Cummins, R. Reversible Middle Cerebral Artery Occlusion without Craniectomy in Rats. *Stroke* **1989**, *20* (1), 84–91.

(109) Phillips, J. B.; Williams, A. J.; Adams, J.; Elliott, P. J.; Tortella, F. C. Proteasome Inhibitor PS519 Reduces Infarction and Attenuates

Leukocyte Infiltration in a Rat Model of Focal Cerebral Ischemia. *Stroke* **2000**, *31* (7), 1686–1693.

(110) Krzyzanowska, W.; Pomierny, B.; Budziszewska, B.; Filip, M.; Pera, J. N-Acetylcysteine and Ceftriaxone as Preconditioning Strategies in Focal Brain Ischemia: Influence on Glutamate Transporters Expression. *Neurotoxic. Res.* **2016**, *29* (4), 539–550.

(111) Krzyzanowska, W.; Pomierny, B.; Bystrowska, B.; Pomierny-Chamiolo, L.; Filip, M.; Budziszewska, B.; Pera, J. Ceftriaxone- and N-Acetylcysteine-Induced Brain Tolerance to Ischemia: Influence on Glutamate Levels in Focal Cerebral Ischemia. *PLoS One* **2017**, *12* (10), No. e0186243.

(112) Nielsen, M. M. B.; Lambertsen, K. L.; Clausen, B. H.; Meyer, M.; Bhandari, D. R.; Larsen, S. T.; Poulsen, S. S.; Spengler, B.; Janfelt, C.; Hansen, H. S. Mass Spectrometry Imaging of Biomarker Lipids for Phagocytosis and Signalling during Focal Cerebral Ischaemia. *Sci. Rep.* **2016**, *6* (1), 39571.